

# Spallation Neutron Source

## Design Manual

### Chapter 5 Ring & Transfer Lines

June 1998

---

Senior Team Leader

---

Lead Engineer

## RING & TRANSFER LINES

### Table of Contents

5.0 BEAM TRANSPORT AND RING SYSTEMS .....	5.1-1
5.1 INTRODUCTION.....	5.1-1
5.1.1 Scope.....	5.1-1
5.1.2 Performance Requirements .....	5.1-1
5.1.3 Design Description .....	5.1-1
5.2 ACCELERATOR RING LATTICE AND ACCELERATOR PHYSICS DESIGN.....	5.2-1
5.2.1 Lattice Design of the Accumulator Ring .....	5.2-1
5.2.2 Impedance, Coherent Instabilities, and Damping.....	5.2-5
5.3 HIGH ENERGY BEAM TRANSPORT LINE (WBS 1.5.1).....	5.3-1
5.3.1 Scope.....	5.3-1
5.3.2 Design Requirements.....	5.3-1
5.3.3 Description of the HEBT Line .....	5.3-1
5.3.4 References .....	5.3-6
5.4 INJECTION SYSTEM (WBS 1.5.2) .....	5.4-1
5.4.1 Injection System .....	5.4-1
5.4.2. RF Capture .....	5.4-11
5.5 MAGNET SYSTEMS (WBS 1.5.3).....	5.5-1
5.5.1 Scope.....	5.5-1
5.5.2 Design Requirements.....	5.5-1
5.5.3 Quantities and Performance Requirements.....	5.5-1
5.5.4 Magnet Coil Design .....	5.5-1
5.5.5 Corrector Magnets .....	5.5-2
5.5.6 Water Cooling .....	5.5-2
5.5.7 Magnetic Measurements .....	5.5-3
5.5.8 Magnet Cell Assembly and Alignment.....	5.5-3
5.5.9 References .....	5.5-3
5.6 POWER SUPPLY SYSTEM (WBS 1.5.4) .....	5.6-1
5.6.1 Main Ring.....	5.6-1
5.6.2 HEBT and RTBT.....	5.6-3
5.7. RING VACUUM SYSTEM (WBS 1.5.5).....	5.7-1
5.7.1. Scope.....	5.7-1
5.7.2. Design Requirement .....	5.7-1
5.7.3. Ring Vacuum Layout.....	5.7-1
5.7.4. Pump Down, In-situ Bake, and Conditioning .....	5.7-3
5.7.5. Vacuum Instrumentation.....	5.7-4
5.7.6. References .....	5.7-5
5.8 THE RF SYSTEM (WBS 1.5.6) .....	5.8-1
5.8.1 Scope.....	5.8-1
5.8.2 Design Requirements.....	5.8-1
5.8.3 Cavity Design .....	5.8-1
5.8.4 Design of the Power Amplifier.....	5.8-2
5.8.5 Cavity Tuning.....	5.8-2
5.8.6 RF Feedforward and Feedback.....	5.8-2

5.8.7 Barrier Cavity Upgrade.....	5.8-3
5.8.8 References .....	5.8-3
5.9 SNS RING BEAM DIAGNOSTIC INSTRUMENTATION (WBS 1.5.7).....	5.9-1
5.9.1. Beam Loss Monitors.....	5.9-1
5.9.2 Beam Current Monitors .....	5.9-4
5.9.3 Beam Profile Monitor .....	5.9-6
5.9.4 Beam Position Monitors .....	5.9-7
5.9.5 Damper/Tune Measurement.....	5.9-8
5.10 COLLIMATORS AND MOVABLE SHIELDING (WBS 1.5.8) .....	5.10-1
5.10.1 Scope.....	5.10-1
5.10.2 Design requirements for the collimator .....	5.10-1
5.10.3 Design description .....	5.10-1
5.10.4 Analysis and Results .....	5.10-3
5.10.5 References .....	5.10-5
5.11 EXTRACTION (WBS 1.5.9).....	5.11-1
5.11.1 Scope and Requirements.....	5.11-1
5.11.2 Fast Kicker .....	5.11-1
5.11.3 Lambertson Magnetic Septum.....	5.11-2
5.11.4 Timing and Synchronization .....	5.11-3
5.12 RING TO TARGET BEAM TRANSPORT LINE (WBS 1.5.10).....	5.12-1
5.12.1 Scope.....	5.12-1
5.12.2 Design Requirements .....	5.12-1
5.12.3 Design Description and Functions of the RTBT Line .....	5.12-1
5.13 RAM CONSIDERATIONS.....	5.13-1
5.13.1 Sound and Conservative Conceptual Design .....	5.13-1
5.13.2 Conservative Engineering Design and Reliable Components.....	5.13-1
5.13.3 Good Bookkeeping and Maintenance Record of Components .....	5.13-1
5.13.4 Strategic Schedule for Preventive Maintenance.....	5.13-1
5.14 UPGRADE PATH.....	5.14-1
5.15 REQUIRED RING FACILITIES.....	5.15-1
5.15.1 Scope.....	5.15-1
5.15.2 Light Laboratory Area and Technician Shops.....	5.15-1
5.15.3 Assembly Area .....	5.15-1
5.15.4 High Voltage Assembly and Test Lab .....	5.15-1
5.15.5 "Clean" Assembly Area .....	5.15-2
5.15.6 Storage Areas.....	5.15-2

## 5.0 BEAM TRANSPORT AND RING SYSTEMS

### 5.1 INTRODUCTION

#### 5.1.1 Scope

There are three major accelerator systems included in this WBS area. Figure 5.1-1 is a systems diagram for the ring and transport line elements, showing their WBS classifications and their interrelationships with other portions of the project. The first element in this area is the high-energy beam transport (HEBT) system, the second is the accumulator ring (AR) system, and the third is the ring-to-target beam transport (RTBT) system. There are three support buildings to house power supplies, monitoring devices, rf equipment, etc., for those three major systems. They are the HEBT support building, the ring support building, and the RTBT support building.

#### 5.1.2 Performance Requirements

The purpose of the beam transport and ring system is to convert the incoming linac beam of about one ms length into a beam of about 0.5  $\mu$ s length and transport this final beam onto the neutron target. The initial rms un-normalized emittance of the linac beam is  $0.14 \pi$  mm mrad in both horizontal and vertical dimensions. The final emittance of beam on the target is  $120 \pi$  mm mrad in full size. Table 5.1-1 outlines the evolution of the beam emittance from the linac through the accumulator ring to the target.

To maximize the performance and lifetime of the neutron target, a beam spreading system will create a beam on target of 20 cm (H) x 7 cm (V) size with the ratio of peak density to that of the average density no larger than two.

Another major performance requirement will be to hold the average uncontrolled particle loss during the accumulation time to less than  $2 \times 10^{-4}$  per pulse. This stringent requirement will hold down the residual radiation to a level that will permit hands-on maintenance except in a few localized areas, such as the injection, extraction, and collimation systems. To achieve this goal, special care has been exercised in the design of the H<sup>-</sup> stripping, the rf stacking, and the collimator systems. Ongoing accelerator R&D and computer tracking studies of the space-charge effects and halo formation will ensure the achievement of this performance goal.

#### 5.1.3 Design Description

The HEBT system provides the link between the linac and the accumulator ring. The beam coming out of the linac is a 1.0-GeV H<sup>-</sup> beam, approximately one ms long, with a peak current of 28 mA. The beam has a 402.5-MHz microstructure and is chopped to lengths of 546 ns with 295 ns gaps. The transverse rms un-normalized emittance of the linac beam will be  $0.14 \pi$  mm mrad in both planes, and the longitudinal emittance will be  $300 \pi$  keV degrees. The total length of the HEBT line will be 192 m, and the total bending angle will be 90°. The line will provide locations for beam scraping of the halo particles from the linac in both betatron and momentum phase space. A debuncher system will be provided for the proper control of the momentum spread of the beam injected into the accumulator ring. At the injection point, the linac beam will be matched to the ring lattice for the H<sup>-</sup> injection process.

The proton accumulator ring is one of the major systems in the design of the SNS. The primary function of the AR is to take a one ms long 1.0-GeV  $H^-$  beam from the linac and compress it into a 0.5  $\mu$ s long beam by accumulating it in the AR in 1158 turns. The final beam will have  $10^{14}$  protons per pulse, meeting the design specification of 1-MW design average beam power at a 60-Hz repetition rate. Provisions have been reserved for a future upgrade to 2 MW of beam power by a doubling of the stored current to  $2 \times 10^{14}$  protons per pulse without changes to either the magnet or the vacuum system. The lattice structure of the AR is a simple FODO lattice with fourfold symmetry. A missing magnet design is used to reduce the dispersion function to zero at the straight sections. The total circumference of the ring will be 220.688 meters. The transition gamma is about 4.93, much higher than the operating energy of 1.0 GeV. A sketch of the HEBT and AR is given in Fig. 5.1-2 for reference. Other salient design parameters are listed in Table 5.2-1.

**Table 5.1-1**

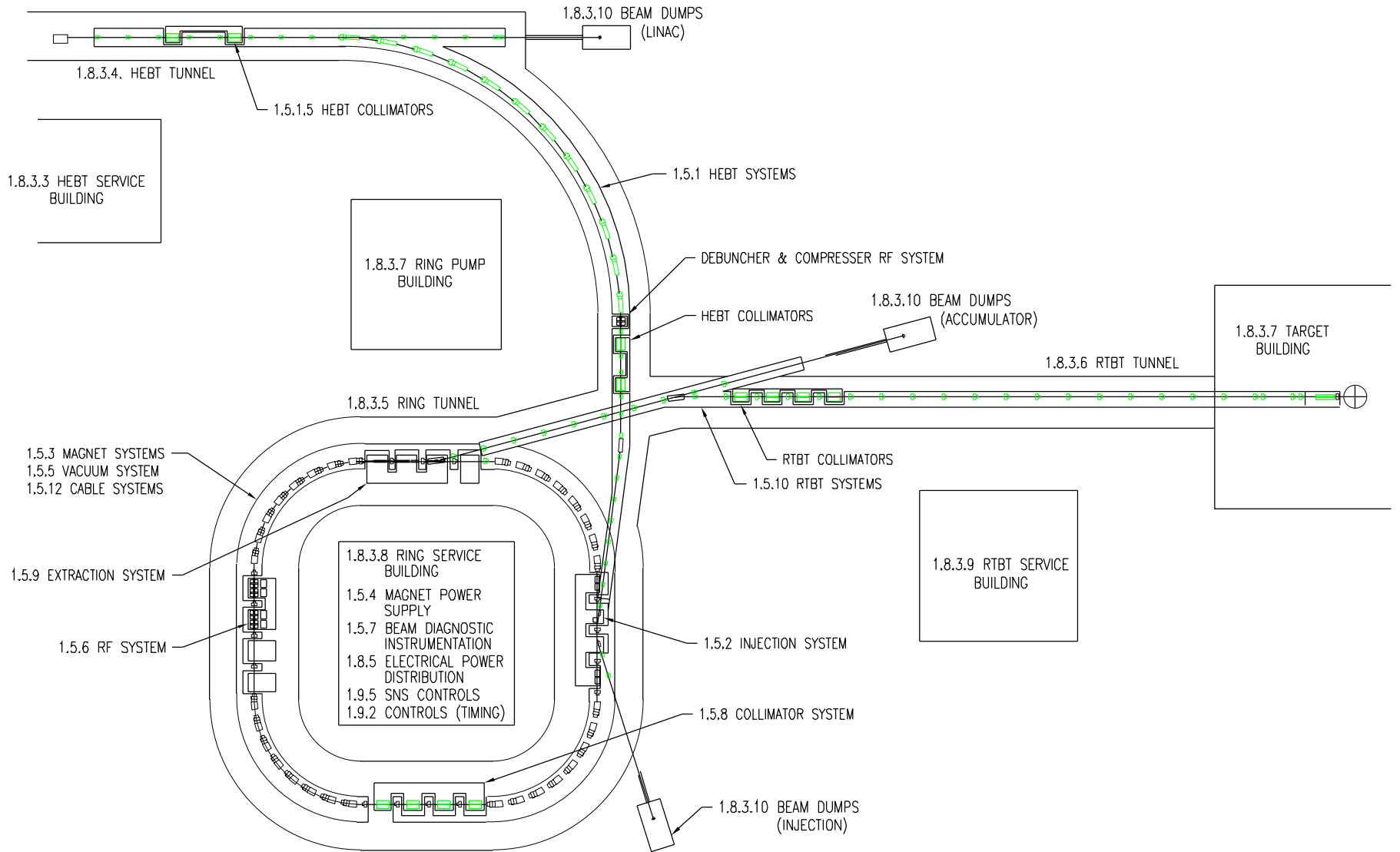
**Evolution of Beam Parameters**

	<b>Linac</b>	<b>HEBT</b>	<b>Ring</b>	<b>RTBT</b>
<b>Energy (GeV)</b>	1.0	1.0	1.0	1.0
<b><math>\epsilon_h \pi</math> mm mrad</b>	0.14 (rms)	0.14 (rms)	120 (full)	120 (full)
<b><math>\epsilon_v \pi</math> mm mrad</b>	0.14 (rms)	0.14 (rms)	120 (full)	120 (full)
<b><math>\epsilon_l</math></b>	300 pi keV-deg	300 pi keV-deg	10 eV-s	10 eV-s
<b>Pulse Length</b>	1 ms	1 ms	560 ns	590 ns

The Ring to Target Beam Transport system will take the extracted beam from the AR and transport it to the neutron target. The extraction starts with an 8-module kicker array to deflect the circulating beam vertically by 16.8 mrad followed by a Lambertson magnet to bend the beam horizontally out of the ring. A small vertical dipole magnet brings the beam back to the horizontal resulting in a beam height about one foot above the ring beam height. The magnet apertures in this line will be sized to allow for malfunctions of one of the eight extraction kickers, protecting the line against excessive losses. A beam shape control section will be provided for the final beam profile tuning for the target. Additional focusing control will provide compensation for the window scattering before the target. The total length of the RTBT line will be 180 meters and the total horizontal bend angle will be 15 degrees.

Sections 5.2.1 and 5.2.2 cover the accumulator ring lattice design and the accelerator physics designs that achieve the needed high intensity and low loss performance. Sections 5.3 to 5.12 cover the engineering systems and their design parameters.

Fig. 5.1-1 SKETCH OF HEBT, AR, AND RTBT SHOWING WBS CLASSIFICATIONS



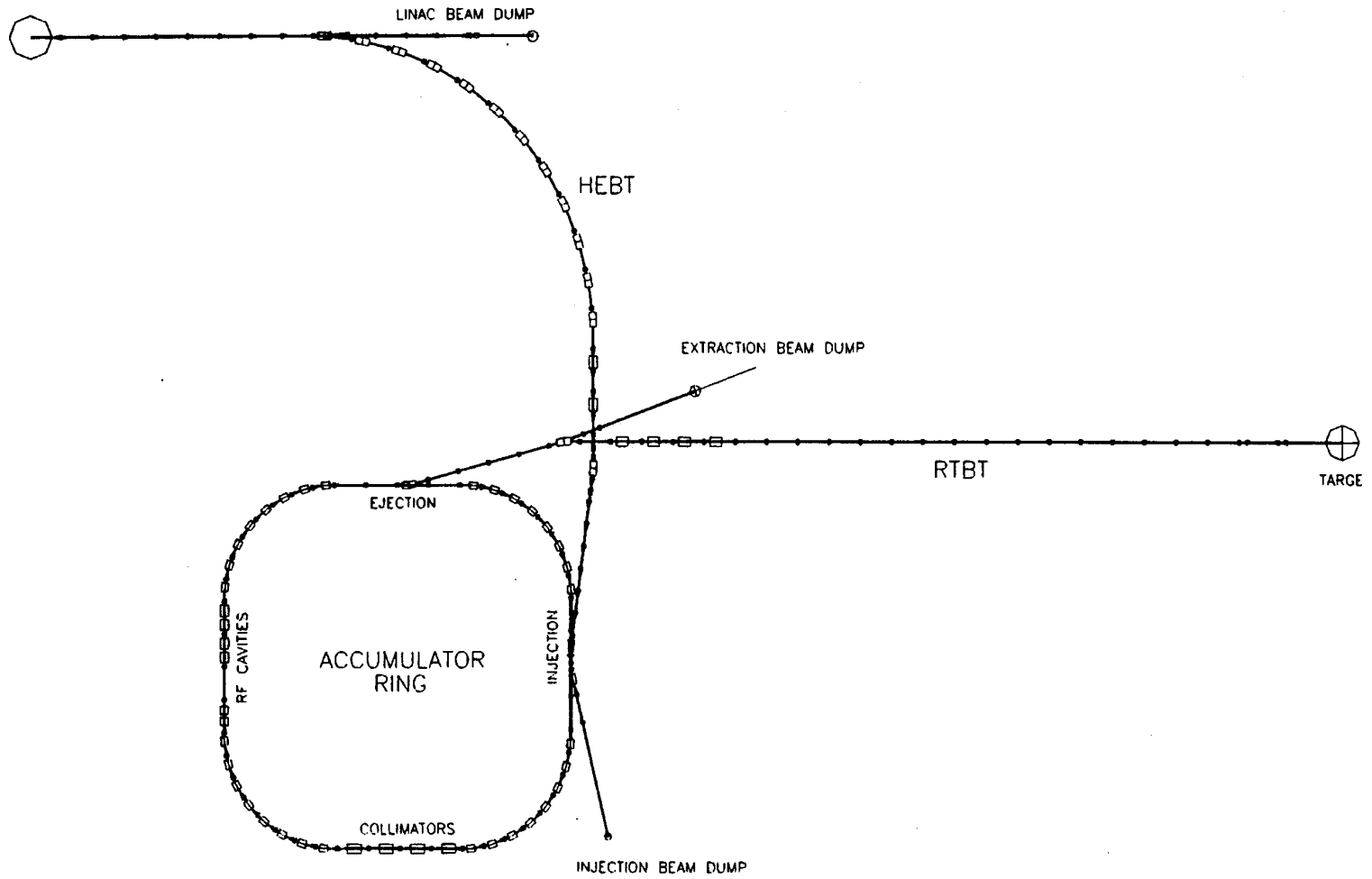


Fig.5.1-2 Layout of Beam Transports and Accumulator Ring

## 5.2 ACCELERATOR RING LATTICE AND ACCELERATOR PHYSICS DESIGN

### 5.2.1 Lattice Design of the Accumulator Ring

#### 5.2.1.1 The Lattice

The accumulator ring of SNS will have a four-fold symmetric lattice. The lattice will accommodate the long straight sections required for the injection system, the extraction system, the rf cavities, and the beam scraping system. The straight sections will be nearly dispersion free, which is desirable, especially for the rf cavities and the injection system. The lattice will provide ease of betatron tuning and flexibility of operation. Unlike lattices of lower symmetry, a lattice of four-fold symmetry will assure that there are no dangerous betatron structure resonances in the vicinity of the working point.

The accumulator ring will consist of four superperiods, each containing a  $90^\circ$  arc and a long straight section, shown schematically in Fig. 5.2-1. Four FODO cells, with a total phase advance of  $2\pi$ , will make up the arc section. Each half-cell will consist of one-half of a quadrupole, a 1.55-meter space, a 1.5-meter long dipole, a 0.45-meter space, and one half of a second quadrupole. The total length of the arc half-cell will be 4 meters. Four full cells of  $\pi/2$  phase advance each will ensure zero dispersion at either end of the arc. However, the introduction of a fixed orbit bump in the injection straight disturbs the symmetric nature of the lattice and creates a 0.3-meter dispersion in all the straight sections. Two FODO cells without dipoles will form each long straight section. The half-cell length for the straight sections will be 5.793 meters. The phase advance in the straight sections will be adjusted to make the horizontal tune of the ring be 5.82 and the vertical tune be 5.80. The lattice functions for all the superperiods are shown in Fig.5.2-2. The relevant ring parameters are given in Table 5.2-1.

The beam will have a full emittance, both horizontal and vertical, of  $120\pi$  mm mr and the ring will have a full acceptance of  $360\pi$  mm mr, which is over twice the full beam emittance plus 1 cm for the maximum possible orbit errors. The ring must also accept a maximum beam momentum spread of plus or minus 1%. The quadrupoles at the center of the arcs will be 50% larger than the normal quadrupoles to meet this requirement. The quadrupoles in the center of the straight sections will have these larger apertures to allow for the injection orbit bumps and for the extraction kicker and septum displacements.

The primary assignments for the long straight sections are for the injection system, the ejection system, the rf cavities, and the beam scraping system. The half-cells not being used for the primary functions will be used for other functions such as the tune meter kicker and the transverse damping system. The super-periods will be named A, B, C, and D. The injection system will be in the A super-period. The extraction system will be in the D super-period. The rf cavities will be in the C super-period. The beam scraping system will be in the B super-period. Each super-period will start at the beginning of an arc, and the magnets in the A super-period will be designated: DHA1, QVA1, DHA2, QHA2, ..., DHA8, QHA8, QVA9, QHA10, QVA11, and QHA12. The B, C, and D super-periods will be similar. The 1.55-m space between a quadrupole and a dipole will be occupied by a beam position monitor, by a vacuum pumping port, and either by a correction dipole combined with a skew quadrupole or by a correction dipole with a combination of higher order correctors.

The injection straight section contains a three dipole chicane to produce one fixed horizontal orbit bump to accommodate  $H^-$  injection. Horizontal and vertical dynamic bumps are used to paint the injected protons in the transverse phase space.

It has been demonstrated that the tune of the lattice is quite flexible and can be changed over one half of a tune unit without adverse change in the beta functions. The lattice has structure resonances at betatron tune values of 5 and 6, which is expected from 4-fold symmetry. However, there are no structure resonances at fractional tunes between 5 and 6, except for one at 5.333, which is some distance away from the working point.

### 5.2.1.2 Accumulator Ring Magnets

Table 5.2-2 lists the main magnetic elements required for the accumulator ring. For the stability of the ring, and for economy, it is advantageous to connect as many magnetic elements as possible to a single power supply. All the dipoles will be connected to one power supply. The quadrupoles will be divided into three families. Each family will be connected to its own main power supply. To achieve this there will be quadrupoles of four different lengths, the precise lengths being determined by magnetic field measurements on prototypes. One family (the Arc Quads) will be the arc quadrupoles, Q1 through Q7, which will include the large aperture quadrupole, Q4. The second family (the H Quads) will be the quadrupoles at both ends of the arc and the center quadrupole in the straight section (Q8, Q10, and Q12). The third family (the V Quads) will be the defocusing quadrupoles in the straight sections (Q9 and Q11). (The quadrupole designations used are generic; H, V and superperiod designations are omitted.) The second and third group of the quadrupoles will be used to adjust the tune of the ring. The main power supply connections are shown in the Fig 5.2-1. The poles of the quadrupoles will be carefully shaped to eliminate multi-pole errors. In addition small trim windings and trim supplies will provide additional fine-tuning. Transients or eddy current effects do not exist since the ring is dc. The magnet types listed in Table 5.2-2 are defined in Tables 5.5-1 and 2. Table 5.2-2 also lists the integrated dipole and quadrupole fields required for each type of magnet. The current in each string is calculated from these values and the projected magnet properties in Section 5.5.

The three dipole chicane magnets that produce a fixed orbit bump for the injection straight are special dipoles. Two of them, IDH1 and IDH3, are septum magnets that accommodate the incoming linac beam and the outgoing  $H^0$  beam respectively. The large aperture C-magnet, IDH2, is a special magnet to accommodate the stripping foil mechanism and the stripped electron dump. Because of the special scheme to minimize uncontrolled proton loss due to the stripping of excited  $H^0$ 's in the magnetic field, the downstream edge of this magnet is carefully shaped to give the desired fringe field shape and integral. Table 5.2-3 gives the properties of the chicane magnets. All magnets described in this section will be operated in dc fashion. The dynamic or painting magnet systems are described in Section 5.4.1.7.

### 5.2.1.3 Lattice Functions

Table 5.2-4 gives a complete listing of the lattice functions of the accumulator ring.

**Table 5.2-1 SNS Accumulator Ring Parameters**

KINETIC ENERGY	1.0 GEV
MAGNETIC RIGIDITY	5.6575 T m
CIRCUMFERENCE	220.688 m
PERIODICITY	4
STRUCTURE	24 FODO
BEAM EMITTANCES	120 $\pi$ mm mr
RING ADMITTANCE	360 $\pi$ mm mr
$\beta_{\max}$ x/y	19.2/19.2
Xp max	4.1 m
$\nu_{x/y}$	5.82 / 5.80
Natural $\xi_{x/y}$	-6.5 / -7.3
$\gamma_T$	4.93

**Table 5.2-2 SNS Ring Magnets\***

<b>ELEMENT*</b>	<b>NO.</b>	<b>TYPE</b>	<b>B*Le (T m)</b>	<b>I** (A)</b>
<b>DIPOLES</b>	32	17D140	1.111	3988.3
<b>QUADRUPOLES</b>	<b>NO.</b>	<b>TYPE</b>	<b>G*Le (T)</b>	<b>I** (A)</b>
<b>Arc Quads</b>				
<b>Arc Defocusing Q1,Q3,Q5,Q7</b>	16	20Q50	2.062	569.6
<b>Arc Focusing Q2,Q6</b>	8	20Q47	1.942	569.5
<b>Arc Focusing Q4</b>	4	30Q49	1.942	569.5
<b>H Quads</b>				
<b>Arc End Q8,Q12</b>	8	20Q50	1.630	450.3
<b>Straight Section Q10</b>	4	30Q40	1.319	450.2
<b>V Quads</b>				
<b>Straight Section Q9,Q11</b>	8	20Q50	1.319	364.4

\*designations H, V, and superperiod are omitted from name designation  
 \*\*Calculated from projected magnet properties in Tables 5.5-1 and 2.

**Table 5.2-3 Injection Chicane Dipoles**

<b>MAGNET</b>	<b>IDH1</b>	<b>IDH2</b>	<b>IDH3</b>
<b>Type</b>	Septum	C Magnet	Septum
<b>Length* (m)</b>	0.5	0.781	0.5
<b>Gap (cm)</b>	17	20	17
<b>Width (cm)</b>	20	30	20
<b>Field (T)</b>	0.315	0.3	0.153
<b>Septum Thickness (cm)</b>	3		3

\* For IDH1 and IDH3, the length and field can be changed while keeping the field integral.

## 5.2.2 Impedance, Coherent Instabilities, and Damping

### 5.2.2.1 Scope

The Spallation Neutron Source is a high intensity machine. For 2 MW operation the average beam current just before extraction is 39 Amperes, with peak currents as high as 94 Amperes. This current level, coupled with the 0.02 % loss limit, necessitates a careful investigation of coherent instabilities. Estimates of machine impedance and the effect this impedance has on the beam have been made (Blaskiewicz, 1998) and are summarized herein. Preliminary damper requirements are included.

### 5.2.2.2 Impedance Estimates

Impedance estimates from some sources such as space charge, beam position monitors and the resistivity of the vacuum chamber wall are calculable with a high degree of confidence. Impedances from other devices, such as kicker magnets, are difficult to estimate and should be measured. This section provides best guess impedance estimates for these devices.

The transverse impedance due to space charge is similar in both horizontal (x) and vertical (y) directions and is given by:

$$Z_x = Z_y = 10 \text{ M}\Omega/\text{m}.$$

The longitudinal (s) space charge impedance is:

$$Z_s/n = i 150 \text{ }\Omega,$$

where n is the frequency measured in units of the revolution frequency. The total transverse impedance due to stripline beam positions monitors is the same in the horizontal and vertical directions and is given by:

$$Z_x = 0.024 \frac{\sin^2(kl) - i \sin(kl) \cos(kl)}{kl} \text{ M}\Omega/\text{m}$$

In this equation  $k = \omega/c$  is the wave number and  $l = 20$  cm.

The total longitudinal impedance due to striplines is:

$$Z_s = 180 (\sin^2(kl) - i \sin(kl) \cos(kl)) \text{ }\Omega$$

The impedance contribution from the position monitors is essentially reactive. The resistivity of the vacuum chamber adds a longitudinal contribution of:

$$Z_s = 0.74 (1 - i \operatorname{sgn}(n)) \sqrt{n} \text{ }\Omega$$

The vertical transverse resistive wall impedance is:

$$Z_y = 0.0059 \frac{(1 - i \operatorname{sgn}(f))}{\sqrt{n}} \text{ M}\Omega / m$$

The horizontal transverse impedance is slightly smaller.

Bellows and pipe transitions add low frequency transverse and longitudinal contributions:

$$Z_x = Z_y = -i(0.36) \text{ M}\Omega / m$$

$$Z_s / n = -i45 \text{ }\Omega$$

At frequencies near the cutoff frequency for microwave propagation down the beam pipe these equations are unreliable. However, these frequencies are several hundred MHz and should not play a significant role in the beam dynamics.

The most difficult object to assess is the extraction kicker. Its impedance estimate should be viewed as a rough guess. The longitudinal impedance of the extraction kicker is given by:

$$Z_s = \frac{0.0073}{1 - 3i(f / 60\text{MHz} - 60\text{MHz} / f)} \text{ M}\Omega$$

The vertical transverse impedance is:

$$Z_y = \frac{0.025}{f / 120\text{MHz} - 0.6i(1 - (f / 120\text{MHz})^2)} \text{ M}\Omega / m$$

The horizontal impedance of the extraction kicker should be small compared to the vertical impedance.

The RF cavities are the final impedance sources considered. The cavity gaps will be only a few inches long so the transverse impedance should be negligible. The longitudinal impedance of higher order modes will be considered in the early design stages and the final product will have negligible impedance for modes other than the fundamental.

### 5.2.2.3 Instabilities

For longitudinal instabilities, a coasting beam model, with a peak current of 100Amperes and a root mean square energy spread of 4 MeV, gives growth rates of  $8 \text{ s}^{-1}$  per Ohm. For frequencies of  $n < 700$  the beam position monitors (BPMs) and the resistivity of the vacuum chamber contribute no more than  $200\Omega$ , corresponding to a peak growth rate of 1600/s, and do not present any problem. The extraction kicker could be a problem. For a frequency near 60MHz a coasting beam growth rate of 58000/s is predicted and might result in longitudinal emittance growth.

For transverse instabilities a 100 Amperes cold coasting beam approximation yields a growth rate of  $200 \text{ s}^{-1}$  for  $\text{Re}(Z_y)$  equals 0.001 megohms per meter. The most unstable mode due to wall resistivity yields a growth rate of 2600/s, which is probably benign. For the extraction kicker the growth rate of 6000/s corresponds to 6 e-folding times in one millisecond for a current of 100 A. If the kicker impedance is accurate this growth rate should not be a problem.

It should be pointed out that these coasting beam growth rates are probably overestimates, especially for the kicker contribution. This is due to the fact that the gap in the beam allows the high frequency low Q modes to substantially decay from one turn to the next. Additional studies are underway.

#### 5.2.2.4 Damping

Of the instabilities predicted for the SNS, only the resistive wall instability is easily damped. Assuming that the coherent pickup is able to detect a coherent betatron oscillation of amplitude  $x$ , the minimum kicker strength required is

$$\Delta x' = Tx / \beta\tau$$

In this equation T is the revolution period,  $\beta$  is the average beta function, and  $\tau$  is the e-folding time of the instability. Setting  $x=5 \text{ mm}$  gives a  $2 \text{ } \mu\text{rad}$  kick which is easily obtained.

The instabilities due to the kicker are more difficult. For a transverse instability with a 5-mm amplitude the minimum kick amplitude would be  $4.2 \text{ } \mu\text{rads}$  at a frequency near 60MHz.

#### 5.2.2.5 References

Blaskiewicz, M., BNL SNS Tech Note 42, (1998)

# Accumulator Ring Consisting of Four Superperiods.

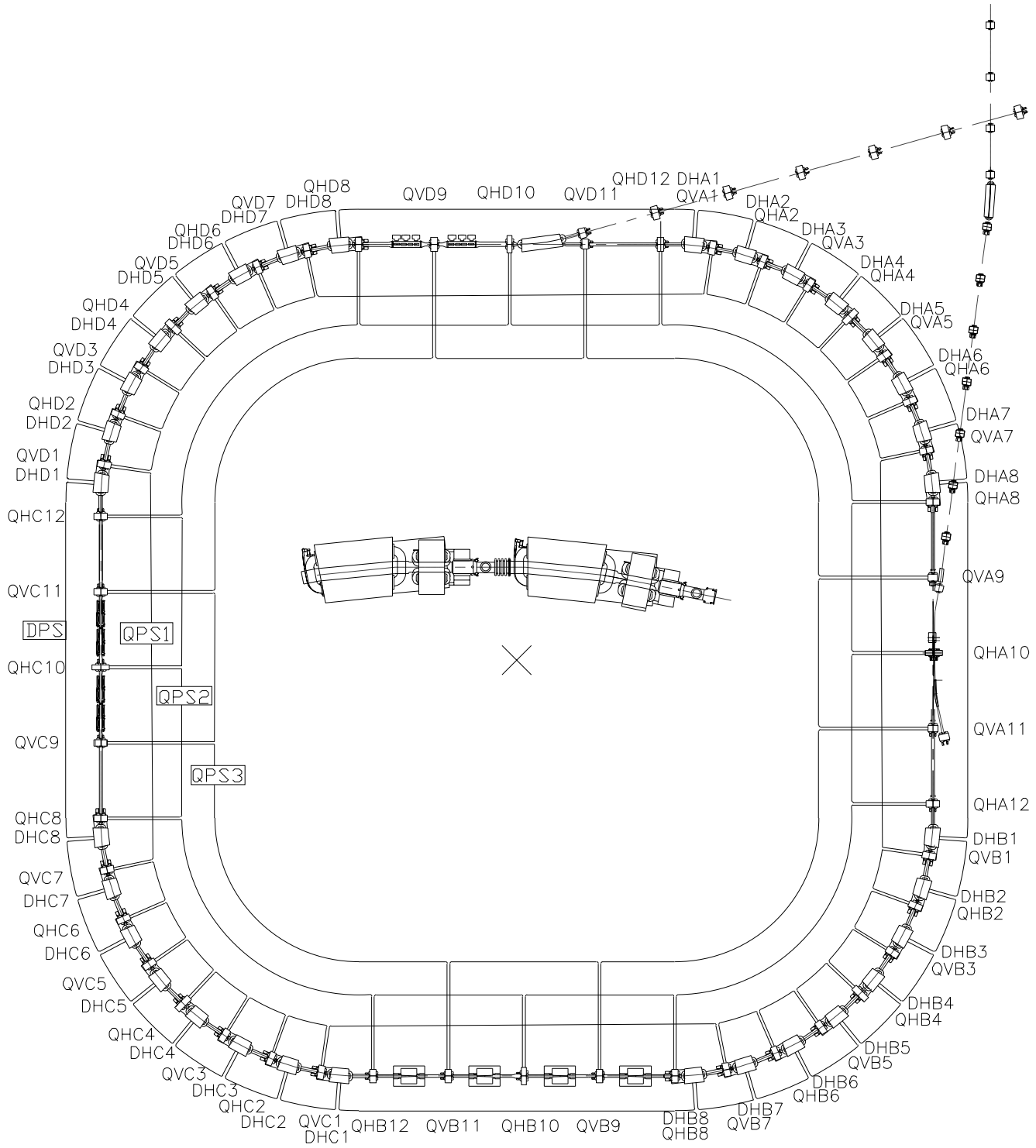
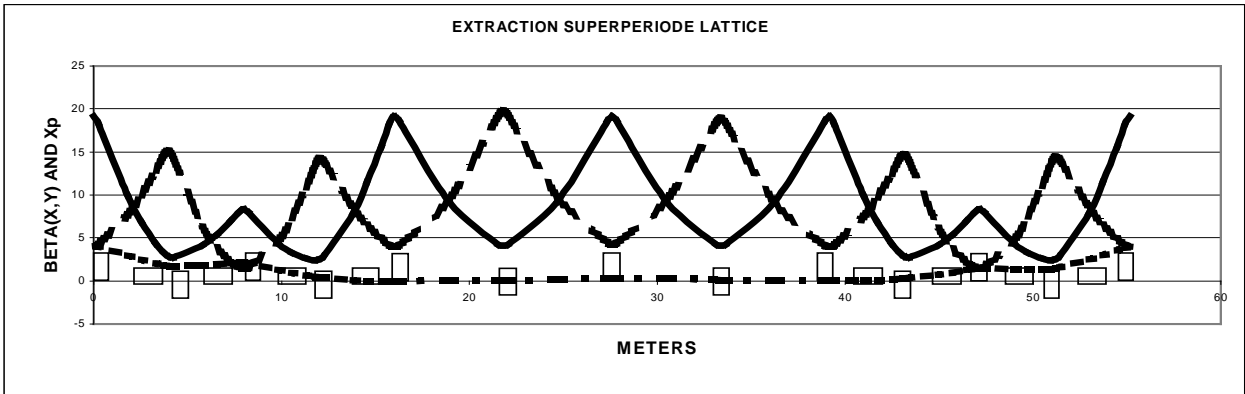
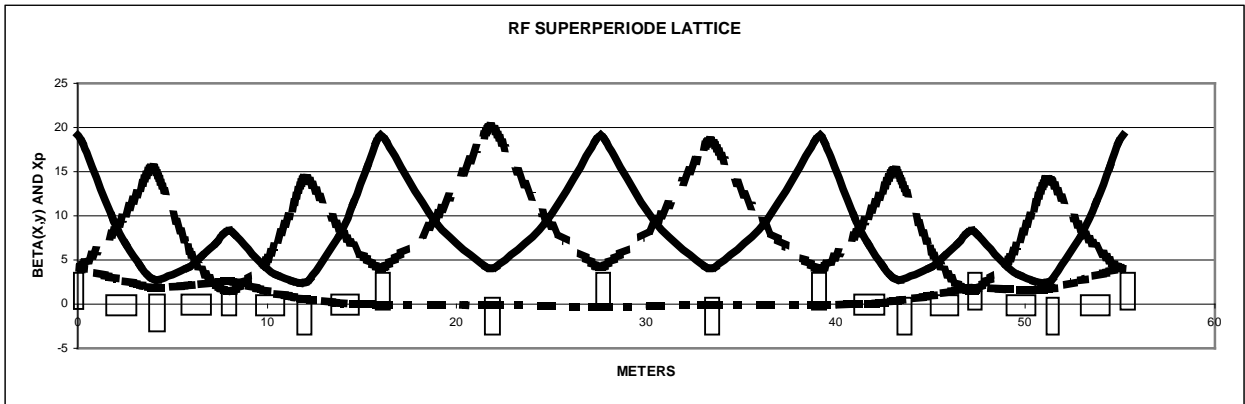
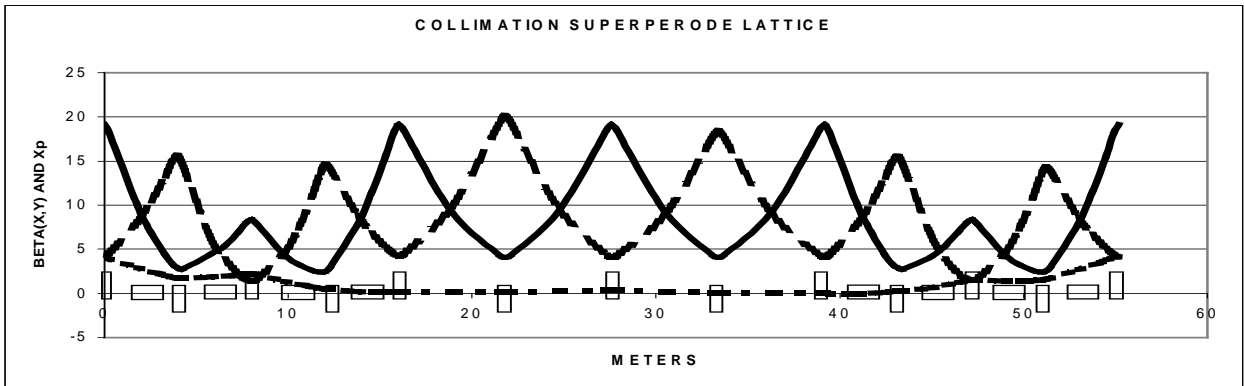
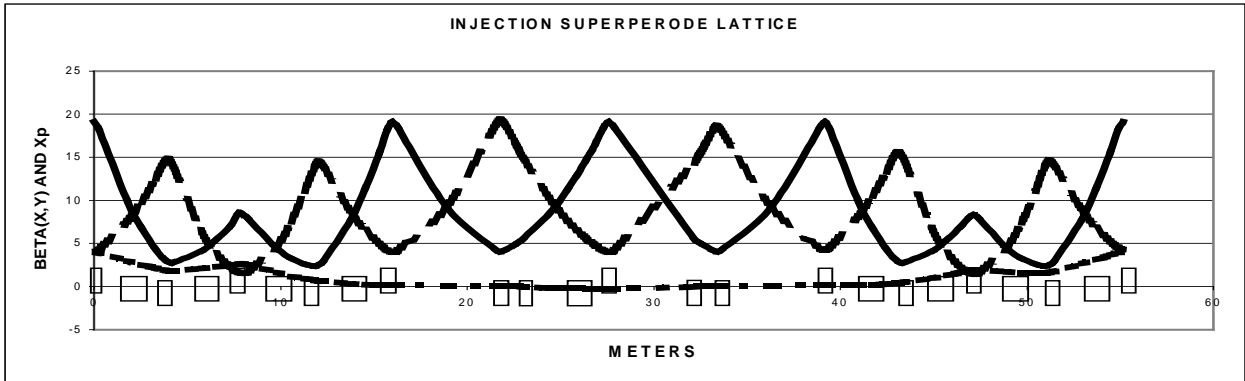


Fig. 5.2-1



**Fig. 5.2-2 Accumulator Ring Lattice Functions**

**Table 5.2-4 LATTICE FUNCTIONS 1GeV SPALLATION NEUTRON SOURCE ACCUMULATOR RING**

No.	ELEMENT	S meters	NU(x) 2 Pi	NU(y) 2 Pi	BETA(x) meters	BETA(y) meters	Xp meters	ALPHA(x)	ALPHA(y)	dXp/dS	Magnet
0	QF	0	0	0	19.44602	4.13817	0.26823	0.01667	0	-0.00414	QHB10
1	QF	0.25	0.00207	0.00951	18.88082	4.27497	0.26331	2.22219	-0.5525	-0.03514	
2	L	2.8965	0.03403	0.0783	9.32155	9.33782	0.17032	1.38985	-1.36054	-0.03514	
3	L	5.543	0.10382	0.11041	4.16786	18.67764	0.07733	0.55751	-2.16858	-0.03514	
4	QD	5.793	0.11359	0.1125	4.02524	19.22507	0.06962	0.01843	0	-0.02666	QVB11
5	QD	6.043	0.12338	0.11459	4.14907	18.67764	0.06393	-0.5185	2.16858	-0.01895	
6	L	8.6895	0.19452	0.1467	9.03541	9.33782	0.01377	-1.32784	1.36054	-0.01895	
7	L	11.336	0.22759	0.21549	18.20558	4.27497	-0.03639	-2.13718	0.5525	-0.01895	
8	QF	11.586	0.22974	0.225	18.74801	4.13817	-0.04057	-0.01148	0	-0.01446	QHB12
9	QF	11.836	0.23189	0.23447	17.9641	4.33355	-0.0433	3.10215	-0.79267	-0.00724	
10	OO	13.386	0.25056	0.27772	9.76819	7.69357	-0.05452	2.18553	-1.37508	-0.00724	
11	BM2	14.136	0.26526	0.29137	6.74865	9.96755	-0.0229	1.82759	-1.65689	0.09151	DHC1
12	BM2	14.886	0.2874	0.302	4.32059	12.66424	0.08252	1.39941	-1.9387	0.18938	
13	O	15.336	0.30671	0.30729	3.19978	14.48516	0.16774	1.09129	-2.10779	0.18938	
14	QD	15.586	0.32005	0.30998	2.82884	14.88062	0.21928	0.41492	0.55007	0.2245	QVC1
15	QD	15.836	0.33438	0.31272	2.77214	13.95165	0.28084	-0.18469	3.10921	0.26989	
16	OO	17.386	0.40904	0.33948	4.24089	6.15	0.69918	-0.76289	1.92411	0.26989	
17	BM2	18.136	0.43371	0.36463	5.54631	3.69392	0.93469	-0.97207	1.35067	0.35764	DHC2
18	BM2	18.886	0.45269	0.40804	7.13839	2.09799	1.23478	-1.14388	0.77723	0.44194	
19	O	19.336	0.46204	0.44814	8.23337	1.55331	1.43365	-1.28941	0.43317	0.44194	
20	QF	19.586	0.46676	0.475	8.53157	1.44654	1.51271	0.11373	0	0.18826	QHC2
21	QF	19.836	0.4715	0.50186	8.12287	1.55331	1.52711	1.49762	-0.43317	-0.07346	
22	OO	21.386	0.51305	0.59871	4.43938	4.73305	1.41325	0.87882	-1.61827	-0.07346	
23	BM2	22.136	0.54434	0.61868	3.3108	7.59054	1.38822	0.62112	-2.19171	0.00678	DHC3
24	BM2	22.886	0.58551	0.63158	2.58797	11.30819	1.4234	0.33955	-2.76515	0.08695	
25	O	23.336	0.61459	0.63728	2.36965	13.95165	1.46252	0.14562	-3.10921	0.08695	
26	QD	23.586	0.63133	0.64002	2.43154	14.88062	1.51786	-0.39695	-0.55007	0.35744	QVC3
27	QD	23.836	0.64677	0.64271	2.77876	14.48516	1.64261	-1.01294	2.10779	0.64428	
28	OO	25.386	0.70127	0.66456	7.67057	8.85375	2.64124	-2.14307	1.52538	0.64428	
29	BM2	26.136	0.71414	0.67999	11.19968	6.77704	3.14775	-2.54728	1.24357	0.70531	DHC4
30	BM2	26.886	0.72326	0.70031	15.26341	5.12304	3.69751	-2.8536	0.96176	0.75954	
31	O	27.336	0.72758	0.71553	17.95295	4.33355	4.0393	-3.12316	0.79267	0.75954	
32	QF	27.586	0.72974	0.725	18.74801	4.13817	4.14151	-0.01148	0	0.05518	QHC4
33	QF	27.836	0.73189	0.73447	17.9641	4.33355	4.0667	3.10215	-0.79267	-0.65153	
34	OO	29.386	0.75056	0.77772	9.76819	7.69357	3.05682	2.18553	-1.37508	-0.65153	
35	BM2	30.136	0.76526	0.79137	6.74864	9.96755	2.59102	1.82759	-1.65689	-0.5896	DHC5
36	BM2	30.886	0.7874	0.802	4.32059	12.66424	2.17384	1.39941	-1.9387	-0.52199	
37	O	31.336	0.80671	0.80729	3.19978	14.48516	1.93895	1.09129	-2.10779	-0.52199	
38	QD	31.586	0.82005	0.80998	2.82884	14.88062	1.85179	0.41492	0.55007	-0.17795	QVC5
39	QD	31.836	0.83438	0.81272	2.77214	13.95165	1.8493	-0.18469	3.10921	0.15796	
40	OO	33.386	0.90904	0.83948	4.24089	6.15	2.09413	-0.76289	1.92411	0.15796	
41	BM2	34.136	0.93371	0.86463	5.5463	3.69392	2.23911	-0.97207	1.35067	0.22834	DHC6

42	BM2	34.886	0.9527	0.90804	7.13838	2.09799	2.43609	-1.14388	0.77723	0.29653	
43	O	35.336	0.96204	0.94814	8.23337	1.55331	2.56953	-1.28941	0.43317	0.29653	
44	QF	35.586	0.96676	0.975	8.53156	1.44654	2.58822	0.11372	0	-0.14754	QHC6
45	QF	35.836	0.9715	1.00186	8.12287	1.55331	2.49629	1.49762	-0.43317	-0.58532	
46	OO	37.386	1.01305	1.09871	4.43938	4.73305	1.58905	0.87882	-1.61827	-0.58532	
47	BM2	38.136	1.04434	1.11868	3.3108	7.59054	1.1799	0.62112	-2.19171	-0.50487	DHC7
48	BM2	38.886	1.08551	1.13158	2.58798	11.30819	0.83296	0.33955	-2.76515	-0.41956	
49	O	39.336	1.11459	1.13728	2.36965	13.95165	0.64416	0.14562	-3.10921	-0.41956	
50	QD	39.586	1.13133	1.14002	2.43155	14.88062	0.5532	-0.39695	-0.55007	-0.31089	QVC7
51	QD	39.836	1.14677	1.14271	2.77876	14.48516	0.48753	-1.01294	2.10779	-0.21643	
52	OO	41.386	1.20127	1.16456	7.67058	8.85375	0.15206	-2.14307	1.52538	-0.21643	
53	BM2	42.136	1.21414	1.17999	11.19969	6.77704	0.02605	-2.54728	1.24357	-0.11932	DHC8
54	BM2	42.886	1.22326	1.20031	15.26341	5.12304	-0.02664	-2.8536	0.96176	-0.02107	
55	O	43.336	1.22758	1.21553	17.95296	4.33355	-0.03612	-3.12316	0.79267	-0.02107	
56	QF	43.586	1.22974	1.225	18.74801	4.13817	-0.04058	-0.01147	0	-0.01446	QHC8
57	QF	43.836	1.23188	1.23451	18.21684	4.27497	-0.04358	2.11555	-0.5525	-0.00956	
58	L	46.4825	1.26479	1.3033	9.12446	9.33782	-0.06887	1.32007	-1.36054	-0.00956	
59	L	49.129	1.33471	1.33541	4.24254	18.67764	-0.09416	0.5246	-2.16858	-0.00956	
60	QD	49.379	1.34428	1.3375	4.118	19.22507	-0.09793	-0.02166	0	-0.02064	QVC9
61	QD	49.629	1.35383	1.33959	4.26462	18.67764	-0.10453	-0.57045	2.16858	-0.03232	
62	L	52.2755	1.42223	1.3717	9.4608	9.33782	-0.19008	-1.39297	1.36054	-0.03232	
63	L	54.922	1.45384	1.44049	19.01056	4.27497	-0.27562	-2.21548	0.5525	-0.03232	
64	QF	55.172	1.45589	1.45	19.56851	4.13817	-0.27966	0.00537	0	0.00006	QHC10
65	QF	55.422	1.45795	1.45951	19.00529	4.27497	-0.27559	2.2256	-0.5525	0.03244	
66	L	58.0685	1.48964	1.5283	9.41913	9.33782	-0.18972	1.3966	-1.36054	0.03244	
67	L	60.715	1.55857	1.56041	4.22088	18.67764	-0.10386	0.5676	-2.16858	0.03244	
68	QD	60.965	1.56822	1.5625	4.07459	19.22507	-0.09721	0.02317	0	0.02084	QVC11
69	QD	61.215	1.57789	1.56459	4.19725	18.67764	-0.09339	-0.51854	2.16858	0.00984	
70	L	63.8615	1.64849	1.5967	9.05929	9.33782	-0.06733	-1.31862	1.36054	0.00984	
71	L	66.508	1.68157	1.66549	18.15611	4.27497	-0.04128	-2.11869	0.5525	0.00984	
72	QF	66.758	1.68372	1.675	18.69069	4.13817	-0.03823	0.00116	0	0.01448	QHC12
73	QF	67.008	1.68588	1.68447	17.90308	4.33355	-0.03382	3.10412	-0.79267	0.02069	
74	OO	68.558	1.70464	1.72772	9.70754	7.69357	-0.00176	2.18332	-1.37508	0.02069	
75	BM2	69.308	1.71944	1.74137	6.69338	9.96755	0.05052	1.82263	-1.65689	0.11863	DHD1
76	BM2	70.058	1.7418	1.752	4.27471	12.66424	0.17589	1.3919	-1.9387	0.21542	
77	O	70.508	1.76133	1.75729	3.16115	14.48516	0.27283	1.08268	-2.10779	0.21542	
78	QD	70.758	1.77484	1.75998	2.79301	14.88062	0.33334	0.41214	0.55007	0.27044	QVD1
79	QD	71.008	1.78936	1.76272	2.73638	13.95165	0.40908	-0.18215	3.10921	0.33782	
80	OO	72.558	1.86486	1.78948	4.20817	6.15	0.9327	-0.76739	1.92411	0.33782	
81	BM2	73.308	1.88968	1.81463	5.52315	3.69392	1.21795	-0.98028	1.35067	0.42224	DHD2
82	BM2	74.058	1.90871	1.85804	7.13015	2.09799	1.56505	-1.15549	0.77723	0.5026	
83	O	74.508	1.91806	1.89814	8.23641	1.55331	1.79122	-1.30287	0.43317	0.5026	
84	QF	74.758	1.92277	1.925	8.54127	1.44654	1.87769	0.10091	0	0.18671	QHD2
85	QF	75.008	1.92751	1.95186	8.13836	1.55331	1.88391	1.48762	-0.43317	-0.13716	
86	OO	76.558	1.96885	2.04871	4.47524	4.73305	1.67131	0.87568	-1.61827	-0.13716	
87	BM2	77.308	1.99983	2.06868	3.3485	7.59054	1.59734	0.6218	-2.19171	-0.05992	DHD3

88	BM2	78.058	2.0405	2.08158	2.6218	11.30819	1.58157	0.34402	-2.76515	0.01789	
89	O	78.508	2.06921	2.08728	2.39856	13.95165	1.58962	0.15207	-3.10921	0.01789	
90	QD	78.758	2.08575	2.09002	2.45819	14.88062	1.63046	-0.39419	-0.55007	0.31013	QHV3
91	QD	79.008	2.10105	2.09271	2.80484	14.48516	1.74586	-1.01338	2.10779	0.61656	
92	OO	80.558	2.15523	2.11456	7.6825	8.85375	2.70154	-2.1335	1.52538	0.61656	
93	BM2	81.308	2.16809	2.12999	11.19361	6.77704	3.18699	-2.53293	1.24357	0.67695	DHD4
94	BM2	82.058	2.17723	2.15031	15.23255	5.12304	3.71533	-2.83502	0.96176	0.73082	
95	O	82.508	2.18156	2.16553	17.90421	4.33355	4.0442	-3.102	0.79267	0.73082	
96	QF	82.758	2.18372	2.175	18.69069	4.13817	4.13917	0.00116	0	0.02624	QHD4
97	QF	83.008	2.18588	2.18447	17.90308	4.33355	4.05722	3.10412	-0.79267	-0.67946	
98	OO	84.558	2.20464	2.22772	9.70754	7.69357	3.00406	2.18332	-1.37508	-0.67946	
99	BM2	85.308	2.21944	2.24137	6.69338	9.96755	2.5176	1.82263	-1.65689	-0.61672	DHD5
100	BM2	86.058	2.2418	2.252	4.27471	12.66424	2.08047	1.3919	-1.9387	-0.54803	
101	O	86.508	2.26133	2.25729	3.16114	14.48516	1.83385	1.08268	-2.10779	-0.54803	
102	QD	86.758	2.27484	2.25998	2.79301	14.88062	1.73773	0.41214	0.55007	-0.22388	QVD5
103	QD	87.008	2.28936	2.26272	2.73637	13.95165	1.72106	-0.18215	3.10921	0.09003	
104	OO	88.558	2.36486	2.28948	4.20817	6.15	1.8606	-0.76739	1.92411	0.09003	
105	BM2	89.308	2.38968	2.31463	5.52315	3.69392	1.95585	-0.98028	1.35067	0.16374	DHD6
106	BM2	90.058	2.40871	2.35804	7.13015	2.09799	2.10582	-1.15549	0.77723	0.23588	
107	O	90.508	2.41806	2.39814	8.23641	1.55331	2.21197	-1.30287	0.43317	0.23588	
108	QF	90.758	2.42278	2.425	8.54127	1.44654	2.22324	0.10091	0	-0.14599	QHD6
109	QF	91.008	2.42751	2.45186	8.13836	1.55331	2.13949	1.48762	-0.43317	-0.52162	
110	OO	92.558	2.46885	2.54871	4.47524	4.73305	1.33098	0.87568	-1.61827	-0.52162	
111	BM2	93.308	2.49983	2.56868	3.34851	7.59054	0.97078	0.6218	-2.19171	-0.43817	DHD7
112	BM2	94.058	2.5405	2.58158	2.62181	11.30819	0.67479	0.34402	-2.76515	-0.35049	
113	O	94.508	2.56921	2.58728	2.39857	13.95165	0.51707	0.15207	-3.10921	-0.35049	
114	QD	94.758	2.58575	2.59002	2.45819	14.88062	0.4406	-0.39419	-0.55007	-0.26358	QVD7
115	QD	95.008	2.60105	2.59271	2.80484	14.48516	0.38428	-1.01338	2.10779	-0.18871	
116	OO	96.558	2.65523	2.61456	7.6825	8.85375	0.09177	-2.1335	1.52538	-0.18871	
117	BM2	97.308	2.66809	2.62999	11.19361	6.77704	-0.01319	-2.53293	1.24357	-0.09097	DHD8
118	BM2	98.058	2.67723	2.65031	15.23255	5.12304	-0.04446	-2.83502	0.96176	0.00766	
119	O	98.508	2.68156	2.66553	17.90421	4.33355	-0.04101	-3.102	0.79267	0.00766	
120	QF	98.758	2.68372	2.675	18.69069	4.13817	-0.03823	0.00116	0	0.01448	QHD8
121	QF	99.008	2.68587	2.68451	18.15498	4.27497	-0.03408	2.12088	-0.5525	0.0187	
122	L	101.6545	2.71897	2.7533	9.05028	9.33782	0.01541	1.3194	-1.36054	0.0187	
123	L	104.301	2.78969	2.78541	4.1878	18.67764	0.0649	0.51793	-2.16858	0.0187	
124	QD	104.551	2.79939	2.7875	4.06521	19.22507	0.07054	-0.02285	0	0.02651	QVD9
125	QD	104.801	2.80906	2.78959	4.21109	18.67764	0.07822	-0.56629	2.16858	0.0351	
126	L	107.4475	2.87813	2.8217	9.40504	9.33782	0.17111	-1.39629	1.36054	0.0351	
127	L	110.094	2.90986	2.89049	18.99216	4.27497	0.26399	-2.22628	0.5525	0.0351	
128	QF	110.344	2.91191	2.9	19.55611	4.13817	0.26889	-0.0076	0	0.00402	QHD10
129	QF	110.594	2.91397	2.90951	18.99961	4.27497	0.26599	2.21196	-0.5525	-0.02718	
130	L	113.2405	2.94559	2.9783	9.46402	9.33782	0.19407	1.39114	-1.36054	-0.02718	
131	L	115.887	3.0139	3.01041	4.27299	18.67764	0.12215	0.57033	-2.16858	-0.02718	
132	QD	116.137	3.02343	3.0125	4.12664	19.22507	0.11709	0.02071	0	-0.01337	QVD11
133	QD	116.387	3.03298	3.01459	4.25188	18.67764	0.11543	-0.5265	2.16858	0.00005	

134	L	119.0335	3.10275	3.0467	9.14252	9.33782	0.11555	-1.32147	1.36054	0.00005	
135	L	121.68	3.1356	3.11549	18.24092	4.27497	0.11568	-2.11643	0.5525	0.00005	
136	QF	121.93	3.13774	3.125	18.77182	4.13817	0.11401	0.01344	0	-0.01335	QHD12
137	QF	122.18	3.13989	3.13447	17.9748	4.33355	0.10826	3.12894	-0.79267	-0.03249	
138	OO	123.73	3.1586	3.17772	9.71731	7.69357	0.0579	2.19848	-1.37508	-0.03249	
139	BM2	124.48	3.17341	3.19137	6.68397	9.96755	0.07009	1.83297	-1.65689	0.06494	DHA1
140	BM2	125.23	3.19583	3.202	4.25366	12.66424	0.15516	1.39703	-1.9387	0.16175	
141	O	125.68	3.21549	3.20729	3.13685	14.48516	0.22795	1.08477	-2.10779	0.16175	
142	QD	125.93	3.22911	3.20998	2.76695	14.88062	0.27391	0.41724	0.55007	0.2073	QVA1
143	QD	126.18	3.24378	3.21272	2.70683	13.95165	0.33239	-0.1731	3.10921	0.26232	
144	OO	127.73	3.32022	3.23948	4.1576	6.15	0.73899	-0.76289	1.92411	0.26232	
145	BM2	128.48	3.34532	3.26463	5.468	3.69392	0.96865	-0.97869	1.35067	0.3496	DHA2
146	BM2	129.23	3.36453	3.30804	7.07484	2.09799	1.26254	-1.15688	0.77723	0.4335	
147	O	129.68	3.37395	3.34814	8.18297	1.55331	1.45762	-1.30562	0.43317	0.4335	
148	QF	129.93	3.37869	3.375	8.49161	1.44654	1.53407	0.08875	0	0.17592	QHA2
149	QF	130.18	3.38345	3.40186	8.09673	1.55331	1.54495	1.46811	-0.43317	-0.08918	
150	OO	131.73	3.42487	3.49871	4.48185	4.73305	1.40672	0.86407	-1.61827	-0.08918	
151	BM2	132.48	3.45573	3.51868	3.36952	7.59054	1.36996	0.61428	-2.19171	-0.00878	DHA3
152	BM2	133.23	3.49603	3.53158	2.65082	11.30819	1.39357	0.3409	-2.76515	0.0717	
153	O	133.68	3.52441	3.53728	2.42928	13.95165	1.42584	0.15141	-3.10921	0.0717	
154	QD	133.93	3.54074	3.54002	2.49032	14.88062	1.4765	-0.39927	-0.55007	0.33511	QVA3
155	QD	134.18	3.55583	3.54271	2.84079	14.48516	1.59467	-1.02382	2.10779	0.61384	
156	OO	135.73	3.60943	3.56456	7.74681	8.85375	2.54612	-2.14136	1.52538	0.61384	
157	BM2	136.48	3.62219	3.57999	11.26808	6.77704	3.03029	-2.53858	1.24357	0.67624	DHA4
158	BM2	137.23	3.63127	3.60031	15.3137	5.12304	3.55885	-2.83824	0.96176	0.73212	
159	O	137.68	3.63559	3.61553	17.98786	4.33355	3.8883	-3.10434	0.79267	0.73212	
160	QF	137.93	3.63774	3.625	18.77183	4.13817	3.98693	0.01344	0	0.05407	QHA4
161	QF	138.18	3.63989	3.63447	17.9748	4.33355	3.91514	3.12894	-0.79267	-0.62629	
162	OO	139.73	3.6586	3.67772	9.71731	7.69357	2.94439	2.19848	-1.37508	-0.62629	
163	BM2	140.48	3.67341	3.69137	6.68397	9.96755	2.49804	1.83297	-1.65689	-0.56304	DHA5
164	BM2	141.23	3.69583	3.702	4.25366	12.66424	2.10119	1.39703	-1.9387	-0.49436	
165	O	141.68	3.71549	3.70729	3.13685	14.48516	1.87873	1.08477	-2.10779	-0.49436	
166	QD	141.93	3.72911	3.70998	2.76695	14.88062	1.79716	0.41724	0.55007	-0.16074	QVA5
167	QD	142.18	3.74378	3.71272	2.70682	13.95165	1.79775	-0.1731	3.10921	0.16552	
168	OO	143.73	3.82022	3.73948	4.1576	6.15	2.05431	-0.76288	1.92411	0.16552	
169	BM2	144.48	3.84532	3.76463	5.46799	3.69392	2.20515	-0.97869	1.35067	0.23639	DHA6
170	BM2	145.23	3.86453	3.80804	7.07484	2.09799	2.40833	-1.15688	0.77723	0.30497	
171	O	145.68	3.87395	3.84814	8.18296	1.55331	2.54556	-1.30562	0.43317	0.30497	
172	QF	145.93	3.87869	3.875	8.49161	1.44654	2.56686	0.08875	0	-0.1352	QHA6
173	QF	146.18	3.88345	3.90186	8.09673	1.55331	2.47845	1.46811	-0.43317	-0.5696	
174	OO	147.73	3.92487	3.99871	4.48186	4.73305	1.59557	0.86407	-1.61827	-0.5696	
175	BM2	148.48	3.95573	4.01868	3.36952	7.59054	1.19816	0.61428	-2.19171	-0.48931	DHA7
176	BM2	149.23	3.99603	4.03158	2.65082	11.30819	0.86279	0.3409	-2.76515	-0.40431	
177	O	149.68	4.02441	4.03728	2.42928	13.95165	0.68085	0.15141	-3.10921	-0.40431	
178	QD	149.93	4.04074	4.04002	2.49033	14.88062	0.59457	-0.39927	-0.55007	-0.28855	QVA7
179	QD	150.18	4.05583	4.04271	2.84079	14.48516	0.53547	-1.02382	2.10779	-0.18599	
180	OO	151.73	4.10943	4.06456	7.74681	8.85375	0.24718	-2.14136	1.52538	-0.18599	

181	BM2	152.48	4.12219	4.07999	11.26809	6.77704	0.14351	-2.53858	1.24357	-0.09025	DHA8
182	BM2	153.23	4.13127	4.10031	15.3137	5.12304	0.11202	-2.83824	0.96176	0.00636	
183	O	153.68	4.13559	4.11553	17.98786	4.33355	0.11488	-3.10434	0.79267	0.00636	
184	QF	153.93	4.13774	4.125	18.77183	4.13817	0.11401	0.01344	0	-0.01335	QHA8
185	QF	154.18	4.13988	4.13451	18.22774	4.27497	0.10903	2.14176	-0.5525	-0.02636	
186	L	156.8265	4.17293	4.2033	9.03826	9.33782	0.03928	1.33056	-1.36054	-0.02636	
187	L	159.473	4.24412	4.23541	4.14245	18.67764	-0.03048	0.51936	-2.16858	-0.02636	
188	QD	159.723	4.25392	4.2375	4.01804	19.22507	-0.03754	-0.01692	0	-0.03028	QVA9
189	QD	159.973	4.26371	4.23959	4.1597	18.67764	-0.04569	-0.55517	2.16858	-0.03508	
190	DLI1	161.1817	4.30273	4.25155	5.96124	13.88138	-0.08809	-0.93531	1.79954	-0.03508	
191	BMI1	161.4317	4.30915	4.25451	6.44733	13.00069	-0.0986	-1.00893	1.7232	-0.04894	
192	BMI1	161.6817	4.31509	4.25768	6.97004	12.15818	-0.11256	-1.08177	1.64687	-0.06279	
193	DLI2	163.945	4.35262	4.29942	13.46178	6.26747	-0.25468	-1.78649	0.95583	-0.06279	
194	BMI2	164.2555	4.35615	4.30769	14.59735	5.70334	-0.27158	-1.87043	0.86103	-0.0461	
195	BMI2	164.566	4.3594	4.31677	15.78443	5.19808	-0.2833	-1.95234	0.76623	-0.02939	
196	BMI3	164.646	4.3602	4.31925	16.09847	5.07743	-0.28548	-1.97311	0.7418	-0.02508	
197	BMI3	164.726	4.36098	4.32178	16.41582	4.9607	-0.28731	-1.99373	0.71737	-0.02077	
198	DLI5	165.266	4.3659	4.34049	18.65743	4.27497	-0.29853	-2.15739	0.5525	-0.02077	
199	QF	165.516	4.36799	4.35	19.19658	4.13817	-0.29937	0.02172	0	0.0141	QHA10
200	QF	165.766	4.37008	4.35951	18.63613	4.27497	-0.29152	2.19832	-0.5525	0.04856	
201	DLI3	170.059	4.43958	4.45078	5.52942	14.6458	-0.08307	0.85473	-1.86326	0.04856	
202	BMI4	170.309	4.44706	4.45341	5.12138	15.59651	-0.07177	0.77742	-1.93959	0.0418	
203	BMI4	170.559	4.45512	4.45589	4.75202	16.58539	-0.06217	0.69997	-2.01592	0.03504	
204	DLI4	171.059	4.47312	4.46041	4.13044	18.67764	-0.04465	0.5432	-2.16858	0.03504	
205	QD	171.309	4.48297	4.4625	3.99396	19.22507	-0.03649	0.00794	0	0.03036	QVA11
206	QD	171.559	4.49283	4.46459	4.12234	18.67764	-0.02939	-0.52639	2.16858	0.02656	
207	L	174.2055	4.56404	4.4967	9.07832	9.33782	0.04089	-1.34627	1.36054	0.02656	
208	L	176.852	4.59688	4.56549	18.3739	4.27497	0.11117	-2.16614	0.5525	0.02656	
209	QF	177.102	4.59901	4.575	18.92594	4.13817	0.11616	-0.02054	0	0.0133	QHA12
210	QF	177.352	4.60114	4.58447	18.13888	4.33355	0.11698	3.12363	-0.79267	-0.00678	
211	OO	178.902	4.61961	4.62772	9.8804	7.69357	0.10648	2.20442	-1.37508	-0.00678	
212	BM2	179.652	4.63413	4.64137	6.83256	9.96755	0.13768	1.84629	-1.65689	0.08991	DHB1
213	BM2	180.402	4.65599	4.652	4.37704	12.66424	0.24113	1.41722	-1.9387	0.18573	
214	O	180.852	4.67505	4.65729	3.24073	14.48516	0.3247	1.10791	-2.10779	0.18573	
215	QD	181.102	4.68823	4.65998	2.86328	14.88062	0.37891	0.42472	0.55007	0.24958	QVB1
216	QD	181.352	4.7024	4.66272	2.80299	13.95165	0.45044	-0.17991	3.10921	0.32486	
217	OO	182.902	4.77657	4.68948	4.24557	6.15	0.95397	-0.75079	1.92411	0.32486	
218	BM2	183.652	4.80126	4.71463	5.53024	3.69392	1.22941	-0.95661	1.35067	0.40907	DHB2
219	BM2	184.402	4.82033	4.75804	7.09699	2.09799	1.56659	-1.12567	0.77723	0.48934	
220	O	184.852	4.82974	4.79814	8.17479	1.55331	1.78679	-1.26943	0.43317	0.48934	
221	QF	185.102	4.83449	4.825	8.46551	1.44654	1.87007	0.12321	0	0.17449	QHB2
222	QF	185.352	4.83927	4.85186	8.05507	1.55331	1.87341	1.495	-0.43317	-0.14782	
223	OO	186.902	4.88126	4.94871	4.38544	4.73305	1.64429	0.8725	-1.61827	-0.14782	
224	BM2	187.652	4.91295	4.96868	3.26813	7.59054	1.56248	0.61245	-2.19171	-0.07019	
225	BM2	188.402	4.95463	4.98158	2.55986	11.30819	1.53918	0.32887	-2.76515	0.00812	DHB3
226	O	188.852	4.98399	4.98728	2.35154	13.95165	1.54284	0.13406	-3.10921	0.00812	
227	QD	189.102	5.00083	4.99002	2.41868	14.88062	1.58015	-0.40667	-0.55007	0.29156	QVB3

228	QD	189.352	5.01634	4.99271	2.77068	14.48516	1.68972	-1.02263	2.10779	0.58832	
229	OO	190.902	5.07075	5.01456	7.71475	8.85375	2.60163	-2.16709	1.52538	0.58832	
230	BM2	191.652	5.08354	5.02999	11.28442	6.77704	3.06642	-2.57717	1.24357	0.65013	DHB4
231	BM2	192.402	5.09259	5.05031	15.39667	5.12304	3.57525	-2.88821	0.96176	0.70567	
232	O	192.852	5.09687	5.06553	18.11892	4.33355	3.89281	-3.16124	0.79267	0.70567	
233	QF	193.102	5.09901	5.075	18.92594	4.13817	3.98477	-0.02054	0	0.02742	QHB4
234	QF	193.352	5.10114	5.08447	18.13888	4.33355	3.90642	3.12363	-0.79267	-0.652	
235	OO	194.902	5.11961	5.12772	9.8804	7.69357	2.89582	2.20442	-1.37508	-0.652	
236	BM2	195.652	5.13413	5.14137	6.83256	9.96755	2.43044	1.8463	-1.65689	-0.588	DHB5
237	BM2	196.402	5.15599	5.152	4.37703	12.66424	2.01523	1.41722	-1.9387	-0.51833	
238	O	196.852	5.17506	5.15729	3.24072	14.48516	1.78198	1.10791	-2.10779	-0.51833	
239	QD	197.102	5.18823	5.15998	2.86328	14.88062	1.69215	0.42472	0.55007	-0.20303	QVB5
240	QD	197.352	5.2024	5.16272	2.80299	13.95165	1.6797	-0.17991	3.10921	0.10299	
241	OO	198.902	5.27657	5.18948	4.24556	6.15	1.83934	-0.75079	1.92411	0.10299	
242	BM2	199.652	5.30126	5.21463	5.53024	3.69392	1.94439	-0.95661	1.35067	0.17692	DHB6
243	BM2	200.402	5.32033	5.25804	7.09699	2.09799	2.10428	-1.12567	0.77723	0.24913	
244	O	200.852	5.32974	5.29814	8.17478	1.55331	2.21639	-1.26943	0.43317	0.24913	
245	QF	201.102	5.33449	5.325	8.46551	1.44654	2.23086	0.12321	0	-0.13377	QHB6
246	QF	201.352	5.33927	5.35186	8.05507	1.55331	2.14998	1.495	-0.43317	-0.51096	
247	OO	202.902	5.38126	5.44871	4.38544	4.73305	1.358	0.8725	-1.61827	-0.51096	
248	BM2	203.652	5.41295	5.46868	3.26813	7.59054	1.00565	0.61245	-2.19171	-0.4279	DHB7
249	BM2	204.402	5.45463	5.48158	2.55987	11.30819	0.71718	0.32887	-2.76515	-0.34073	
250	O	204.852	5.48399	5.48728	2.35155	13.95165	0.56385	0.13407	-3.10921	-0.34073	
251	QD	205.102	5.50083	5.49002	2.41868	14.88062	0.49091	-0.40667	-0.55007	-0.245	QVB7
252	QD	205.352	5.51634	5.49271	2.77068	14.48516	0.44042	-1.02263	2.10779	-0.16048	
253	OO	206.902	5.57075	5.51456	7.71475	8.85375	0.19168	-2.16709	1.52538	-0.16048	
254	BM2	207.652	5.58354	5.52999	11.28442	6.77704	0.10738	-2.57717	1.24357	-0.06414	DHB8
255	BM2	208.402	5.59259	5.55031	15.39668	5.12304	0.09562	-2.88821	0.96176	0.0328	
256	O	208.852	5.59687	5.56553	18.11893	4.33355	0.11038	-3.16124	0.79267	0.0328	
257	QF	209.102	5.59901	5.575	18.92594	4.13817	0.11616	-0.02054	0	0.0133	QHB8
258	QF	209.352	5.60113	5.58451	18.39405	4.27497	0.11779	2.12743	-0.5525	-0.00035	
259	L	211.9985	5.63367	5.6533	9.2377	9.33782	0.11687	1.33237	-1.36054	-0.00035	
260	L	214.645	5.70273	5.68541	4.28963	18.67764	0.11596	0.5373	-2.16858	-0.00035	
261	QD	214.895	5.7122	5.6875	4.15998	19.22507	0.11755	-0.01373	0	0.01313	QVB9
262	QD	215.145	5.72165	5.68959	4.30362	18.67764	0.12255	-0.56637	2.16858	0.02698	
263	L	217.7915	5.78976	5.7217	9.4509	9.33782	0.19396	-1.37857	1.36054	0.02698	
264	L	220.438	5.82148	5.79049	18.89716	4.27497	0.26537	-2.19077	0.5525	0.02698	
265	QF	220.688	5.82355	5.8	19.44602	4.13817	0.26823	0.01667	0	-0.00414	QHB10

**NUX = 5.82355**                      **dNUX/(dP/P) = -6.49203**  
**NUY = 5.8**                              **dNUY/(dP/P) = -7.29861**

**Circumference = 220.688 m**                      **Transition gamma = 4.93152**  
**Radius = 35.1236 m**                              **(dS/S)/(dP/P) = 0.041119**

**MAXIMA BETX(64)= 19.56851**                      **BETY(132)= 19.22507**                      **Xp(32)= 4.14151**  
**MINIMA BETX(226)= 2.35154**                      **BETY(221)= 1.44654**                      **Xp(199)= -0.29937**

### 5.3 HIGH ENERGY BEAM TRANSPORT LINE (WBS 1.5.1)

#### 5.3.1 Scope

The SNS High Energy Beam Transport line (HEBT) connects the 1-GeV linac to the accumulator ring. The HEBT matches the beam into the accumulator and determines the beam quality at injection.

#### 5.3.2 Design Requirements

Table 5.3-1 gives the required Twiss parameters at the entrance (middle of the last linac quadrupole) and exit (injection stripping foil) of the HEBT. In addition, a major requirement of all parts of this accelerator is minimization of uncontrolled beam losses to allow hands-on maintenance. This is achieved by maintaining adequate tolerances on elements, appropriately located collimators, and sufficient beam diagnostics.

**Table 5.3-1 Twiss parameters at the entrance and exit of the HEBT for 1 MW**

Twiss parameters	Entrance (end of Linac)	Exit (stripping foil)	Units
$\alpha_X$	0.00	-1.955	
$\beta_X$	12.811	15.690	mm/mrad
$\epsilon_X$	0.70	0.70	$\pi$ mm mrad (5 rms, un-norm.)
$\alpha_Y$	0.00	0.7753	
$\beta_Y$	9.181	5.162	mm/mrad
$\epsilon_Y$	0.70	0.70	$\pi$ mm mrad (5 rms, un-norm.)
$\alpha_Z$	0.0005	0.14	
$\beta_Z$	0.005	0.05	deg/keV
$\epsilon_Z$	1500	1500	$\pi$ keV deg (5 rms)

#### 5.3.3 Description of the HEBT Line

The HEBT has following functions: (a) matching of the beam from the linac into the transport line, (b) momentum selection, (c) momentum compaction, (d) preparation of the beam for injection, (e) characterization of the beam out of the linac and before injection, and (f) halo cleanup. We have decoupled the first four of these functions, and can consider the HEBT to have three sections: Linac-Achromat Matching Section (LAMS), Achromat, and Achromat-Ring Matching Section (ARMS). In addition to the 90° bend to the ring, there is a 0° beamline used for linac beam characterization, leading to the linac beam dump, as shown in Fig 5.3-1.

The first four cells (11.4 m/cell) after the linac (LAMS) are used to characterize the linac beam, match the beam into the achromat, collimate the beam halo, and maintain space for the kicker required in a future upgrade to 4 MW operation. Following this section, the six cell long achromat (14.0 m/cell) bends the beam 90° and provides momentum selection by cleaning up the beam energy halo at the point of maximum dispersion ( $\eta=8.9$  m). The bunch rotator rf cavity is located in the first cell following the achromat (in the ARMS), where the dispersion and its derivative are zero. The remaining six cells (8 m/cell) are used for matching the beam into the

accumulator ring, diagnostics, and for beam halo scrapers. A small dipole magnet for steering the beam in the quadrupole focusing-plane follows every quadrupole in the HEBT.

To reduce the probability of uncontrolled beam losses, HEBT is equipped with nine sets of beam halo scrapers. The collimators are the minimum apertures in the line, chosen to be 10 times the rms beam size. The maximum magnetic field in dipoles and quadrupoles is kept less than 3 kG, to keep H stripping losses below 0.1 nA/m. The alignment tolerances required to keep the beam losses low (Raparia, 97) are given in Table 5.3-2.

**Table 5.3-2 Alignment tolerances for the HEBT magnets**

Type of Error	Tolerance
Translation (x and y)	±0.1 mm
Pitch and yaw	±1 mrad
Rotation	±0.5 deg

### 5.3.3.1 Linac to Achromat Matching Section

The linac has a FDOO lattice with a phase advance of about 19°/cell, and the achromat has a FODO lattice with 60°/cell phase advance. The first two cells (four quadrupoles) of the HEBT provide a smooth transition between the two. To remove any linac beam halo, there are two movable and two fixed collimators located in the 2nd to 5th half-cells in this section (details of the configuration are discussed in the section on halo scraping). The 6th and 7th half-cells are reserved for kickers required in a future upgrade. The space between quadrupoles in the first cell of the HEBT is occupied by beam diagnostics, as discussed in a later section.

### 5.3.3.2 Momentum Selection Achromat

A 90° achromatic bend starts at the fifth cell of the HEBT line, and finishes in six cells, containing twelve 7.5° dipoles. The total phase advance in the achromat is 360°. A beam energy-halo scraper is located at the middle cell of the achromat, where the dispersion is maximum (8.9 m). Figure 5.3-2 shows amplitude functions ( $\beta_x$ ,  $\beta_y$ ) and dispersion function ( $\eta$ ) along the HEBT. The first dipole of the achromat is a switching magnet to provide beam to the 0° linac dump.

### 5.3.3.3 Bunch Rotation

Bunch Rotation is accomplished with a 2.6 meter long, 16 cell, 805 MHz rf cavity, operating at a gradient of 1.375 MV/m. This cavity is similar to the last cavity of linac. The cavity is located in the first half-cell after the achromat (130 m from the linac), where the dispersion and its derivative both have zero values. This location of the cavity can provide the desired momentum spread for a 1 MW (28 mA) beam, as well as a 2 MW (56 mA) beam. For beam stability in the ring, it is desirable to have  $\Delta P/P \approx \pm 0.5\%$ . Table 5.3-3 shows different values

of  $\Delta P/P$  that can be achieved by changing the phase and amplitude of the cavity.

**Table 5.3-3 Energy and Momentum Spread at the Injection Foil**

Cavity Parameters		Beam at Injection	
$E_0T$ (MV/m)	$\phi_S$ (degree)	$\Delta E$ (MeV)	$\Delta P/P$ ( $10^{-3}$ )
1.375	-90	$\pm 0.084$	$\pm 0.005$
0.000		$\pm 1.597$	$\pm 1.08$
1.375	+90	$\pm 2.928$	$\pm 1.97$
6.000	+90	$\pm 7.546$	$\pm 5.08$

### 5.3.3.4 Ring Matching Section

After the achromat, two cells are provided for the diagnostics and beam collimators. At the end of the achromat this line is parallel to the ring straight section, but offset by 10 m, allowing one to have the required dogleg for injection into the ring. These bends are necessary to allow the dispersion and its derivative to be zero at the injection stripper foil. As shown in Fig. 5.3-2, the dispersion has a minimum and maximum of similar amplitude but opposite sign through the dogleg. This section has enough adjustments (quadrupoles) to match the six variables, which are four amplitude functions and two dispersion functions. There is no vertical bend and no vertical dispersion. The locations of the dipoles are determined by the injection scheme discussed in Section 5.4. Fig. 5.3-3 shows the calculated phase space particle distribution at the foil.

### 5.3.3.5 Magnets and Support

The magnet and support system for the HEBT is described in detail in Section 5.5. Table 5.3-4 lists the magnet requirements for the HEBT.

**Table 5.3-4 Magnet requirements for the HEBT**

	Type	Location	No.	Field	Aperture	Length
<b>Dipoles</b>	8D250	Achromat ARMS	13	0.3 T	8 cm gap	2.5m
	12C20	LAMS, ARMS, LDUMP	25	0.03 T	12 cm x 12 cm	0.2 m
	20C30	Achromat	12	0.02 T	20 cm x 20 cm	0.3m
<b>Quadrupoles</b>	12Q50	LAMS, ARMS	25	4 T/m	12 cm $\phi$	0.5 m
	20Q50	Achromat	12	3.4 T/m	20 cm $\phi$	0.5m
	12Q80	LDUMP	2	4 T/m	12 cm $\phi$	0.8m

### 5.3.3.6 Power Supplies

The power supply system for the HEBT is described in detail in Sections 5.6.1 and 5.6.2. Table 5.3-5 shows the power supply requirements for the HEBT.

**Table 5.3-5 Power supply requirements for the HEBT**

	Type	Location	Number Magnets	Number PS
<b>Dipoles</b>	8D250	Achromat/ ARMS	12	1
	8D250	Achromat	1	1
	12C20	LAMS, ARMS LDUMP	25	25
	20C30	Achromat	12	12
<b>Quadrupoles</b>	12Q50	LAMS, ARMS	21	14
	20Q50	Achromat	12	2
	12Q50	LDUMP	4	2
	12Q80	LDUMP	2	2

### 5.3.3.7 Vacuum

The HEBT will have a vacuum of less than  $5 \times 10^{-8}$  Torr. The estimated losses due to H stripping, assuming 50% hydrogen ( $\sigma \approx 10^{-19}$  cm<sup>2</sup>/atom) and 50 % oxygen/nitrogen ( $\sigma \approx 10^{-18}$  cm<sup>2</sup>/atom), is 0.18 nA/m. Table 5.3-6 shows the required vacuum components.

**Table 5.3-6 Vacuum components required for the HEBT.**

Equipment	Number
Sector Valves	6
Ion Pumps	20
Roughing Pumps	5
Vacuum Gauges	5

### 5.3.3.8 Instrumentation and Diagnostics

In addition to the 0° linac diagnostic line, there must be diagnostic devices spread over the entire HEBT to determine the beam loss and the beam quality before injection. There are one beam loss monitor per quadrupole and one per dipole, with another 27 left for additional critical locations. Beam position monitors (x and y) are located near each quadrupole. Harps, which will only be used at low repetition rate, due to thermal constraints, will allow beam profile measurements to be made at the entrance to the achromat, in the middle of the achromat, and at the entrance to the ring. Profiles from four crawling-wire profile monitors located between four consecutive quadrupole magnets determine the beam emittance. There will be two of these four-

profile units, one at the exit of the linac, and one before the entrance to the ring. Bunch shape monitors (detailed bunch shape), wall current monitors (continuous monitoring of coarse bunch shape), and time-of-flight energy monitors (continuous monitoring of beam energy) will be located at the output of the linac and at the output of the debuncher cavity (with an additional wall current monitor at the entrance to the debuncher). Finally, beam current monitors (current toroids) will provide continuous monitoring of beam current at four locations. Fig. 5.3-4 shows the diagnostics, and Table 5.3-7 lists the devices. Some of the diagnostic devices, those listed in parentheses, are the responsibility of LANL and will be supplied by LANL. These devices will be located in the zero degree beam line and used by LANL to characterize the beam from the Linac.

**Table 5.3-7 Diagnostic Devices in the HEBT\***

Device	Number
Beam Loss Monitor (BLM)	77
Beam Current Monitor (BCM)	4 (1)
Beam Position Monitor (BPM)	33
Wall Current Monitor (WCM)	3 (1)
Harp (PrM)	3 (1)
Bunch Shape Monitor (BSM)	2 (1)
Time of Flight Energy Monitor (TF)	2 (1)
Crawling Wire Scanner(PrM)	8 (4)

\*Los Alamos will provide the number of devices in parentheses

### 5.3.3.9 Scraper & Collimator (Halo scraping)

There are nine collimators in the HEBT, one for momentum collimation and eight for transverse collimation. Four transverse collimators (two each in x and y) are located just after the linac, and the other four are in a zero-dispersion region just after the bunch rotator cavity. The four horizontal collimators are movable foils, which strip the  $H^-$  to  $H^+$ . After horizontal defocusing, the  $H^+$  beam is dumped in the same dump that is used for fixed vertical collimation. This reduces costs, and has the added advantage of being adjustable in the bending plane.

The momentum collimator is located at the maximum dispersion point in the achromat. This scraper is a pair of movable stripping foils in the middle of the bend section, followed by an off-line beam dump for the oppositely bent protons. All collimators are designed to handle  $10^{-3}$  of the beam intensity, but we expect any one collimator to intercept less than  $10^{-4}$ . Section 5.10 gives details of the collimators, and Fig. 5.3-5 shows the collimator configuration schematically.

### 5.3.3.10 Bunch Rotator RF System

The bunch rotator rf cavity is similar to the last cavity of the side-coupled linac and will be built by LANL. Table 5.3-8 gives the requirements for this cavity.

**Table 5.3-8 Bunch rotator specifications**

Type	No.	Field	Aperture	Length
16 cell SCC	1	3.5MV/m	4.8 cm $\phi$	2.6 m

### 5.3.3.11 Linac Dump

In addition to the 90<sup>0</sup> bend to the accumulator ring, there is an additional 35-m long beam line after the LAMS section for linac beam characterization and beam dumping. Fig. 5.3-6 shows the TRANSPORT output for this line including the LAMS section of the HEBT.

### 5.3.4 References

Raparia, D, Alessi, J., Lee, Y.Y., Ruggiero, A.G., Soukas, A., Tuozzolo, J., Weng, W.T., Witkover, R.L., NSNS/BNL Tech. Note 2 (1997).

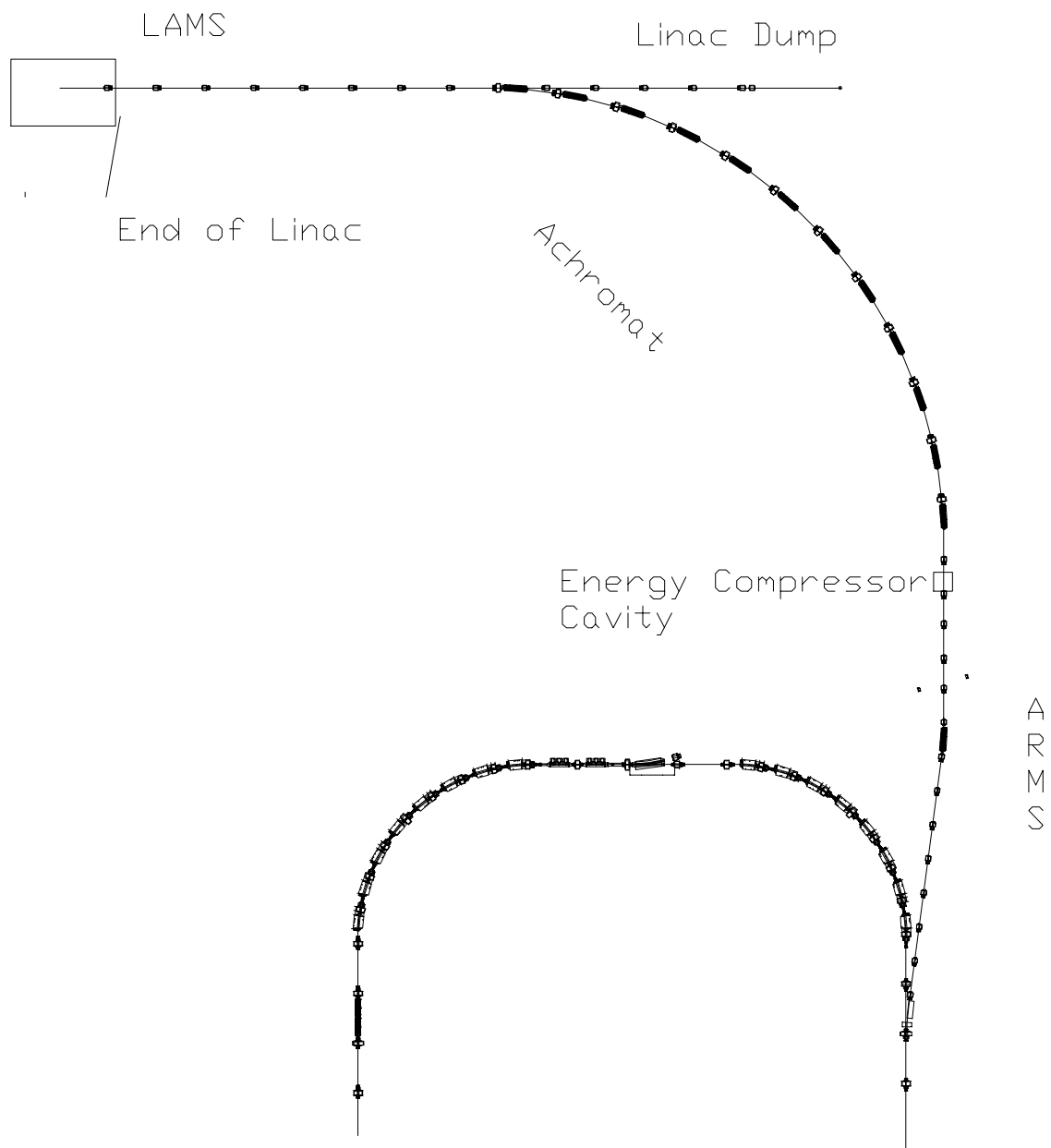


Figure 5.3-1. Layout of the HEBT line.

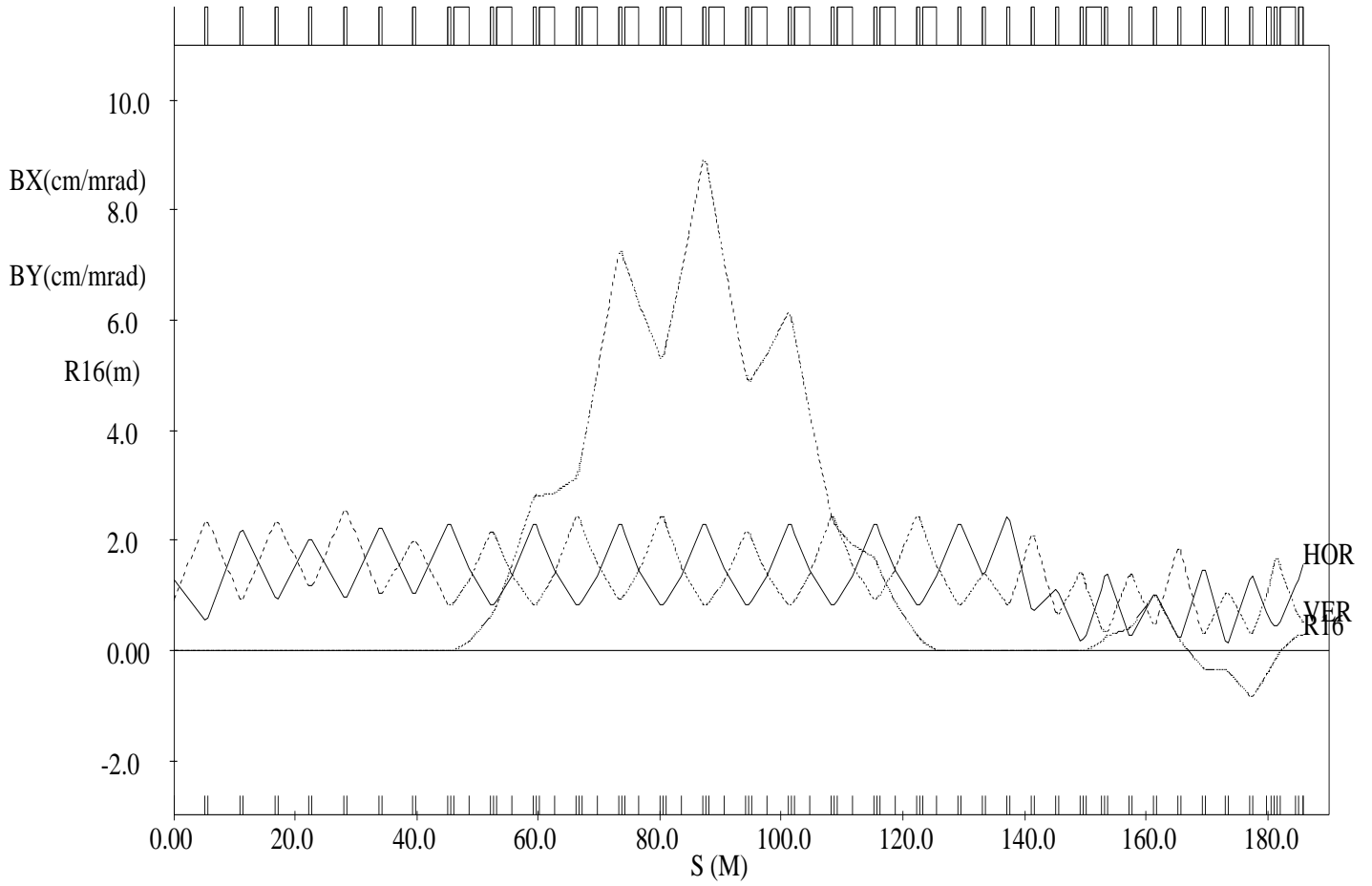
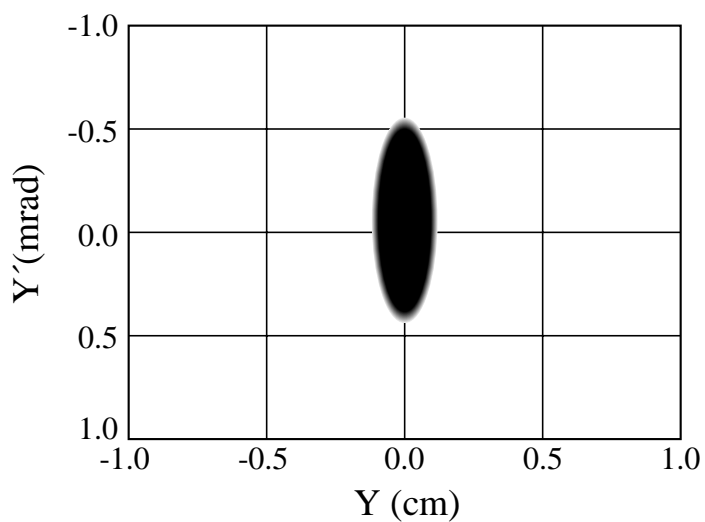
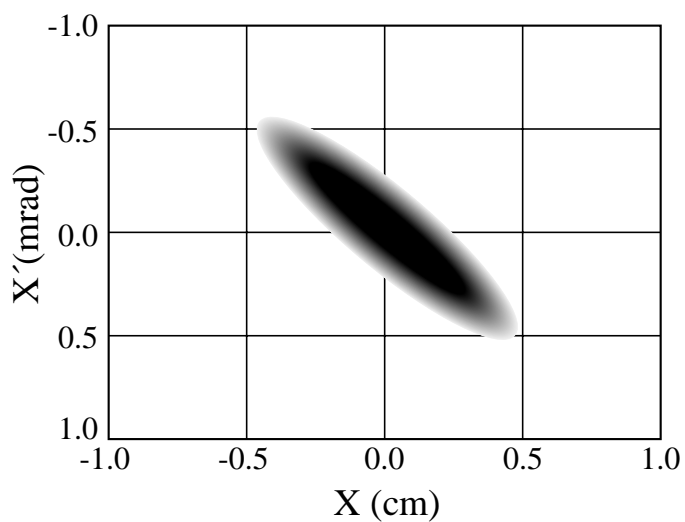
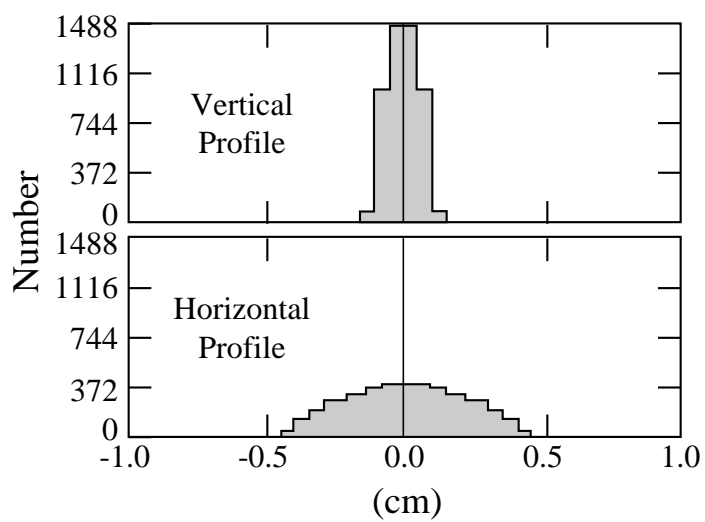
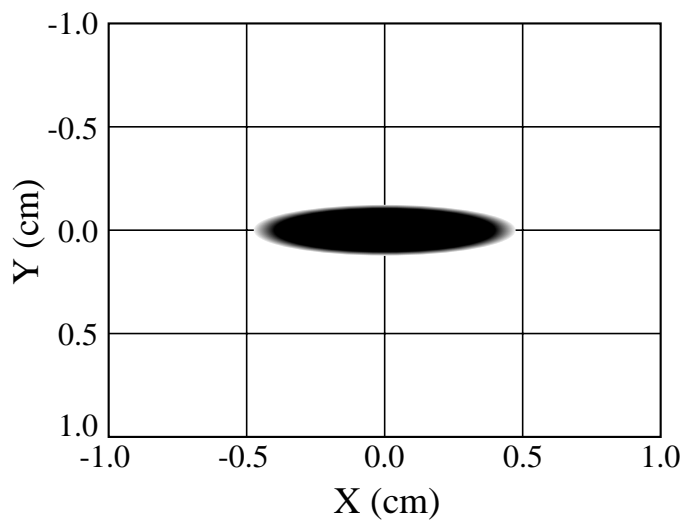


Figure 5.3-2. TRANSPORT output for the beta functions and dispersion function (R16) along the HEFT.



**Fig. 5.3-3. The Phase space and beam size at the injection foil.**

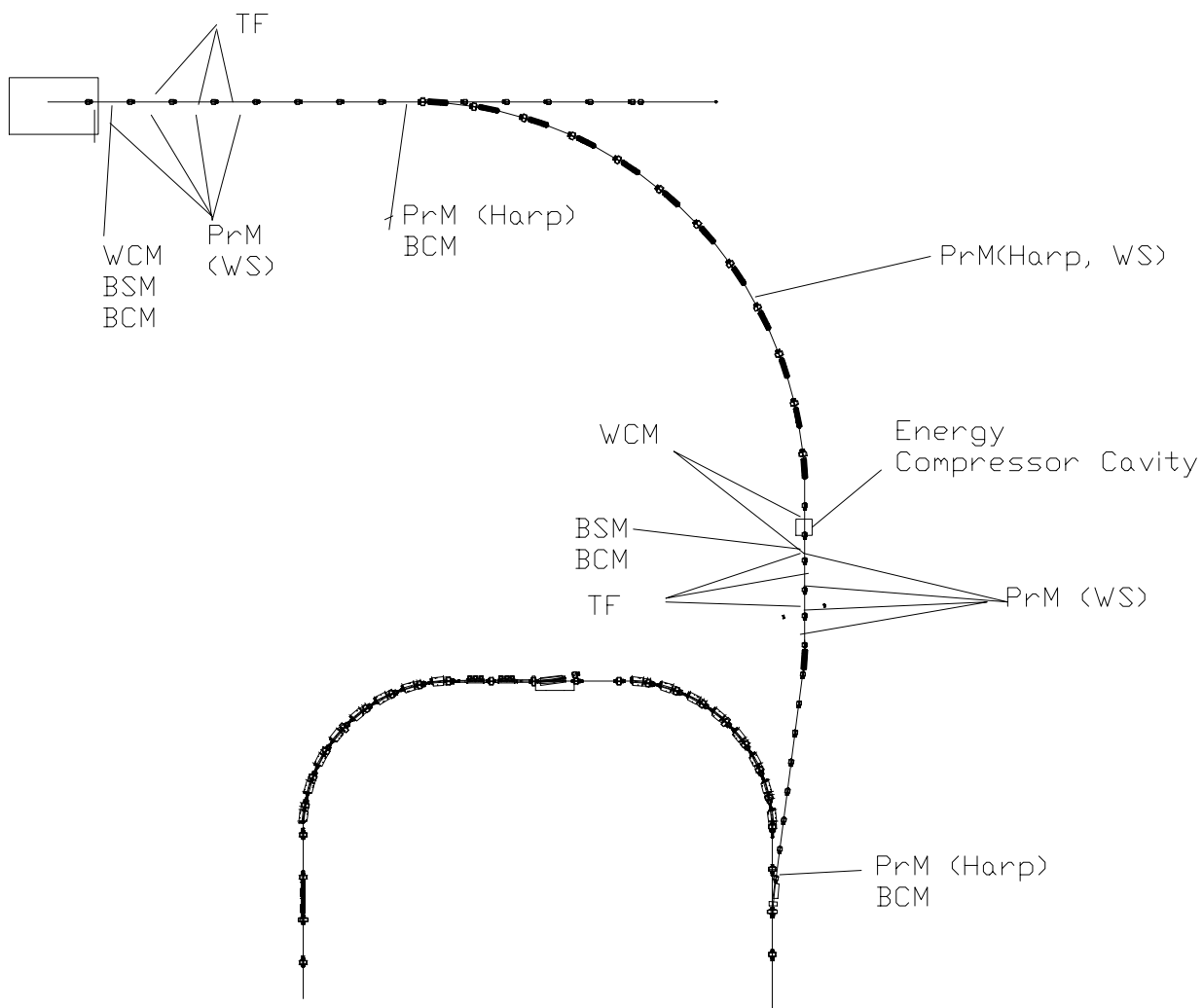


Figure 5.3-4. Schematic showing the location of the diagnostics in the HEBT line.

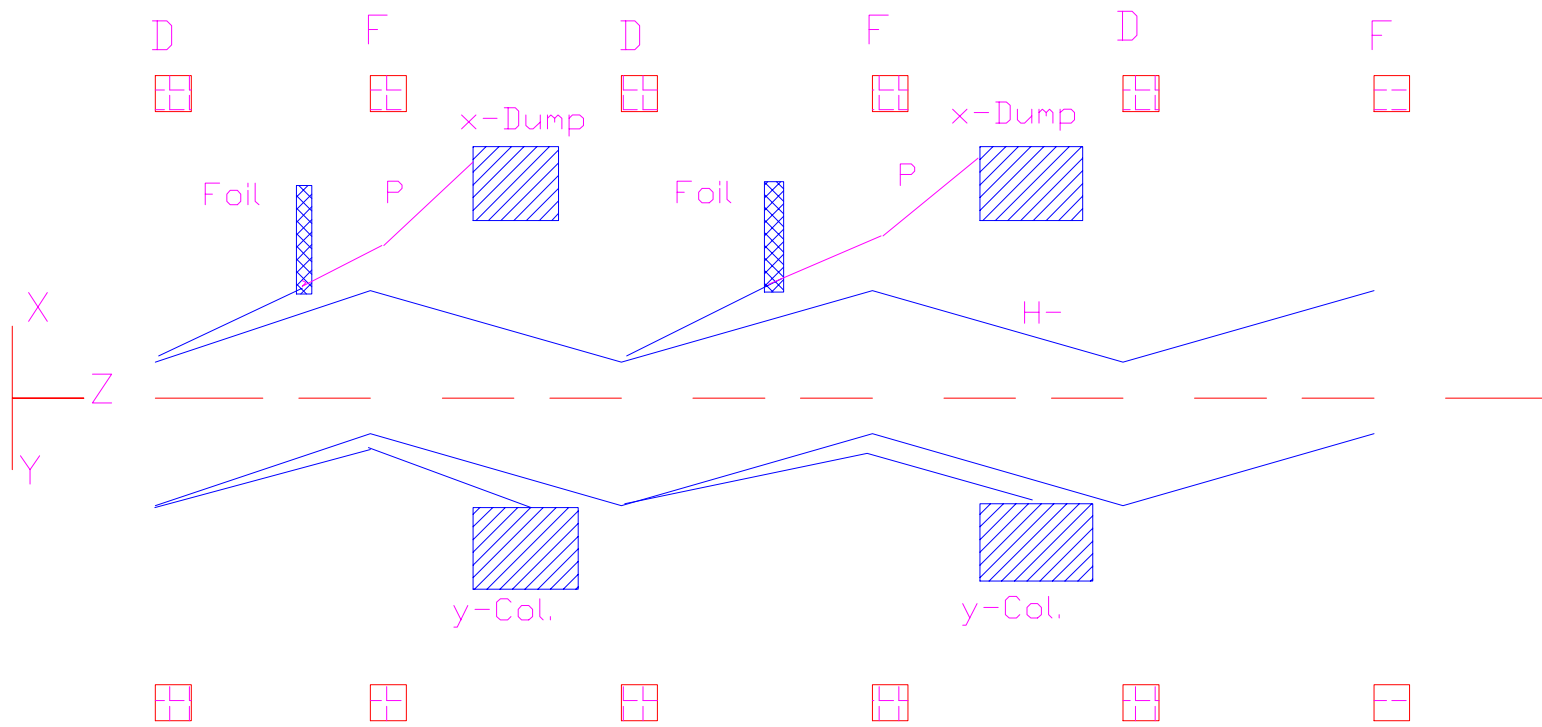


Figure 5.3-5. Schematic of the HEBT collimator configuration.

# SNS LINAC DUMP LINE

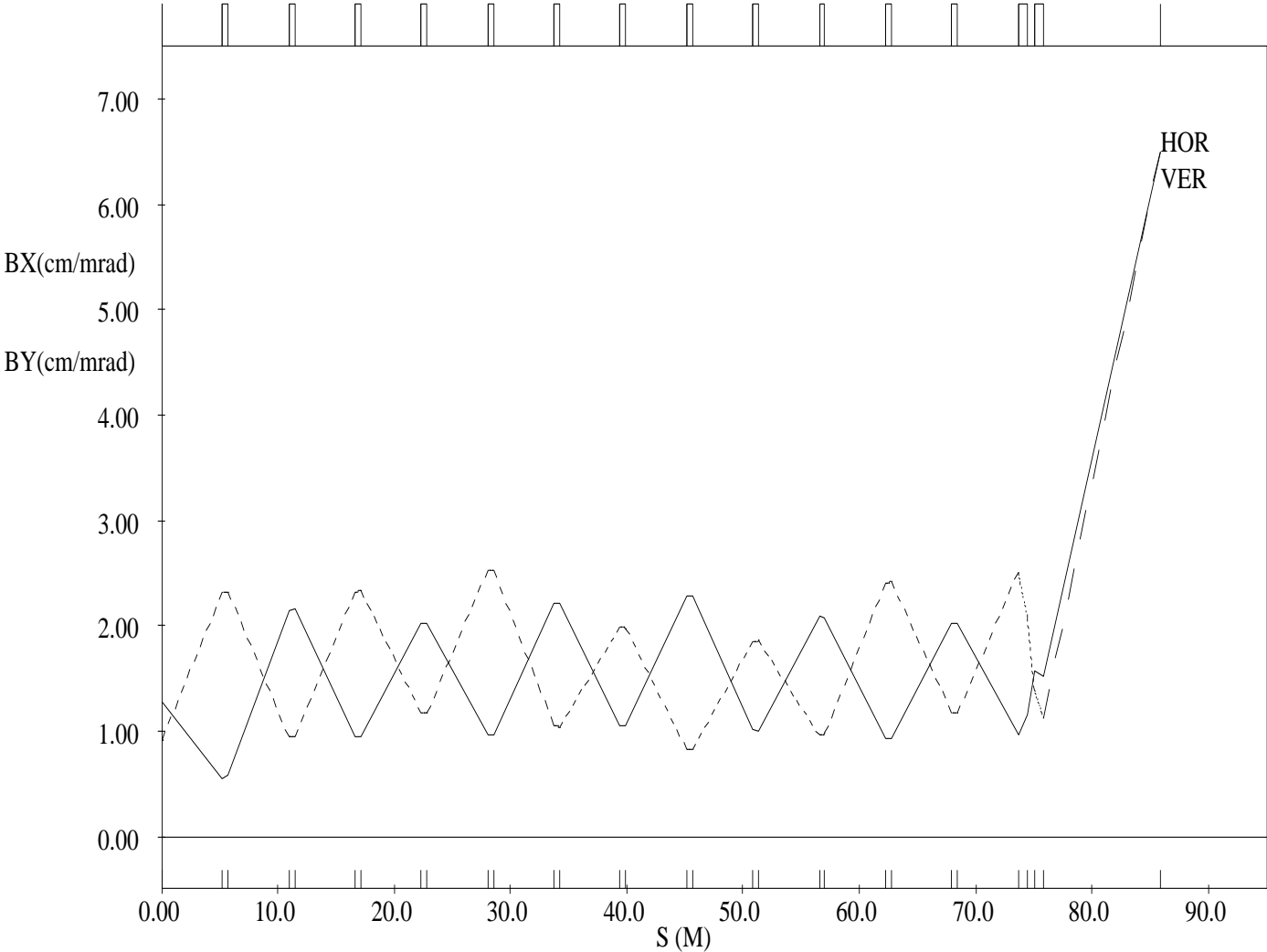


Figure 5.3-6. TRANSPORT calculation of the beam optics to the linac dump.

## 5.4 INJECTION SYSTEM (WBS 1.5.2)

### 5.4.1 Injection System

#### 5.4.1.1 Scope

In this section, the design and implementation of the injection and accumulation processes into the main ring are presented. Injection into the accumulator ring is an  $H^-$  charge exchange process that allows beam to accumulate in already occupied phase space. As described earlier, the beam from the linac is chopped in the revolution frequency of the ring, ensuring there will be a gap in the circulating proton beam. The following sections describe the process, the choice of the stripping foil, the different loss mechanisms, the disposal of non-captured ions, the dc and dynamic injection orbit bumps, and the hardware needed to implement the process.

#### 5.4.1.2 Injection Process

Injection takes place in one of the near-dispersion-free regions (straight section A) of the ring. The process is controlled by a large, especially designed, fixed orbit bump. The fixed orbit bump is a chicane consisting of three dipole magnets (IDH1-A9, IDH2-A9, and IDH3-A10) around the center of the straight section with the center magnet just upstream of the wide aperture quadrupole (QHA10) in the center of the straight section. To facilitate the dumping of the  $H^0$  ions excited by the stripping foil, injection takes place in the downstream fringe field of the center dipole (IDH2). This dipole, which is a C-type magnet, has a central magnetic field of 3 kG. However the stripping foil is located at the edge of the magnet in a 2.5-kG field region. The magnetic field value is important because the electric field felt by the moving, excited  $H^0$ 's is such that the principal quantum numbers of  $n=4$  or less survive the field, whereas those of  $n=5$  or higher strip immediately. The spatially decreasing nature of the fringe field assures that the excited  $H^0$ 's that are not stripped immediately will probably not be stripped at all because the field is decreasing, and hence the electric field felt by the  $H^0$ 's will be too low. The uncontrolled loss by the Stark stripping of the excited  $H^0$ 's is estimated to be on the order of  $10^{-8}$  of the injected  $H^-$  beam. Even if the energy gap between the  $n=4$  and  $n=5$  states is completely miscalculated, the uncontrolled loss rate would be  $10^{-6}$ .

A schematic of the injection straight section and the orbit bump is shown in Fig. 5.4.1-1. At the upstream end of the chicane, in the HEBT injection line, there are a 1.9 degree dipole (HDH14) and a 2.5 meter long septum magnet (HDH15) with a 3 kG field to bring the beam from the HEBT line to the foil, while avoiding the upstream quadrupole (QVA9) and the circulating beam. At the downstream of the center quadrupole (QHA10), there is a 2-meter long septum magnet (DDH1) with a field of 5 kG to take the unstripped  $H^-$  and  $H^0$  ions to the external injection dump. In addition, a water-cooled copper block is located immediately downstream and 2.5 cm outside of the stripping foil to intercept the stripped electrons from the  $H^-$  injected beam.

Two sets of kickers (pulsed dipoles), a set of four (4) for each plane (IKDH1 through IKDH4 and IKDV1 through IKDV4), are used to create dynamic orbit bumps in order to paint the optimum phase space of the injected proton population. The kickers are located in the space between QHA8 and QVA9 as well as between QVA11 and QHA12. The optimum distribution will be determined by computer simulation and by experimentation. However, the present plan is to charge the bump magnets to an initial direct current and, at the proper time in the injection process, to discharge them through an external resistor creating an exponentially decaying

magnetic field. The initial amplitude and the decay time constant impart the spatial distribution to the circulating protons. This scheme has the advantages of simplicity and reliability of operation. Fig. 5.4.1-2 shows the basic scheme of painting in phase space.

The injection loss and subsequent beam loss due to all injection mechanisms has to be kept manageable. There are several injection loss mechanisms. These are: 1) the linac beam missing the stripping foil, 2)  $H^0$ 's emerging from the foil, which is a function of the thickness of the foil, 3)  $H^-$ 's emerging from the foil, which is calculated to be negligible, and 4) circulating beam loss due to Coulomb and nuclear scattering on the foil. Loss mechanism 1) is related to the stripping foil size and this loss should be kept to less than a few percent. This beam loss along with loss due to mechanism 3) is well known and a controlled dumping of the waste beam is planned. Loss mechanism 4) is directly related to the thickness of the foil and the amount of circulating beam hitting it, which is proportional to the foil size. The foil size is chosen such that it provides a compromise between mechanisms 1) and 4). The thickness of the foil is determined by mechanisms 2), 4) and the foil heating problem described later. Present plans call for a carbon foil of size of 8 mm x 4 mm and a thickness of  $300 \mu\text{g}/\text{cm}^2$ .

### 5.4.1.3 Disposal of Unstored Protons

The  $H^-$  ions that miss the stripping foil and the  $H^0$ 's emerging from the foil should be disposed of in a proper beam dump. The size of the stripping foil is chosen such that a distribution tail of about 2% of the incoming linac beam misses the foil. This is a compromise between this loss and the loss due to Coulomb and nuclear scattering of the stored protons. Recently very precise measurements of the cross-sections for  $H^-$  in carbon have been obtained by Gulley (1996) as follows:

$$\begin{aligned}\sigma_{-1,0} &= (6.76 \pm 0.09) 10^{-19} \text{cm}^2 \\ \sigma_{0,1} &= (2.64 \pm 0.05) 10^{-19} \text{cm}^2 \\ \sigma_{-1,1} &= (0.12 \pm 0.06) 10^{-19} \text{cm}^2\end{aligned}$$

For a  $400\text{-}\mu\text{g}/\text{cm}^2$  thick foil, about 0.82 % and for a  $300\text{-}\mu\text{g}/\text{cm}^2$  foil about 2% of the incoming  $H^-$  ions will emerge as  $H^0$ . The population of their quantum states is measured to be  $n^{-2.8}$ , where n is the principal quantum number.

The  $H^0$ 's that emerge from the foil are converted to protons by a thick foil placed in their path. The downstream quadrupole bends the  $H^-$ 's into the 5-kG septum magnet, but because of the high magnetic field a small fraction will be stripped to neutral particles. If a thick foil is placed in their paths inside the septum, they will be converted to protons. Placement of the foil will be determined after careful measurement of the magnetic field, so that the median of the protons emerging from the septum will be parallel with the protons from the  $H^0$ 's. The plan is to place the foil inside the magnet where the field integral is equal to the field integral traveled by the  $H^-$ . A set of two 30-cm aperture quadrupoles and two 36C30 corrector magnets placed downstream in the injection dump line will focus and steer the protons on the water-cooled dump.

#### 5.4.1.4 Stripped Electron Sweeping and Collection

The stripped electrons from the incoming H<sup>-</sup> beam have a momentum of 0.923 MeV/c and a magnetic rigidity of 0.003 T-m. Inside the 2.5 kG magnetic field, the electrons will curve with a 1.2-cm radius, and they will be intercepted by a copper block that is placed 0.5 cm downstream and 2.4 cm radially outward of the foil. The collection block is water cooled as the electron power is expected to be about 1/918 of the proton power (i.e. about 1 kW for a 1MW SNS). The generation of free electrons inside the ring has to be minimized in order to reduce the possibility of them causing an instability to the stored protons. The possibility of secondary electrons emerging from the collection block is eliminated by the fact that it is located inside a 2.5-kG field.

#### 5.4.1.5 Carbon Foil Heating Considerations

A carbon foil is used to strip the electrons of the H<sup>-</sup> beam because of the resiliency and high sublimation temperature of the material. The sublimation temperature of carbon is above 3500 degrees C°. The foil is heated by the energy deposited by the proton and the two accompanying electrons. Since they all have the same velocity, they should have the same energy loss in a given material. There is no data available for what fraction of the energy lost by the beam contributes toward heating of the material. At higher energies, the efficiency is estimated to be as low as 30%. However, for our calculations we assume that all the energy loss contributes to the heating of the material.

For a 1 MW SNS injection, the linac has the following parameters. The effective average current over a macropulse at the injection point is 18.2 mA within the un-normalized rms emittances of 0.14 pi mm mr in both planes. The peak current density at the foil, where the horizontal and vertical beta functions are 16 m and 5 m, is about 3700 A/m<sup>2</sup>. The temperature at the spot will rise very quickly toward equilibrium where the heat input and the black body radiation become equal. Since the heat input is proportional to the thickness of the foil, while the black body radiation is proportional to the surface area, a thicker foil results in a higher resultant temperature.

For the linac current assumed for the SNS injection, a carbon foil of up to 400-μg/cm<sup>2</sup> thickness can survive for 1 MW of beam power, whereas thicker foils may reach their sublimation temperature. However, the mechanism of foil breakage is more complicated than just simple foil evaporation. More detailed calculations and experiments will be carried out to determine the optimum thickness of the stripping foil. Presently, a foil thickness of 300 μg/cm<sup>2</sup> is being contemplated.

#### 5.4.1.6 DC Orbit Magnets and Power Supplies

This section describes the number of dc magnets and power supplies (ps) that are required to accomplish the SNS injection. The devices are located in the HEBT injection line, in the ring, and in the injection dump line. The parameters for this equipment are given in Table 5.4.1-1.

The injection line from the end of the HEBT line, contains two (2) dipoles that direct the H<sup>-</sup> beam toward the stripping foil. The first (HDH14) is a 1.9 degree, 0.776 m long magnet. The second (HDH15) is a 7.6 degree, 2.5 m long, 3-kG septum magnet described in Section 5.4.1.2.

The controlled beam loss line to the injection dump begins at the 2-m long, 5-kG septum magnet (DDH1), which is operated dc. In addition, the dump beam line consists of two 30-cm quadrupoles and two 30-cm dipole correctors for steering and pitching (see also Section 5.4.1.3) onto the dump face.

The dc injection orbit chicane bump (see Section 5.4.1.2) will be created by a set of three magnets located around the injection stripping foil. The first dipole (IDH1-A9) will be placed downstream of ring quadrupole QVA9, The next dipole (IDH2-A9) will be placed just upstream of quadrupole QHA10, and the third (IDH3-A10) just upstream of quadrupole QVA11.

The power supplies for all the dc injection magnets will be standard ac-to-dc converter multiphase thyristor controlled types. Wherever possible, ps's will be purchased completely as commercial units. The ratings are shown in Table 5.4.1-1. The larger units, especially for the septum magnets will be 12-pulse types to reduce the output ripple. All units will be equipped with passive output LCRC filters that exhibit low-pass characteristics. The load voltage and current sensing will be by isolated voltage and current dc transducers. Feedback regulation circuitry will provide the required stability. The ps control, protection and interlocks will be handled by a PLC. This device will also provide the digital computer interface to the local IOC. The analog reference/readback will be via waveform generator and MADC modules installed in the local VME chassis. Load interlocking will be provided and wired back to the ps's.

**Table 5.4.1-1 Injection, DC Orbit Bump, and Dump Magnet Parameters**

	<b>HDH14 HEBT</b>	<b>HDH15 INJ Sept</b>	<b>IDH1- A9</b>	<b>IDH2- A9</b>	<b>IDH3- A10</b>	<b>DDH1 DMPL</b>
<b>Kick (mrad)</b>	33	132.5	27.86	41.4	13.54	177
<b>Gap HxV (cm)</b>	8 x 30	3 x 8	17 x 20	20 x 30	17 x 20	5 x 10
<b>Core Length (cm)</b>	77.6	250	33	58.1	33	200
<b>Effective Length (cm)</b>	85	250	50	78.1	50	200
<b>Number of Turns</b>	16	4	24	24	16	4
<b>B (kG)</b>	2.5	3	3.15	3.0	1.54	5.0
<b>I (kA)</b>	1.0	1.8	1.8	2.0	2.0	5.0
<b>Resistance milliohms</b>	2	5	2	2	1.7	1
<b>V<sub>dc</sub>(V)</b>	2	9	2	4	3.5	5
<b>P<sub>max</sub> (kW)</b>	2	17	3.6	8	7	25

### 5.4.1.7 Dynamic Bump Kicker Systems

Kicker magnet systems are defined as those that are capable of producing a controlled dynamic deflection of the beam. More specifically in this case, their magnetic fields are programmable to produce beam position and/or angle changes during the 1-m injection time. The four horizontal kickers are designated as IKDH1- IKDH4 and the four vertical kickers as IKDV1- IKDV4. All will operate as programmable or ramped magnets. Since these magnets have to have high frequency responses, their cores will be made out of ferrite material. The current conductors will be OFHC copper, formed and insulated with G-10 or Kapton spacers. The copper cross sections will be sufficient to permit low current density operation. The parameters for these magnets are given in Table 5.4.1-2.

Since the maximum magnetic field strengths in these kicker magnets are fairly low (<1.0 kG), the choice of ferrite as the core material is a logical one. Losses in the core and conductors have to be minimized. The cores will therefore be rectangular-frame ferrite with approximately a square aperture. All units will be constructed identically, with the same type core and coil. One of the design choices is whether to install the units inside or outside of the vacuum system. Cooling requirements will dictate the final choice. The present design is to install the magnets outside of the vacuum system. The vacuum chamber choices would be to use a thin, high resistivity material (e.g. inconel) or a ceramic metallized type chamber. Eddy current effects in the chamber are being studied.

The power supplies for these magnets fall under the general category of programmable, pulsed devices. The shape of the fields in these magnets is dictated by the ultimate accumulated proton beam distribution in the ring and at the SNS project target. The present design calls for an exponentially decaying field of time constant of 150-200  $\mu$ s. One of the prime concerns is to produce specified beam distributions in a reliable, consistent manner. Thus, the ps's for these magnets have to be simple, standard units that exhibit high reliability. The choices are to use switchmode power supplies, series regulator transistor banks, or triggered current-decay circuitry schemes. While the first two choices have a higher flexibility in that current responses can be arbitrarily shaped, they are also more complicated and have higher component counts. The selected scheme, the last one, uses a dc ps to charge-up the magnet inductance. At the appropriate time a series switch is opened and the current diverts to a passive external resistor so that the stored current decays naturally with the time constant determined by the magnet inductance and the resistor.

Assuming that the exponentially decaying scheme is selected, the injection kicker pulser circuit is shown schematically in Fig. 5.4.1-3. The charging ps is a standard multi-phase rectifier, or switchmode type unit that is commercially available. Its normal charging voltage can be typically 1/10th of the discharge voltage rating. This is given in Table 5.4.1-2 as  $V_{\max}$  Charge. The opening switch is a solid-state gate-turn-off device or an IGBT (insulated gate bipolar transistor) device. These have high current capability and can interrupt the current in microseconds. The decaying current, which will be diverted into an external resistor ( $R_{\text{ext}}$ ), will be measured by a DCCT. The resistor will be constructed of smaller, low-inductance type commercial units to make up the required power rating. This will minimize the induced voltage at turnoff ( $V_{\max}$  Discharge in Table 5.4.1-2). Controls for these kicker magnets will be similar to those indicated for the dc orbit bump magnets. The additional requirement is for timing triggers that will be derived from the project timing system.

**Table 5.4.1-2 Dynamic Bump Kicker Parameters**

PARAMETER	IKDH1	IKDH2	IKDH3	IKDH4	IKDV1	IKDV2	IKDV3	IKDV4
<b>Kick (mrad)</b>	5.3	-3.8	-3.4	4.7	8	-3	-0.5	4.6
<b>Gap (HxV) (cm)</b>	17 x 17							
<b>Core length (cm)</b>	34							
<b>Eff. Length (cm)</b>	50							
<b>Number Of Turns</b>	10							
<b>Induct (μH)</b>	76							
<b>B (kG)</b>	0.6	0.45	0.4	0.53	0.9	0.35	0.06	0.52
<b>I (kA)</b>	0.82	0.62	0.55	0.72	1.23	0.48	0.1	0.71
<b>Cond. Size(cm)</b>	1.6 x 0.8							
<b>Resistance (milliohms)</b>	2							
<b>V=IxR</b>	2	1.5	1.2	1.5	2.5	1	0.2	1.5
<b>I<sub>rms</sub> (A)</b>	220	166	180	193	330	130	30	190
<b>P<sub>max</sub> (W)</b>	100	55	45	75	220	35	2	72
<b>R<sub>ext</sub> (Ohms)</b>	0.38							
<b>V<sub>max</sub> Charge</b>	32	24	21	27	47	18	4	27
<b>V<sub>max</sub> Disch.</b>	312	236	210	274	470	183	40	275

### 5.4.1.8 Stripping Foil Mechanism

The stripping foils will be operated by mechanisms that both support them and locate them accurately in the main ring injection straight section and in the beam dump line. Since individual foils are very fragile and can be easily destroyed, the mechanisms will be capable of supporting a minimum of 4 foils. Capability will be built-in to be able to change the foils remotely and to indicate their position. Initially the remote operation will NOT be completely automatic (most likely it will be manual) to minimize the possible foil damage.

In order to position the main stripping foils vertically, the design of the foil holders is based on the simple principle of hanging the foils and using weight to rotate them into position. Thin carbon filaments will be used to keep them straight and avoid edge curling. The foil frame will not support one edge of the foil. Radial position control will also be provided. Accurately machined stops will be used for final locations, and microswitches will indicate the foil in use.

The stripping foil mechanisms will be equipped with airlock type systems wherever possible, so that entire foil holders can be replaced in a relatively short time in the event of catastrophic type failures. Operational standby units will be constructed. Proper valving and

pumping will be provided to accomplish this. The design and construction of the foil holders and drive mechanisms will be by BNL. The foils will be manufactured by either another laboratory or by commercial vendors.

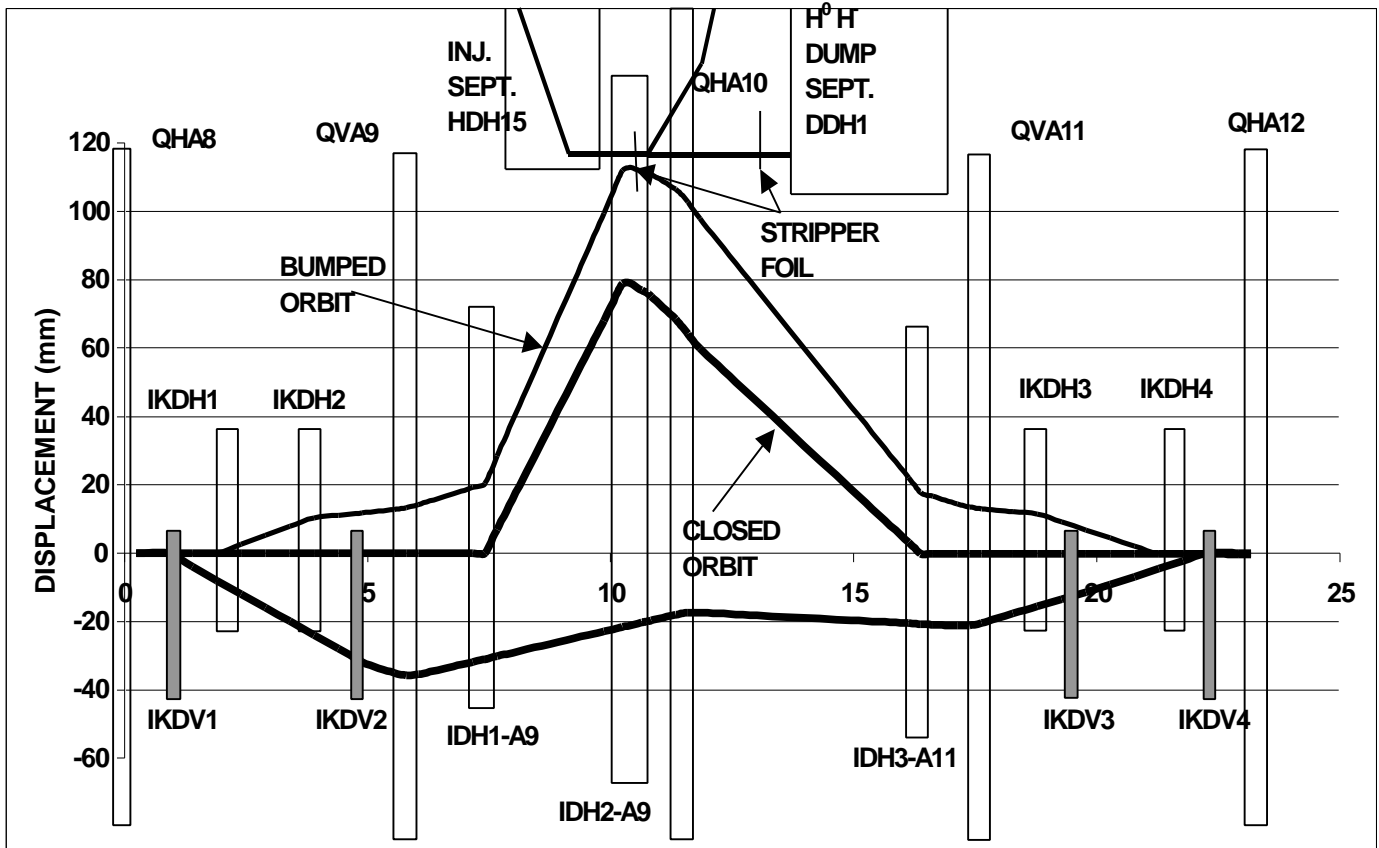


Fig. 5.4.1-1 Orbit Bump at the Injection Area

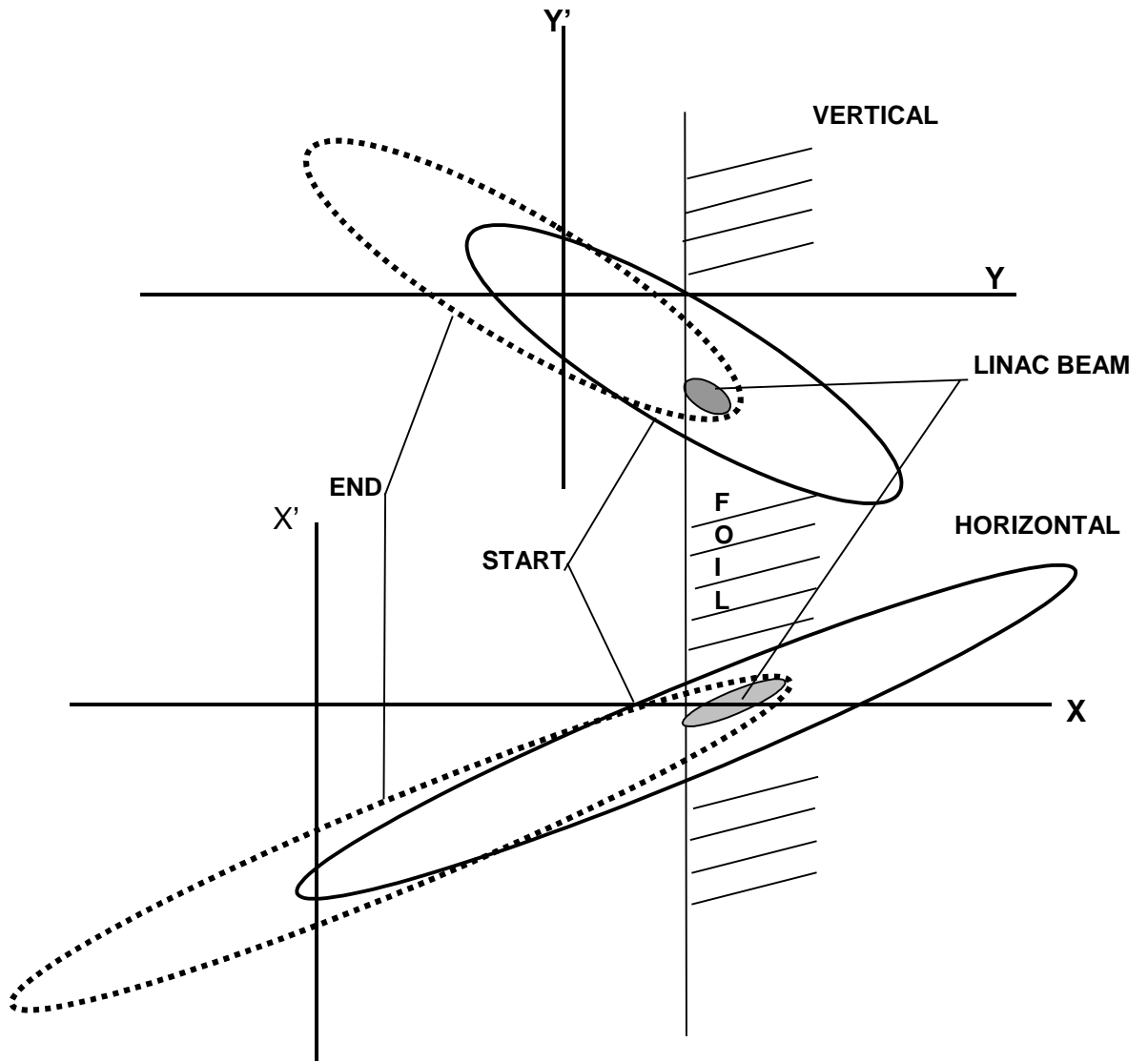
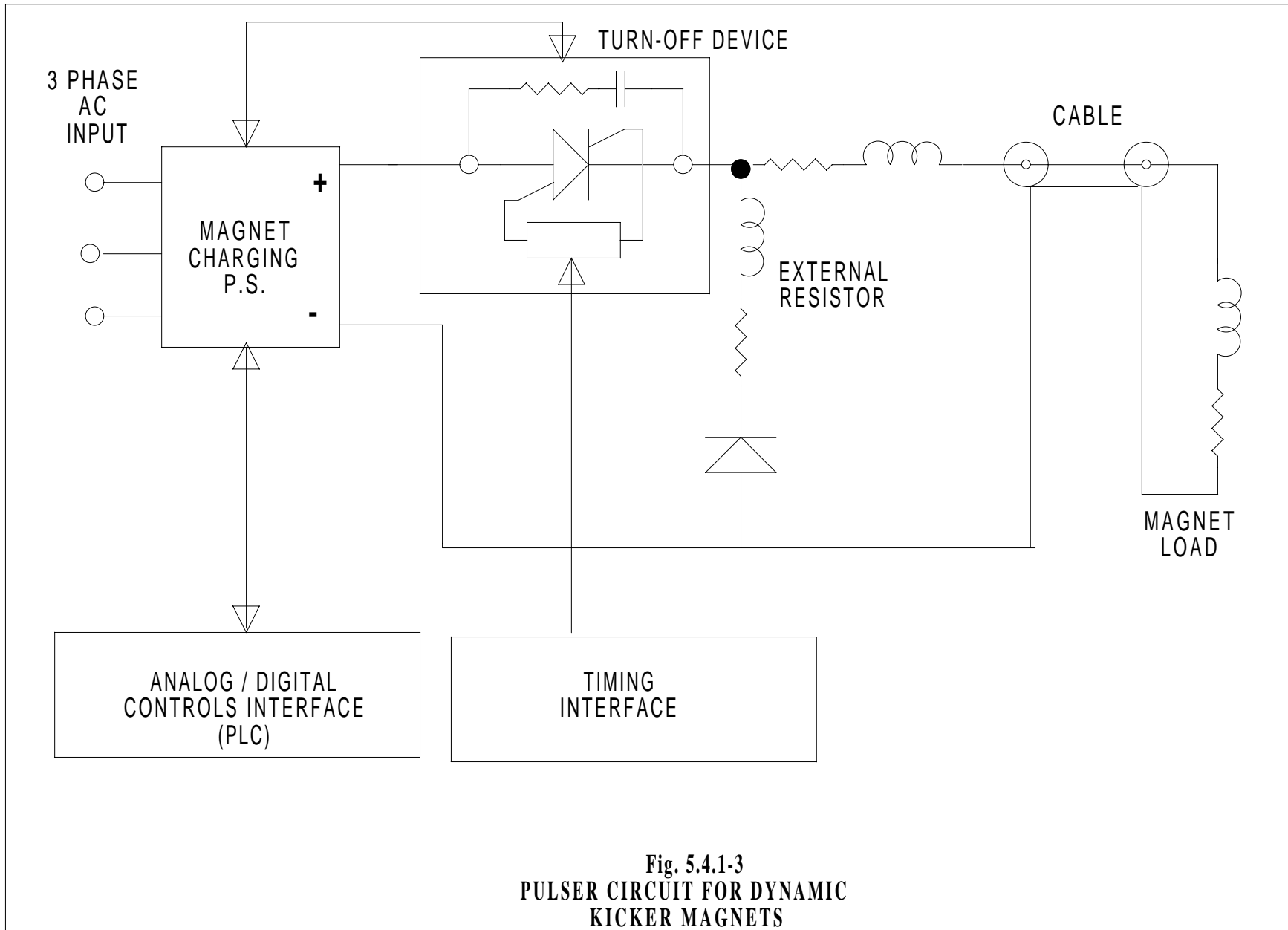


Fig. 5.4.1-2 X and Y Injection Phase Space Diagrams



## 5.4.2. RF Capture

### 5.4.2.1. Introduction

The injection and rf capture process in the accumulator ring is being studied with the code Accsim (Jones 1993). The simulation is 6-dimensional with separate longitudinal and transverse calculations, and with the tracking of a number of representative macro particles through the lattice in the presence of longitudinal and transverse space charge forces and longitudinal beam to wall interactions.

In the simulation we tried to accomplish: (1) injecting a long pulse to decrease the linac average current, (2) obtaining low particle losses, and (3) obtaining at extraction a beam density profile that will yield a final emittance of  $120 \pi$  mm mr and generate an acceptable profile on the neutron producing target (as discussed in Sec.5.11).

An  $H^-$  beam is injected from the linac, stripped to  $H^+$  and moved to the equilibrium orbit. Accsim calculates the scattering in the stripping foil, which is traversed a few times by the beam during the first turns. Losses arise from two main sources:  $H^-$  ions missing the foil or not being converted to protons, and protons hitting the walls during the accumulation process. A general strategy is to try and limit the losses to a specific region of the ring (controlled losses). To decrease the beam diffusion, the beam will be extracted immediately after the injection is completed. To study losses to the level of  $10^{-4}$ , the number of macro particles in the simulation is chosen to be  $10^5$ , with a limit set only by computer time.

### 5.4.2.2. Machine Lattice. Injection

The lattice of the accumulator ring, with super symmetry 4, is described in Sec. 5.2. It consists of an array of FODO cells with 4 straight sections, for injection, for collimation, for the rf, and for extraction. The code MAD (Iselin, 1988) produces the 66 matrices used by Accsim for tracking. To account for beam losses at the wall, collimating apertures were placed at various points along the circumference in the simulation.

The injection system is described in Sec. 5.4.1. For the simulation, the stripping foil is Carbon, with dimensions 8 mm (radial) x 4.58 mm (vertical) and thickness  $220 \mu\text{g}/\text{cm}^2$ . The foil is centered at  $x = 41.33$  mm,  $y = 22.55$  mm with respect to the reference orbit. A plural tabulated scattering distribution (Keil,1960) is used to generate scattering angles in the foil. Nuclear scattering is not currently simulated in Accsim.

The number of protons injected into the accumulator ring is  $2.084 \times 10^{14}$ , for a 2 MW beam. The injection time of 1.031 msec, or 1,225 turns, was used for the simulation. This number of turns and the longitudinal phase bite injected, of  $240^\circ$  or  $2/3$  of the bucket length, were chosen to leave a large longitudinal gap to facilitate extraction.

At injection, the ring equilibrium orbit is distorted with a radial and a vertical bump. Initially, the beam is directed to the foil in correspondence with the center of the phase space acceptance ellipse of the ring, both radially and vertically. The bumps collapse in time, so that at the end of injection the beam sits on the horizontal plane on a less bumped radial orbit. The horizontal and vertical coordinates of the closed orbit displacement at the foil location vs. time are shown in Figs. 5.4.2-1a and 5.4.2-1b, respectively.

The injection line dispersion was matched to the zero ring dispersion at the foil. The  $\alpha$  and  $\beta$  functions of the HEBT at the foil were matched to those of the ring at the foil. Injection

parameters are given in Table 5.4.2-1. The distribution of macro particles at injection is taken as random truncated Gaussian in the radial and vertical phase space, Gaussian in energy, and flat in the longitudinal phase. The values for the transverse un-normalized emittance shown in the table are for  $2\sigma$ .

### 5.4.2.3. RF Capture Losses

Since the beam will be extracted soon after injection process is completed, long-term beam accumulation and rf capture beyond 1 ms are of no concern. For such a high intensity beam, its size and stability are strongly affected by space charge. Tune shift and tune spread are indicative of transverse space charge effects and should be kept small. A design limit for transverse tune shift, both radial and vertical, is  $\Delta\nu = -0.2$ . Space charge issues will be discussed in more detail in Sec. 5.4.2.4.

Following our experience with AGS operation, and in agreement with previous calculations (Blumberg, 1995) we studied the performance of vertically hollow, or "smoke ring" beam in phase space in order to reduce the tune shift. This distribution also produced an acceptable profile on the neutron target.

Beam stacking was studied with the rf system, described in Sec. 5.8, which is a dual harmonic system employing the fundamental harmonic plus a second harmonic. The rf voltage waveform is shown in Fig. 5.4.2-2, compared with a fundamental frequency rf voltage waveform.

With the orbit bumps of Figs.5.4.2-1, we found a solution with no beam losses to the walls in excess of  $10^{-4}$  during the 1,225 turns, at a peak accelerating voltage of 40 kV ( $h = 1$ ) and 20 kV ( $h = 2$ ). The resulting bucket area was 8 eV sec. Transverse tune shifts in the beam were well contained within the design limits of -0.2. Adding a 2nd harmonic to the fundamental improves the longitudinal phase space and the transverse tune shift, creating a more compact beam (Blaskiewicz, 1996).

Accsim snapshots at 1,225 turns, just before extraction, are shown in Fig. 5.4.2-3. The 5 diagrams represent, from left to right and from top to bottom the beam distribution in the radial and vertical phase space, the longitudinal voltage due to space charge, the cross section of the beam in real space (this diagram also shows the location of the stripping injection foil) and the beam distribution in longitudinal phase space. Figs. 5.4.2-4a and 4b show the resulting radial and vertical emittance and the tune shift vs. time during the injection and rf capture process, respectively. Losses and foil traversals are given in Table 5.4.2-2.

### 5.4.2.4. Space Charge Tune Spread

The transverse tune shift is calculated in Accsim for each macro particle with a formalism which computes the amplitude dependent tune shift due to the space charge forces of the instantaneous 2 dimensional betatron amplitude distribution, with walls removed. Individual particles are assumed to perform prescribed oscillations within the beam (Schönauer 1989). In the longitudinal dynamics Accsim includes space charge with perfectly conducting smooth walls. The additional space charge voltage induced on the beam (other than the rf's) is calculated with (Hoffman, 1977)

$$V_{sc} = -\frac{Z_0 c}{4\pi} \left(1 + 2 \ln \frac{b}{a}\right) \frac{d\lambda}{ds}$$

with  $Z_0$  the impedance of free space,  $d\lambda/ds$  the longitudinal gradient of the particle distribution in the beam, and  $b/a$  the ratio between chamber radii and beam. In our simulation we took  $b/a = 3$ . At the present stage in Accsim, no longitudinal impedance budget is yet considered.

For the transverse tune shift in the center of the beam, Accsim agrees with the classical Laslett's expression when the transverse beam profile has only one peak (pseudo Gaussian distribution). In Accsim the algorithm that evaluates the tune distribution in the beam did not prove sufficiently accurate for a general charge distribution (say, a smoke ring). Work is in progress to calculate in a more complete way the space charge force tune shift and orbit kick.

In dealing with space charge, the immediate problem is that the calculation can be very time consuming and therefore impractical when a very large number of representative macro-particles is used. The evolving charge distribution should be continuously updated to calculate transverse kicks on the macro particles due to space charge forces and the tune associated with each particle, in order to evaluate the diffusion of the beam and the growth rate of possible disruptive resonances. Work is under way to devise compromises between the accuracy of the results and computation speed.

Far from the walls, the radial space charge force on a particle can be calculated by an integration on the actual charge distribution. The space charge force produces a tune shift,  $\Delta\nu$ , at each macro particle location. An example of a necktie diagram of the tune spread in the final beam at extraction is shown in Fig. 5.4.2-5a. The Accsim calculated average tune shift in increasing transversal cross sections of the beam is shown in Fig. 5.4.2-5b. The curve shows that the larger tune shifts mostly belong to protons in the outer regions of the beam.

#### 5.4.2.5. References

- Blaskiewicz, M. and Brennan, J.M. 1996. *Fifth European PAC*, p.2373.  
Blumberg, L.N. and Lee Y.Y. 1996. BNL/NSNS Tech. Note 003, Nov. 1.  
Hoffman, A. 1977. CERN 77-13.  
Iselin, F.Ch. and Niederer, J. 1988. *The MAD Program: User's Reference Manual*. CERN/LEP-TH/88 (and later editions). June.  
Jones, F.W. 1993. *User's Guide to ACCSIM*. TRIUMF Design Note TRI-DN90-17 (and later editions).  
Keil, E., Zeitler, E. and Zinn, W. 1960. *Zeit. Naturforschung* **15a**: 1031.  
Schönauer, H. 1989. TRIUMF Design Note TRI-DN-89-K50, August.

**Table 5.4.2-1. Parameters of the injected beam in the accumulator**

	$\alpha$	$\beta$ (m)	$\epsilon$ (mm mr)	Beam size (mm)
Radial phase space	-1.947	15.64	$0.56 \pi$	5.9
Vertical phase space	0.765	5.173	$0.56 \pi$	3.4
Longitudinal phase space	$\Delta\Phi = 240^\circ$		$dE/E = 0.002$ (rms)	

**Table 5.4.2-2. Losses and foil hits**

No. of macro particles	98,000
Total number of particles	$2.084 \times 10^{14}$
% missing foil	2.14
Particles lost elsewhere	$<10^{-5}$
Average foil hits/proton	4.01

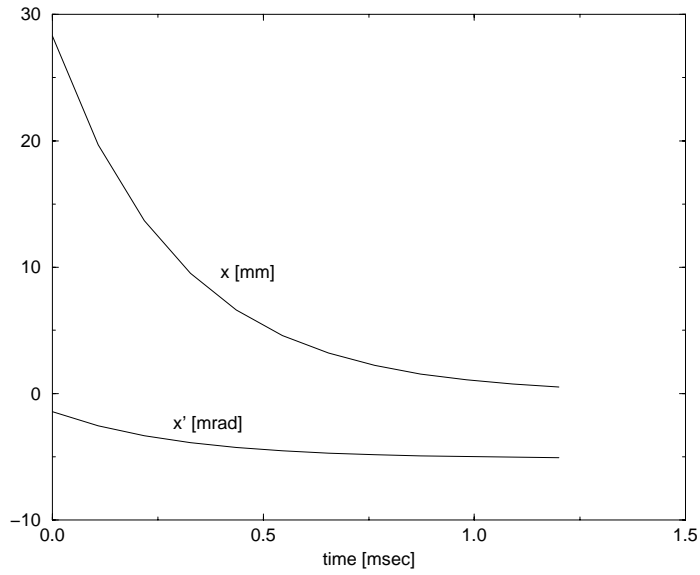


Fig. 5.4.2-1a. Horizontal injection bump

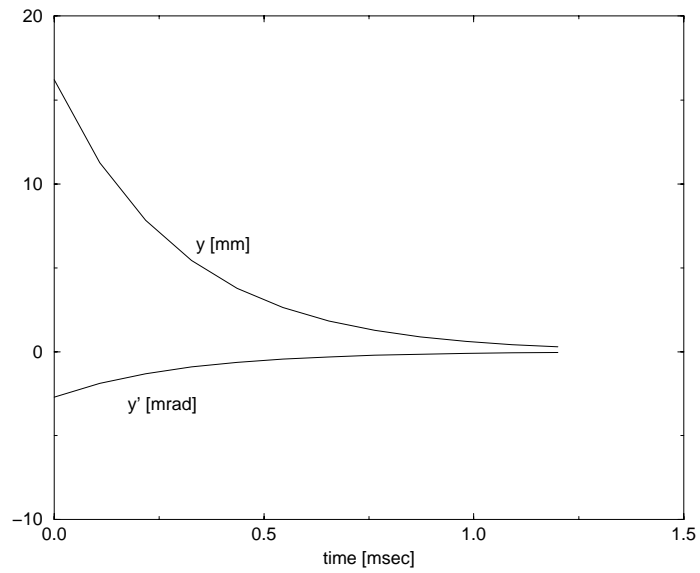


Fig. 5.4.2-1b. Vertical injection bump

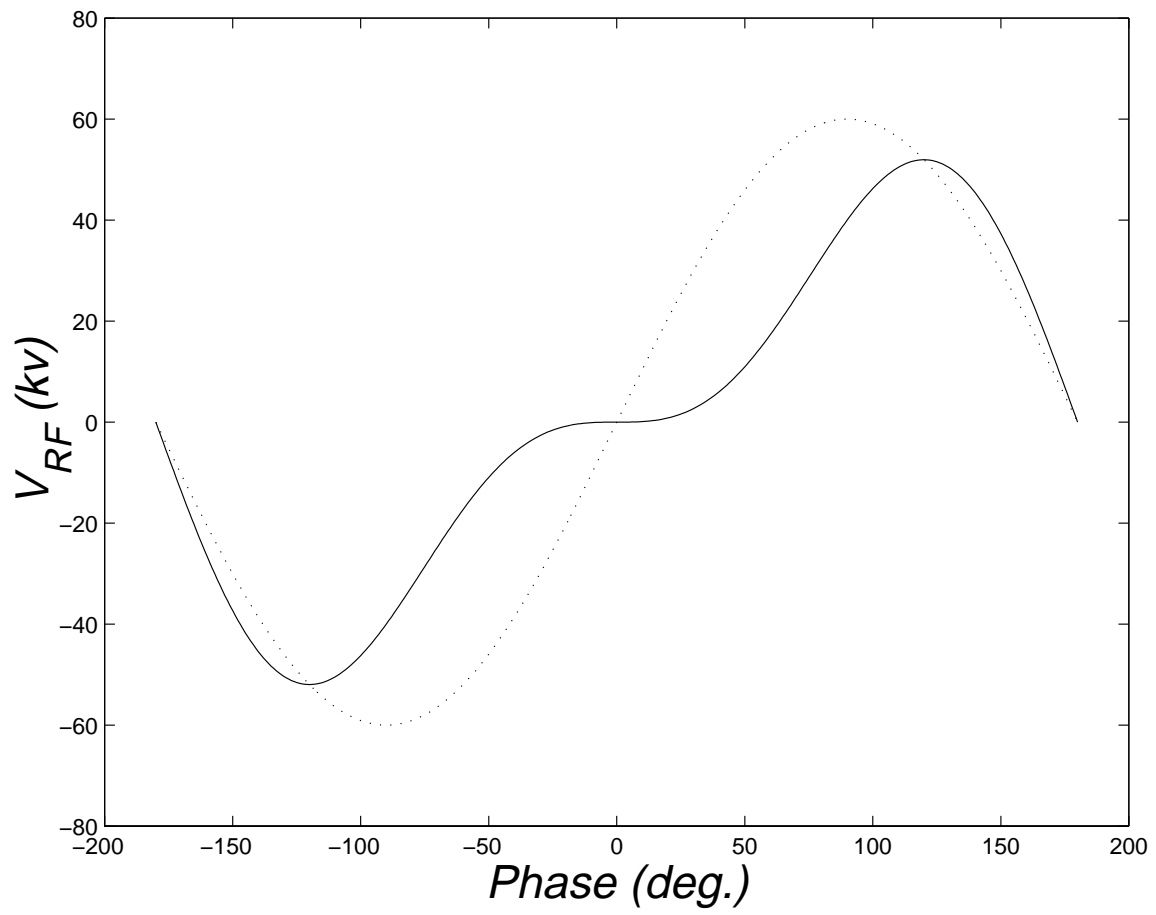


Fig. 5.4.2-2. Dual frequency (solid line) vs. fundamental frequency RF waveform (dotted line).

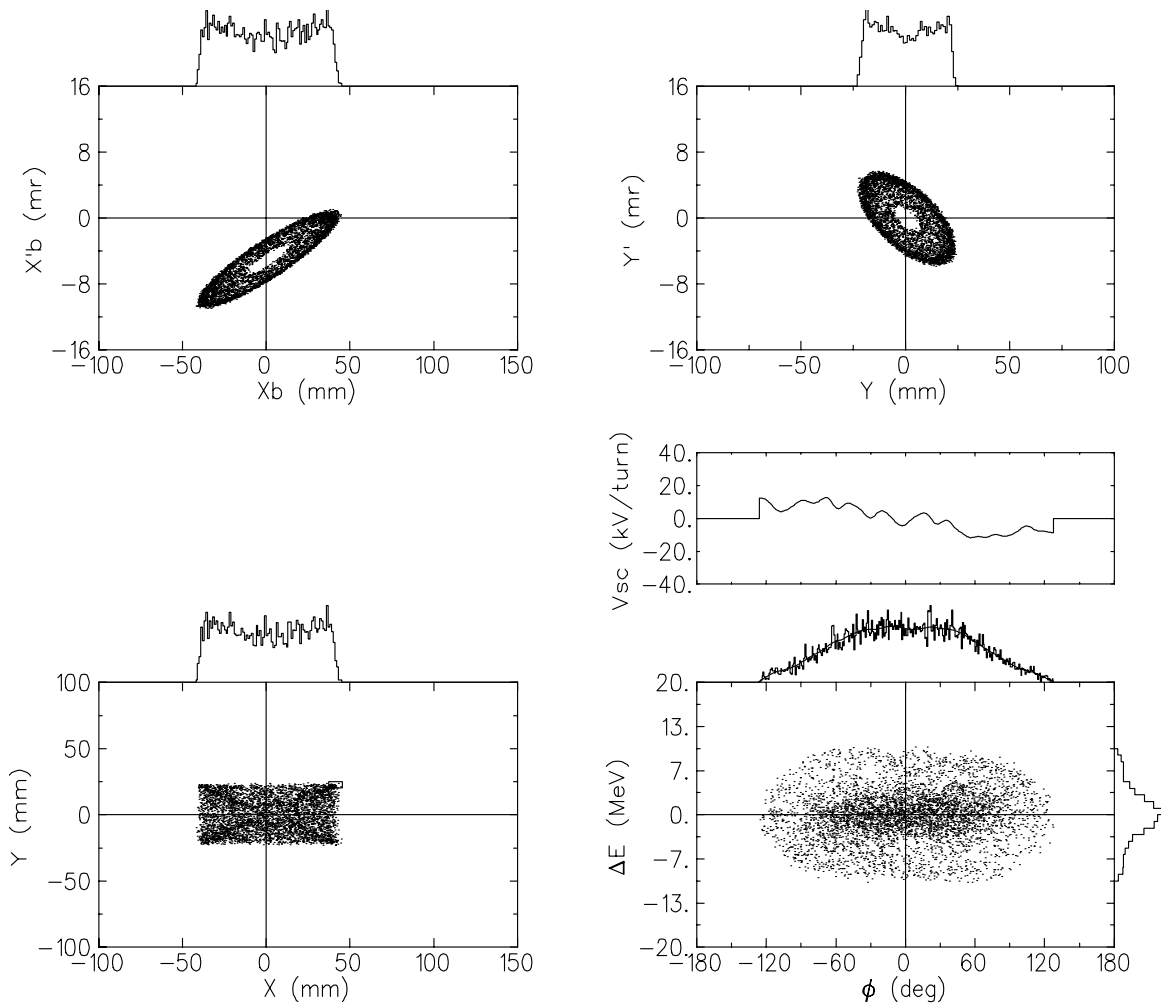


Fig. 5.4.2-3. Beam snapshots at turn number 1,225, just before extraction.

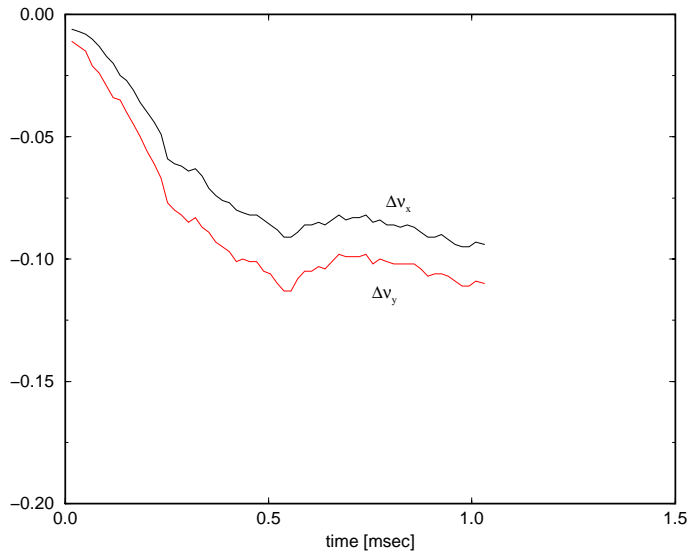


Fig. 5.4.2-4a. Tune shift during injection.

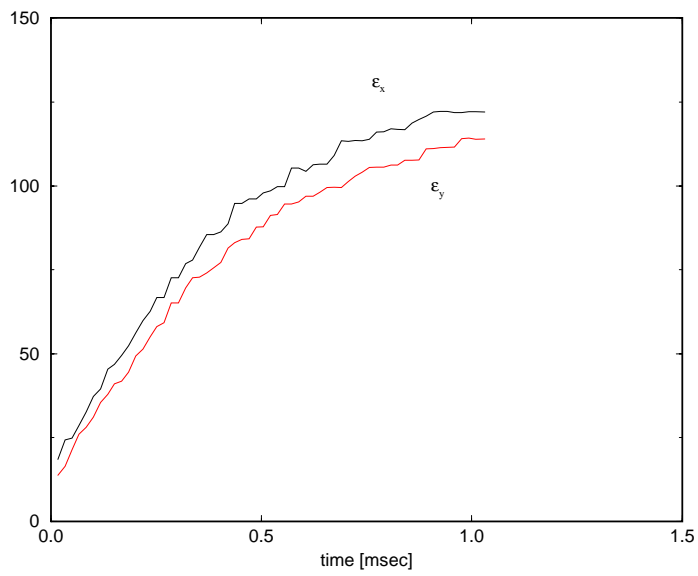


Fig. 5.4.2-4b. Emittance vs. time during injection.

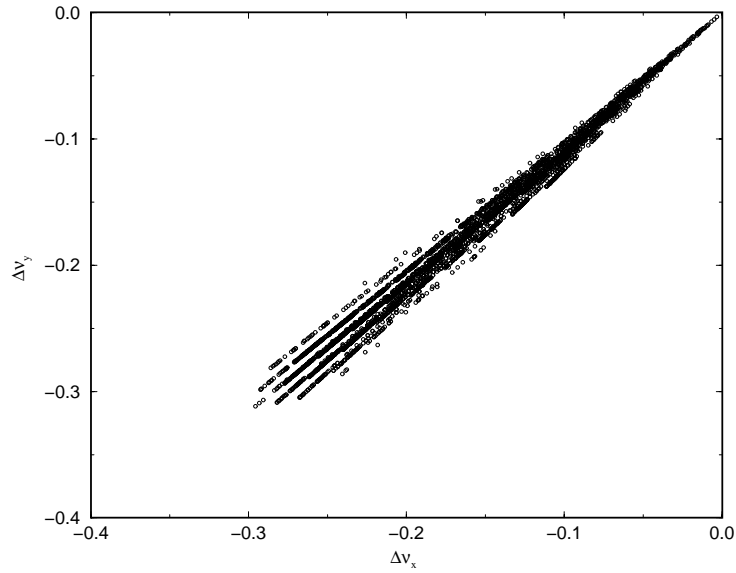


Fig. 5.4.2-5a. Tune spread in the final beam.

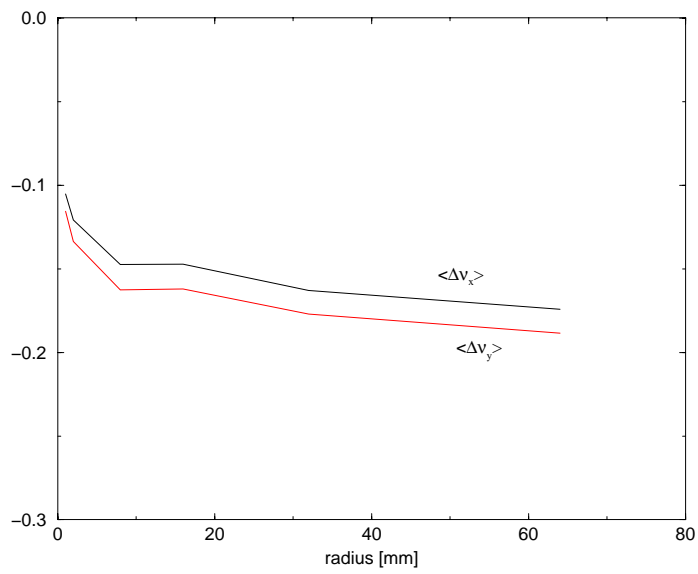


Fig. 5.4.2-5b. Tune spread averaged over final beam cross section.

## 5.5 MAGNET SYSTEMS (WBS 1.5.3)

### 5.5.1 Scope

This section describes the dipole, quadrupole, and corrector magnets required for the accumulator ring, the HEBT transport, and the RTBT transport systems. The special magnets required for injection and extraction are described in the corresponding sections.

### 5.5.2 Design Requirements

Because of the high intensity beam in the accumulator, the magnets must be designed with very precise field shapes and must be manufactured to high tolerances. In addition, beam loss from the high intensity will produce areas of high radiation, requiring magnets of high radiation resistance and very good reliability. All of the magnets for the accumulator ring and for the beam transport systems will operate at fixed fields. The requirements for the magnets are listed in the sections on the ring, HEBT, and RTBT, respectively.

### 5.5.3 Quantities and Performance Requirements

Table 5.5-1 provides a listing of the specifications for the main dipole magnets required for the three systems. Since the bend angle required for each dipole is set quite precisely by the geometry, it is included in this table and is used to calculate the design current. Also specified in the table is the nominal maximum current, which is used to determine the heat load, the cooling requirements, and the power supply ratings.

Table 5.5-2 gives the specifications for the main quadrupoles. Wherever possible magnet designs are shared between the three different systems. In some cases, the quadrupole magnet core length has been shortened to match the lattice requirements but full-length coils are used on the shortened cores to reduce cost and the spares requirements. The current and power requirements listed are the maximum values. When installed the quadrupoles may be run at lower settings depending on their lattice location. For each magnet the table includes a calculated value for the integrated gradient divided by current. This value is used in the sections on each system to calculate the design current. Table 5.5-3 gives the number of quadrupoles allocated to each system.

The cross-sections for the major accumulator ring dipole and quadrupole magnets are shown in Fig. 5.5-1a and Fig. 5.5-1b, respectively. All of the magnets are designed to achieve the required field accuracy without expensive machining, special quality steel, or heat treating of the steel after fabrication. The magnet pole tips will be machined to a tolerance of  $\pm 0.05$  mm. The mating steel pieces within the magnet core must be machined to within  $\pm 0.05$  mm. The core and the pole tips will use 1006 steel throughout.

The magnetic cores will be inexpensive, reliable in a high radiation environment, and easy to maintain. The cores will be manufactured from low carbon steel solid plates or laminations. Using computer controlled numeric machine tools the steel cores will be machined to high accuracy and repeatability. Laminated cores will be used for the ring dipole and quadrupole magnets, whose size and quantities make the laminated core cost effective. The magnets will be built so they can be “split” for easy installation of the coils and vacuum chambers. The vacuum chambers will be built in clean rooms with no welding required after they

are installed in the magnet assembly. The coils and vacuum chambers will be accessible and removable without machining should they fail after long term use.

**Table 5.5-1 Specifications for Main Dipoles in HEBT, Ring, and RTBT\***

<b>DESIGNATION</b>	<b>8D250</b>	<b>17D140</b>	<b>17D310</b>	<b>17DV50</b>	
<b>Location</b>	HEBT	Ring	RTBT	RTBT	
<b>Quantity</b>	13	33	1	1	
<b>Design Bend</b>	7.5	11.25	15.5		degrees
<b>Design Bend</b>	<i>0.1309</i>	<i>0.19635</i>	<i>0.270526</i>	0.0168	radians
<b>B*Le</b>	<i>0.7406</i>	<i>1.1108</i>	<i>1.5305</i>	<i>0.0950</i>	T m
<b>Gap (G)</b>	0.08	0.17	0.17	0.17	m
<b>Pole Width</b>	0.30	0.45	0.45	0.45	m
<b>Iron Length (L)</b>	2.5	1.4	3.1	0.5	m
<b>Magnetic Length (Le)</b>	<i>2.58</i>	<i>1.57</i>	<i>3.27</i>	<i>0.67</i>	m
<b>Design Field (B)</b>	<i>0.287</i>	<i>0.708</i>	<i>0.468</i>	<i>0.142</i>	T
<b>Number of Coils</b>	2	2	2	2	
<b>Turns per Coil</b>	12	12	20	20	
<b>I design</b>	<i>761.4</i>	<i>3988.3</i>	<i>1582.9</i>	<i>479.8</i>	A
<b>I max</b>	800	4200	1800	900	A
<b>Magnet resistance</b>		0.002			ohms
<b>Power max</b>	5.2	27.5	31	2.7	kilowatts
<b>Coil weight</b>	750	2,100			pounds
<b>Steel weight</b>	6,000	20,000			pounds
<b>Construction</b>	Plate	Lamination	Plate	Plate	

\* Values in italics are calculated from the inputs to this table. The magnetic rigidity used is 5.6575 T m.

**Table 5.5-2 Specifications for Main Quadrupoles in HEBT, Ring, and RTBT\***

DESIGNATION	12Q50	12Q80	20Q47	20Q50	
<b>Aperture (diameter)</b>	0.120	0.120	0.200	0.200	m
<b>Iron Length</b>	0.500	0.800	0.465	0.500	m
<b>Magnetic Length (Le)</b>	<i>0.56</i>	<i>0.86</i>	<i>0.57</i>	<i>0.60</i>	m
<b>Number of Poles</b>	4	4	4	4	
<b>Turns per Pole</b>	20	20	24	24	
<b>I max</b>	300	300	600	600	A
<b>Pole Tip Field</b>	<i>0.251</i>	<i>0.251</i>	<i>0.362</i>	<i>0.362</i>	T
<b>Gradient (G)</b>	<i>4.189</i>	<i>4.189</i>	<i>3.619</i>	<i>3.619</i>	T/m
<b>G*Le</b>	<i>2.35</i>	<i>3.60</i>	<i>2.04</i>	<i>2.17</i>	T
<b>G*Le/I</b>	<i>0.007 82</i>	<i>0.012 00</i>	<i>0.003 41</i>	<i>0.003 62</i>	T/A
<b>Magnet resistance</b>			0.022	0.022	ohms
<b>Power max</b>	1.4	2	8	8	kilowatts
<b>Coil weight</b>	300	300	550	550	pounds
<b>Steel weight</b>	1,600			3,950	pounds
<b>Construction</b>					

DESIGNATION	30Q40	30Q49	36Q80	
<b>Aperture</b>	0.300	0.300	0.360	m
<b>Iron Length</b>	0.396	0.486	0.800	m
<b>Magnetic Length (Le)</b>	<i>0.55</i>	<i>0.64</i>	<i>0.98</i>	m
<b>Number of Poles</b>	4	4	4	
<b>Turns per Pole</b>	48	48	48	
<b>I max</b>	600	600	800	A
<b>Pole Tip Field</b>	<i>0.483</i>	<i>0.483</i>	<i>0.536</i>	T
<b>Gradient (G)</b>	<i>3.217</i>	<i>3.217</i>	<i>2.979</i>	T/m
<b>G*Le</b>	<i>1.756</i>	<i>2.046</i>	<i>2.919</i>	T
<b>G*Le/I</b>	<i>0.002 93</i>	<i>0.003 41</i>	<i>0.003 65</i>	T/A
<b>Magnet resistance</b>	0.044	0.044		ohms
<b>Power max</b>	16	16	20	kilowatts
<b>Coil weight</b>	1,100	1,100		pounds
<b>Steel weight</b>		4,800		pounds
<b>Construction</b>				

\* Values in italics are calculated from the inputs to this table.

**Table 5.5-3 Main Quadrupole Allocation**

<b>Designation</b>		<b>12Q50</b>	<b>12Q80</b>	<b>20Q47</b>	<b>20Q50</b>	<b>30Q40</b>	<b>30Q49</b>	<b>36Q80</b>
<b>Location</b>								
<b>HEBT</b>								
	LAMS	7						
	Achromat				12			
	ARMS	14						
	LDUMP	4	2					
	Inj Dump							
<b>RING</b>								
	Arc Defocus				16			
	Arc Focus			8				
	Straight				8			
	Arc End				8			
	Arc Focus						4	
	Straight					4		
<b>RTBT</b>								
	Extraction				7			
	Bend				2			
	Collimat				4			
	Transport				12			
	Expand							5
	Dump				2			
<b>Total Allocated</b>		25	2	8	71	4	4	0
<b>Spares</b>								
<b>Construction Total</b>		25	2		79		10	5

### 5.5.4 Magnet Coil Design

The magnets will be designed with low current density (<350 amps/cm<sup>2</sup>) copper coils wherever possible. The low current density will reduce the resistive energy loss in the coils and keep the voltage drop across the magnets as low as possible. This will reduce the possibility of turn to turn shorts occurring in the coil should the insulation be damaged by radiation. The low current density will also reduce the resistive heat loss in the magnet system. This will lower the power consumption of the accumulator and will reduce the load on the water cooling systems. All of the coils will have a single pass water cooling passage. This will minimize the number of water fittings, which can leak or fail. The exception to this rule will be the high field quadrupoles. Space limitations at the ends require current densities of up to 450 amps/cm<sup>2</sup> but these magnets will be sized for single pass water-cooling.

The coils will use a modified epoxy/glass insulation that is used on accelerator magnets in high radiation areas. This insulation has a Kapton<sup>R</sup> layer (Krempel) in the fiberglass tape. This

material provides the radiation protection of Kapton<sup>R</sup> with the bonding ability of glass fiber and epoxy typically used for accelerator magnets. The manufacturing method for this insulating material is the same as a standard glass wrap insulation with vacuum impregnated epoxy.

Magnesium Oxide mineral insulation will be used for very high radiation resistant coils. This conductor is fabricated with a grounded metal cover that must be terminated with a brazed ceramic feedthrough to keep the insulation material sealed. Also, it must be carefully formed with large radius bends to prevent damage to the insulation. Because of its cost and manufacturing complexity this coil material will only be used in areas where high dose rates are expected such as the last focusing magnets in the RTBT transfer line near the spallation target.

### **5.5.5 Water Cooling**

For radiation resistance and reliability, metal fittings and tubing will be used to carry the cooling water to and from the coils. The water lines will be mounted on insulated stand-offs and routed to a common water manifold on the magnet support frame that will have insulated ceramic breaks. The integrity of the water system will be monitored by klixon temperature sensors on each coil and by return line flow switches.

All of the magnets will be cooled by the closed loop ring water system. This system will also provide cooling for the rf cavities, special injection magnets, and special extraction magnets. In order to prevent corrosion, the water system will see only copper coils, copper cooling plates in the rf cavities, and stainless steel water pipes. The collimators and beam dumps, which contain steel and much higher activation products, will be on separate water systems. The pumps, heat exchangers, and other ancillary equipment for the ring water system will be located in the accumulator water services building. Activated water from the ring will be kept in the tunnel or the service building during normal operation.

### **5.5.6 Corrector Magnets**

Table 5.5-4 gives the specifications for the correction dipoles for the three systems. The corrector magnets will be air-cooled window frame magnets. Kapton<sup>R</sup> coated wire will be wrapped around the steel leg of box or diamond shaped magnets. Each magnet will provide either horizontal or vertical dipole correction. Quadrupole, skew quadrupole, sextupole, and skew sextupole low field correction will also be required (Gardner, 1998). The alternate field configurations will be obtained by positioning trim windings on the magnet cores of the low field dipoles. In the ring the correctors will be located downstream of the quadrupole magnets around the Beam Position Monitor section of the vacuum chamber. Sixteen additional 24C30 multipole correctors will be installed in the straight sections.

**Table 5.5-4 Specifications for Correction Dipoles in HEBT, Ring, and RTBT\***

DESIGNATION	12C20	20C30	24C30	36C30	
<b>Location</b>	HEBT Linac Dump	HEBT Ring Dump RTBT	Ring dipoles & multipoles	Ring RTBT Inj. Dump	
<b>Quantity</b>	25	39	56	15	
<b>Design Bend</b>		0.000 8			radians
<b>B*Le</b>		<i>0.0045</i>			T m
<b>Gap (G)</b>	0.12	0.20	0.24	0.36	m
<b>Pole Width</b>	0.12	0.20	0.24	0.36	m
<b>Iron Length (L)</b>	0.20	0.30	0.30	0.30	m
<b>Magnetic Length (Le)</b>					m
<b>Number of Coils</b>	2	2	2	2	
<b>Turns per Coil</b>	160	180	216	300	
<b>I max</b>	20	20	20	20	A
<b>B max</b>	<i>0.03</i>	<i>0.02</i>	<i>0.02</i>	<i>0.02</i>	T
<b>B*Le</b>					
<b>Bend max</b>					radians
<b>Magnet resistance</b>					ohms
<b>Power max</b>	0.115	0.190	0.230	0.315	kilowatts
<b>Coil weight</b>					pounds
<b>Steel weight</b>					pounds
<b>Construction</b>	Box	Box	Box	Box	

\* Values in italics are calculated from the inputs to this table. The magnetic rigidity used is 5.6575 T m.

### 5.5.7 Magnetic Measurements

Detailed field mapping will be done on each of the first article magnets. Field measurements will be done on all of the production magnets. This will serve as a final check on the quality of all aspects of the magnet assembly, i.e., the coils, the steel core, and the wiring of the coils.

### **5.5.8 Magnet Cell Assembly and Alignment**

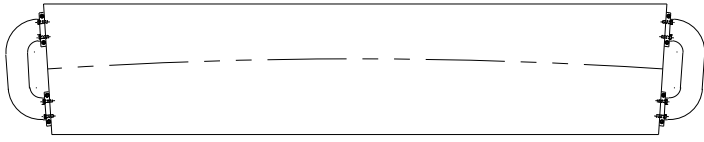
The magnets will be installed and aligned on their support frames outside of the accumulator ring tunnel. In the 90° arcs each large dipole magnet will be mounted with a corrector magnet and quadrupole. In the straight sections the quadrupole will be mounted with a corrector magnet. This assembly will allow installation of a single vacuum chamber within all of the magnets on the frame without unnecessary flange joints or bellows. The support frame will be designed and machined with an accurate positioning hole and slot for the stand jack assembly. The beam position monitor and the magnets will be surveyed on to the support frame using the hole and slot as the reference.

All of the magnets on an individual frame will be plumbed onto a single water manifold on the support frame. The coil heat sensors and flow switches will be wired into a common wiring block. The radiation monitors, beam position monitor wiring, and other ancillary equipment will be installed on the frame assembly as well.

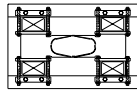
The magnet stands will be positioned in the ring and bolted into the floor. The base of the stand will be located 2 to 4 cm above the floor and the gap between the floor and the base will be filled with concrete grout to evenly distribute the load. The jack frame will then be installed on the stands and the magnet cells will be installed on the jack frame. Fig. 5.5-2 shows the major cell assemblies and lists their associated weights.

### **5.5.9 References**

Gardner, C. J., Sextupole Correctors for the SNS Ring, BNL/SNS Technical Note No. 041,  
January 14, 1998.  
August Krempel Co. Stuttgart, Germany manufactures this special insulation.

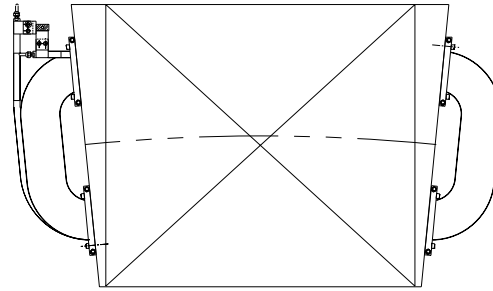


TOP VIEW

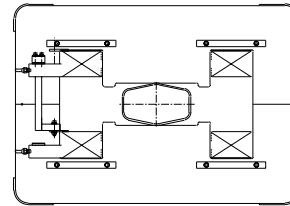


END VIEW

HEBT DIPOLE MAGNET 8D250

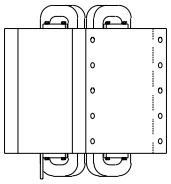


TOP VIEW

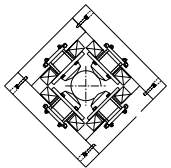


END VIEW

RING DIPOLE MAGNET 17D140

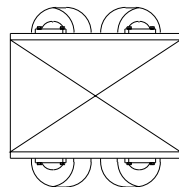


TOP VIEW

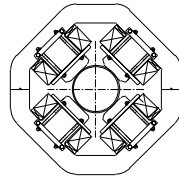


END VIEW

HEBT QUAD 12Q50

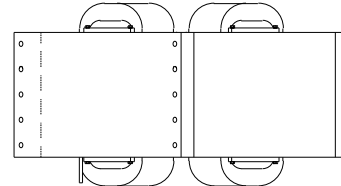


TOP VIEW

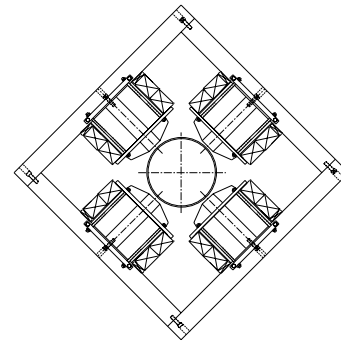


END VIEW

HEBT, RING, AND RTBT  
QUAD MAGNET 20Q50



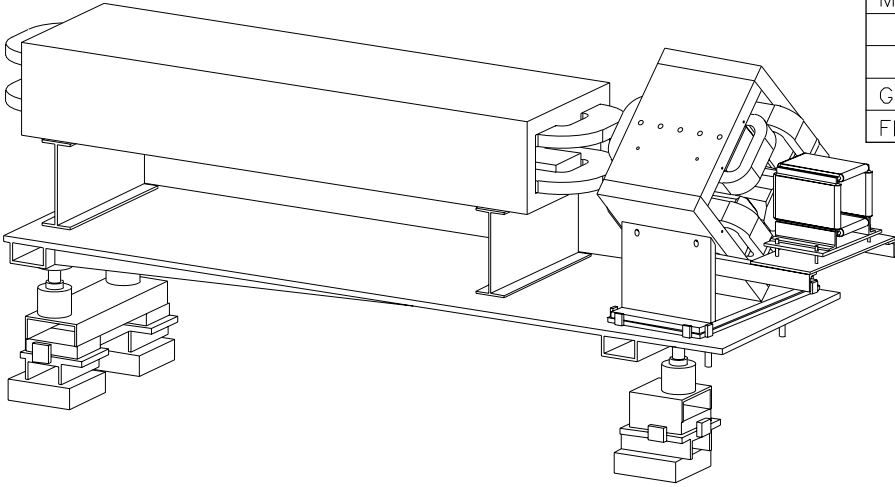
TOP VIEW



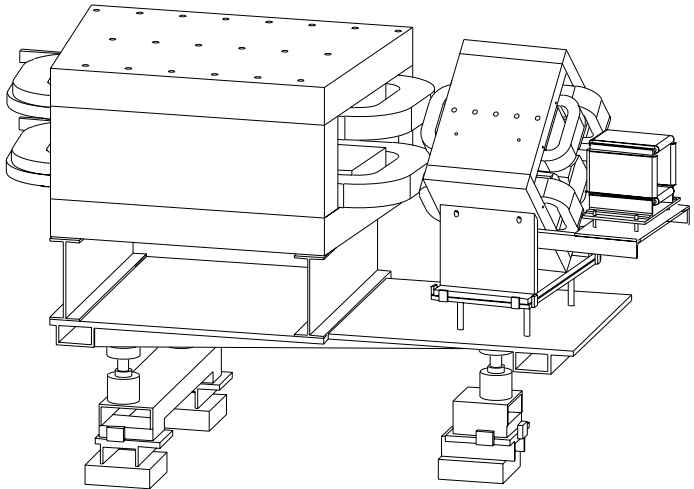
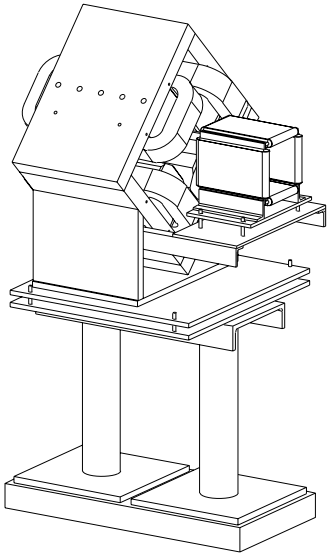
END VIEW

RING QUAD MAGNET 30Q49

CELL ASSEMBLY	HEBT DIPOLE/QUADRUPOLE
MAGNETS	17D140
	20Q50
	20C30
GROSS WEIGHT	18,000 LBS.
FLOOR LOADING	90 PSI. (MAX)



CELL ASSEMBLY	ACCUMULATOR RING LARGE QUADRUPOLE
MAGNETS	30Q49
	36C30
GROSS WEIGHT	8000
FLOOR LOADING	30 PSI. (MAX)



CELL ASSEMBLY	ACCUMULATOR RING DIPOLE/QUADRUPOLE
MAGNETS	17D140
	20Q50/30Q49
	24C30/36C30
GROSS WEIGHT	33500/36000 LBS
FLOOR LOADING	115/120 PSI (MAX)

FIG. 5.5-2

MAGNET CELL ASSEMBLIES

## 5.6 POWER SUPPLY SYSTEM (WBS 1.5.4)

### 5.6.1 Main Ring

The main ring power supplies are conventional for an accumulator ring. All main ring elements are operated essentially in dc fashion, except for the injection and extraction processes. However, even the dc units are provided with adjustability to enable machine tuning for optimization of ring parameters and operating points.

#### 5.6.1.1 High Power Systems

The total power for the ring high power units is large because the magnet apertures are large. This is mainly to provide an extra margin of aperture clearance safety for the high final intensities that the ring must attain. The high intensities also require high performance and reliability so that beam losses and hence residual radiation levels remain within project goals. The parameters for the main ring high power systems are shown in Table 5.6-1.

The large power supplies (ps) for the main ring dipoles and quadrupoles are ac-to-dc converter types with a large number of output phases or pulses that provide smooth dc output voltages and currents. The number of output pulses is 12 per 60-Hertz cycle. With the use of passive output filters, the net output voltage ripple can be made quite small to meet the ring magnetic field accuracy requirements. The other major reason for the use of 12-pulse/cycle operation is to enhance output gain/bandwidth response to disturbances. With high bandwidth and with the use of analog feedback loops, the effects of fast ac line voltage transients and other ps disturbances such as "noise" that may arise will be mitigated. The regulation and ripple will be less than one part in  $10^4$  for the dipole power supplies and less than two parts in  $10^4$  for the quadrupole power supplies.

A simplified schematic of a 12-pulse ps unit, typical of the dipole or quadrupole units, is shown in Fig. 5.6-1. The design uses two full-wave controlled bridges which are displaced 30 electrical degrees and connected in series. The units require symmetrical, balanced arrangements in order to minimize sub-harmonic voltage ripple unbalance in their outputs. Triggering, controls, protection, and computer interface circuitry are shown in the figure. See also section 5.6.3 for computer interface description.

For the main ring dipoles, a set of 33 magnets will be required in series, 32 within the ring enclosure and one in the ring support building as a reference magnet. In the latter, Hall effect probes and a NMR probes will be mounted in the gap to measure the magnetic field intensity, and hence the ring energy in a reproducible manner. This will act as the primary standard for the SNS ring. The interconnection of the main dipoles will be by a fold-back, high-current, water-cooled, copper-bus system. A simplified schematic is shown in Fig. 5.6-2. The figure also shows a ring ground or "loop-break" which shall be respected by all systems that can possibly violate it by metallic bypasses. For the main ring focussing systems, a set of 24 vertical and a set of 24 horizontal quadrupoles will be employed. In order to achieve independent control of the vertical and horizontal machine tunes, the ring quadrupoles will be separated into three families, each family with its own independent power supply. The interconnections for the three families are shown in Fig. 5.6-3. Flexible cables, suitably rated and running in the ring tray system, will make the interconnections. All ring magnets will have water flow, over-temperature, and monitoring protection installed and wired back to the main ps's.

**Table 5.6-1 Accumulator Ring Main Magnet Power Supplies**

	<b>Dipole</b>	<b>Arc Quads</b>	<b>H Quads</b>	<b>V Quads</b>
<b>Number of Magnets</b>	32 + 1 ref	28	12	8
<b>Number of PS's</b>	1	1	1	1
<b>PS Type</b>	DC-SCR	DC-SCR	DC-SCR	DC-SCR
<b>PS Configuration</b>	12-Pulse	12-Pulse	12-Pulse	12-Pulse
<b>Ring Connection</b>	Series Connection - Folded Bus			
<b>Ring BUS</b>	Water/Copper	High Current Cable		
<b>Design Current A (from Table 5.2-2)</b>	3988.3	569.6	450.3	364.4
<b>Max PS Current A</b>	4500	600	500	500
<b>Resistance/Magnet milliohm</b>	2.0	22, 44	22, 44	22
<b>Total String Res. ohms</b>	0.090	0.74	0.38	0.22
<b>Inductance/Magnet mHy</b>	4			
<b>Total String Ind. mHy</b>	130			
<b>PS Max. Voltage V</b>	400	450	200	120
<b>PS Max. Power kW</b>	1,800	270	100	60
<b>Output Filter</b>	Passive LC			
<b>Regulation/Ripple</b>	<1 x 10 <sup>-4</sup>	<2 x 10 <sup>-4</sup>	<2 x 10 <sup>-4</sup>	<2 x 10 <sup>-4</sup>

The three ps's for the quadrupole families will be constructed identically to the main ring dipole system (see Fig. 5.6-1). They however, will range from approximately 1/5 to 1/10 of the dipole power rating (see Table 5.6-1). In addition to the above, there will be a set of four quadrupole trim ps's to enable matching of different types of quadrupole series. These ps units are small and will power isolated trim windings that will be built into each quadrupole. A schematic of this interconnection scheme is shown in Fig. 5.6-4.

The input power for the main ring ps system will be derived from the SNS 13.8 kV voltage distribution system. The ps rectifiers and low-level controls will be located in the ring support building. Water-cooling will be employed, wherever possible, both to reduce component

sizes and to reduce the amount of heat rejected to the building HVAC system. Outdoor switchgear will be used, and the larger rectifier transformers will be outdoor oil-cooled units. Lower power units will be powered from the normal 13.8 kV/480 volt substations supplied by the Conventional Facilities area of the project. Cable tray systems will be required in both the ring buildings and in the main ring. All cables for ac power, dc power, and control and interlocks will be run in the trays. They will be rated for high temperature operation, low oxygen content and low flame propagation, and radiation resistance. For electrical safety, disconnect switches, that are equipped with lockout provisions such as captive-key systems, will be employed in order to meet requirements for safe work practices.

### 5.6.1.2 Low Power Systems

The high intensities that must be attained in the main ring necessitate magnetic field correction systems to eliminate the detrimental effects of machine resonances that can cause beam instabilities and hence beam losses. The most important corrections are dipole or closed orbit errors, quadrupole resonances, skew quadrupole or coupling resonances, and higher-order sextupole and octupole resonances. The correction elements for these resonances that will be introduced into the machine lattice are shown in Table 5.6-2. These magnets will provide for the correction of both main magnet imperfections and survey misalignments.

A large number of independent vertical (24) and horizontal (24) trim dipoles will be provided to reduce closed-orbit distortions. A short dipole will be mounted immediately downstream of each main ring quadrupole and will be connected to its own bipolar correction ps. The ps units will be constructed as bipolar, linear, series regulator, transistor types. These type units generate less switching type electrical noise and hence cause less undesirable coupling to other systems via radiation or conduction. A simplified schematic of a unit that uses linear MOSFET type transistors is shown in Fig. 5.6-5. The unit is self-contained and can operate in either closed loop current or voltage control modes. A programmable logic controller (PLC) provides ac controls, interlocks, and digital computer interfaces. Several units (up to four) will share the CPU and crate, but in order to provide complete isolation between units they will have their own I/O modules and power.

The dipole units will be programmable or tunable from central or host control computers via orbit information obtained from the machine beam position monitors (BPM's). For analog control, the units will be interfaced to waveform generator boards located in the local IOC. A typical control interface to each ps is shown in Fig. 5.6-6.

Families of skew and regular quadrupoles, and regular and skew sextupole magnet strings (see Table 5.6-2) will correct coupling, one-half integer, and one-third integer resonances. A skew quadrupole will be incorporated into each low-field dipole corrector magnet. Regular quadrupole correction windings will be included in each main ring quadrupole magnet. Sextupole and skew sextupole as well as octupole magnets will be built separately and installed downstream of the regular ring quadrupoles to enable higher order corrections. The ps's for these will be similar to the dipole correction units (Fig. 5.6-5) and will be linear-transistor types.

**Table 5.6-2 Accumulator Ring Corrector Systems Power Supplies**

	<b>HDIP Small</b>	<b>HDIP Large</b>	<b>VDIP</b>
<b>Magnet Type</b>	24C30	36C30	24C30
<b>Number of Magnets</b>	16	8	24
<b>Number of Strings</b>	16	8	24
<b>Number of PS's</b>	16	8	24
<b>Current (A)</b>	20	20	20

	<b>QUAD (<math>\frac{1}{2}</math>-INT)</b>	<b>QUAD (SKEW)</b>	<b>SEXT (<math>\frac{1}{3}</math>-INT)</b>	<b>SEXT (SKEW)</b>	<b>OCT</b>
<b>Number of Magnets</b>	12	36	8	8	8
<b>Number of Strings</b>	6	6	4	4	4
<b>Number of PS's</b>	6	6	4	4	4
<b>Length (cm)</b>	50	30	10	10	10
<b>Diameter (cm)</b>	20 small 30 large	24 small 36 large	20	24	20
<b>Current (A)</b>	50	20	50	50	50
<b>Magnet Type</b>	QHCS QHCL QVCS	QSL QSS	SHC SVC	SSHC SSVC	OHC OVC

### 5.6.1.3 Controls Interface

All main ring, HEBT, and RTBT ps's will be interfaced to the SNS EPICS computer control system. The typical ps interface will be accomplished by its tie-in to the local intelligent operations computer or IOC. The typical tie-in consists of digital (OFF/SBY/ON) control and status monitoring, as well as high-resolution analog reference/readback. A typical computer interface diagram is shown schematically in Fig. 5.6-6. As can be seen, the analog connections to the ps are via fiber optic cables, and the digital connection is via the PLC bus-type connection. A multiplexed A/D converter (MADC) system is provided to enable other analog signals to be digitized and stored for diagnostic purposes.

## 5.6.2 HEBT and RTBT

The following paragraphs describe the power supply requirements for the HEBT line from the linac to the main ring and for the RTBT extraction line from the ring to the beam target. For details for these beam transport lines, see their respective Design Manual sections (5.3 and 5.12) as well as the magnet Design Manual section (5.5). The design requirements for both lines fall into two general categories, namely high power and low power. Tables 5.6-3 and 5.6-4 list the major parameters and number of magnet and ps types for the HEBT and RTBT lines respectively. All ps's will be housed in the three available support buildings, namely at the end of the linac klystron gallery, in the ring support building, and along the RTBT transport line. Cable run optimization will dictate the location of ps units. The input power will be from the project 13.8 kV/480 volt substations. Units will be water-cooled wherever possible.

### 5.6.2.1 High Power PS

The high power ps units for the HEBT and RTBT lines will supply the high dc currents required by the large dipoles and quadrupoles. The number required and their ratings are shown in the tables. As can be seen, some of the ps's drive several magnets in series.

The design of the high power units will be ac-to-dc converter types of either 6 or 12 pulse outputs. This will be determined by beam line sensitivity analyses. In either case, the normal scheme will consist of ac switchgear, step-down rectifier transformer(s), SCR (silicon controlled rectifier) full-wave bridges, dc voltage (DCPT) and dc current (DCCT) measuring devices, regulators, ac controls, protection and interlock circuitry, and computer interface. A typical unit is shown in Fig. 5.6-7. The ac controls, protection and interlock, and digital computer interface will be handled by PLC's, one per large unit. The analog references/readbacks will be from/to the local IOC computer, which will be networked to the rest of the SNS control system.

### 5.6.2.2 Low Power PS

Low power units in this case refers to the vertical pitching or horizontal steering trim magnets that are used to control the position of the transported beams at critical locations. The ps's for these magnets will be bipolar, low current, low power units. The system uses stand-alone, series transistor regulators to independently power each magnet. The scheme consists of two ac-to-dc rectifiers, two series pass-banks of transistors, and one set of voltage and current monitors, one bipolar amplifier regulator, ac controls, interlock and protection circuitry and a PLC. The latter will be shared by several units (typically 4) housed in the same rack, however isolation between units will be maintained. The schematic for these type units is the same as for the main ring corrector ps's (see Fig. 5.6-5).

**Table 5.6-3 HEBT Line Electrical Parameters**

<b>SECTION</b>	<b>TYPE</b>	<b>NUMBER OF MAGNETS</b>	<b>NUMBER OF PS'S</b>	<b>VOLTS</b>	<b>AMPS</b>	<b>POWER (KW)</b>
<b>LAMS</b>	12Q50	8	4	20	400	8
	12C20	8	8	30	20	0.6
<b>ACHRO.</b>	8D250	12	1	100	1000	100
	20Q50	12	2	50	400	20
	20C30	12	12	30	20	0.6
<b>ARMS</b>	8D250	1	1	12	1000	12
	12Q50	13	10	20	400	8
	12C20	13	13	30	20	0.6
<b>LDMP</b>	12Q50,	4	4	20	400	8
	12Q80	2				
	12C20	4	4	30	20	0.6

**Table 5.6-4 RTBT Line Electrical Parameters**

<b>SECTION</b>	<b>TYPE</b>	<b>NUMBER OF MAGNETS</b>	<b>NUMBER OF PS'S</b>	<b>VOLTS</b>	<b>AMPS</b>	<b>POWER (KW)</b>
<b>Pre-Bend</b>	17DV50	1 (V)	1	10	1000	10
	20Q50	8	2	30	700	21
	20C30	8	8	30	20	0.6
<b>Post-Bend</b>	17D310	1	1	30	1800	54
	20Q50	17	6	30	700	21
			1	150	700	105
20C30	17	17	30	20	0.6	
<b>Target Spreader</b>	36Q80	5	5	30	1000	30
	36C30	5	5	30	20	0.6
<b>Dump</b>	20Q50	2	2	12	700	8.5
	20C30	2	2	30	20	0.6



# Accumulator Ring Magnet Lattice Plan View

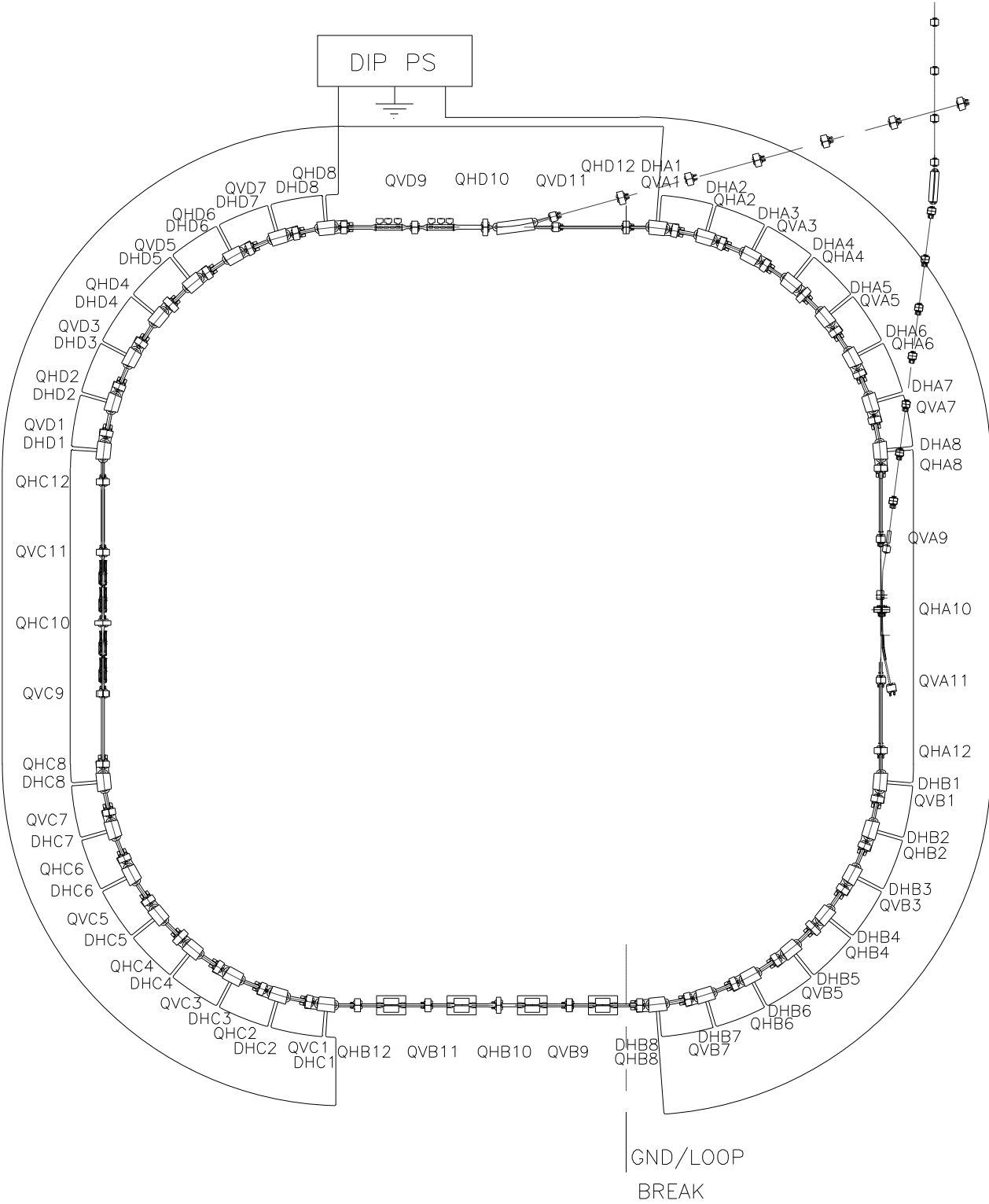


Fig. 5.6-2

# Accumulator Ring Magnet Lattice Plan View

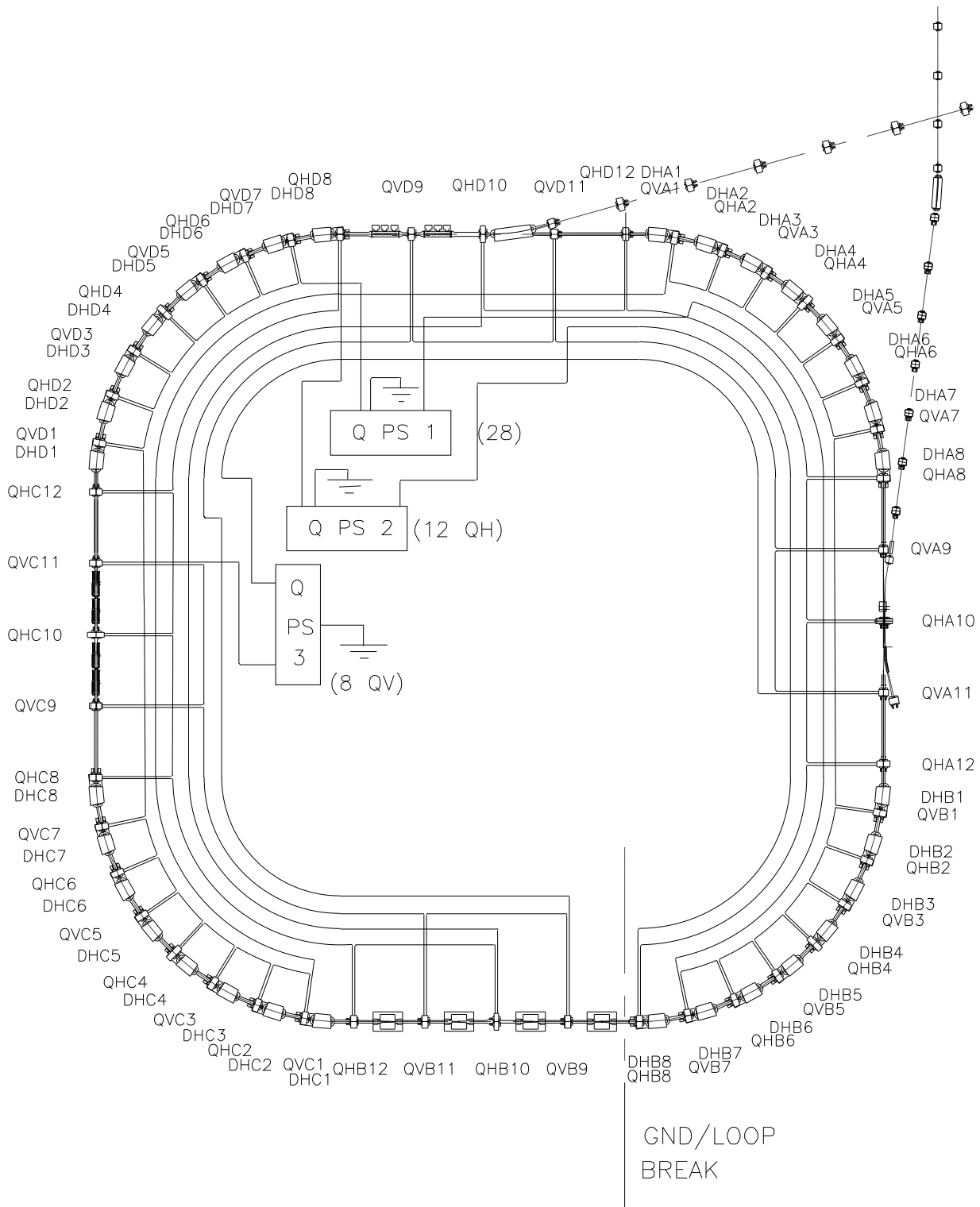


Fig. 5.6-3

# Accumulator Ring Magnet Lattice Plan View

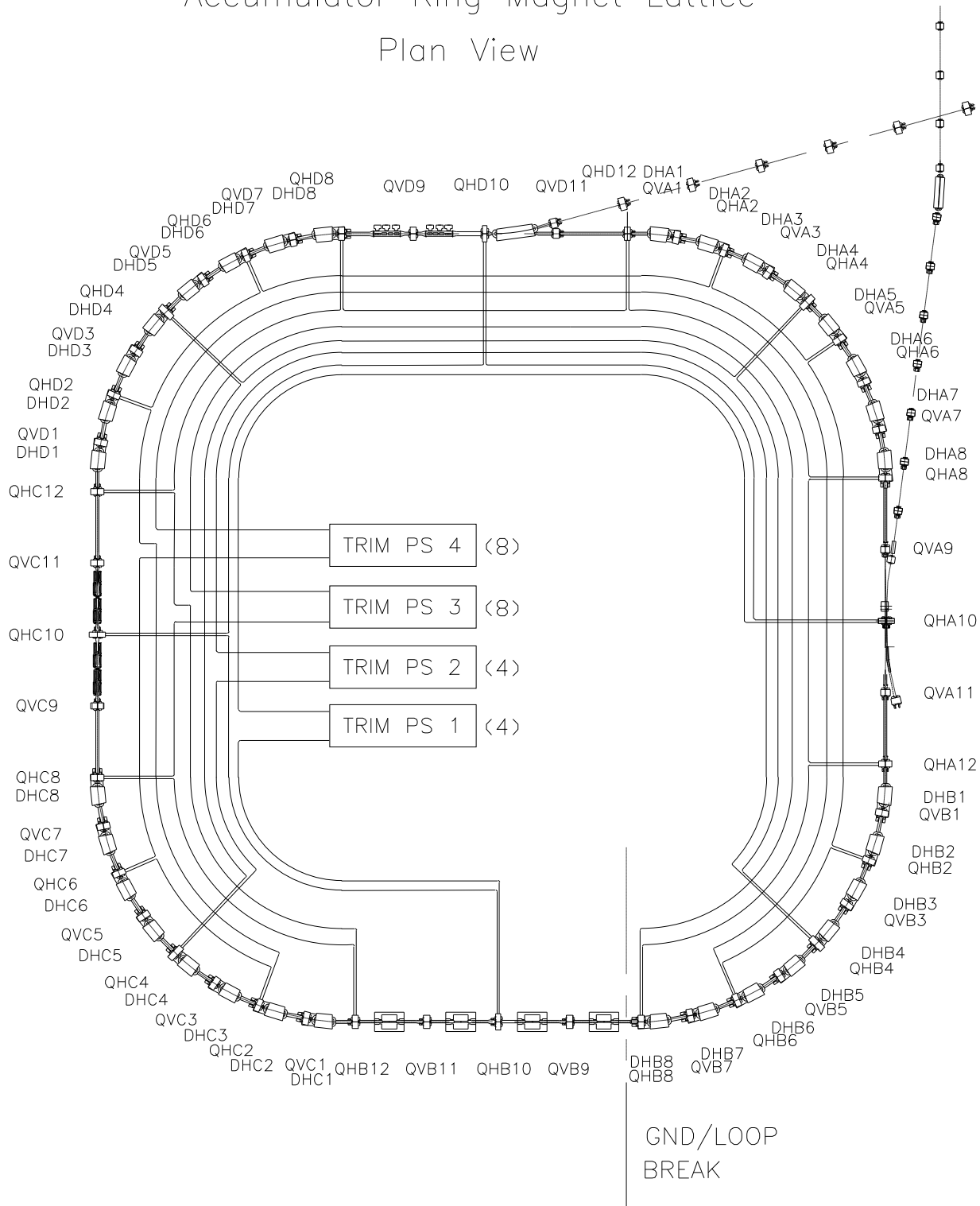


Fig. 5.6-4

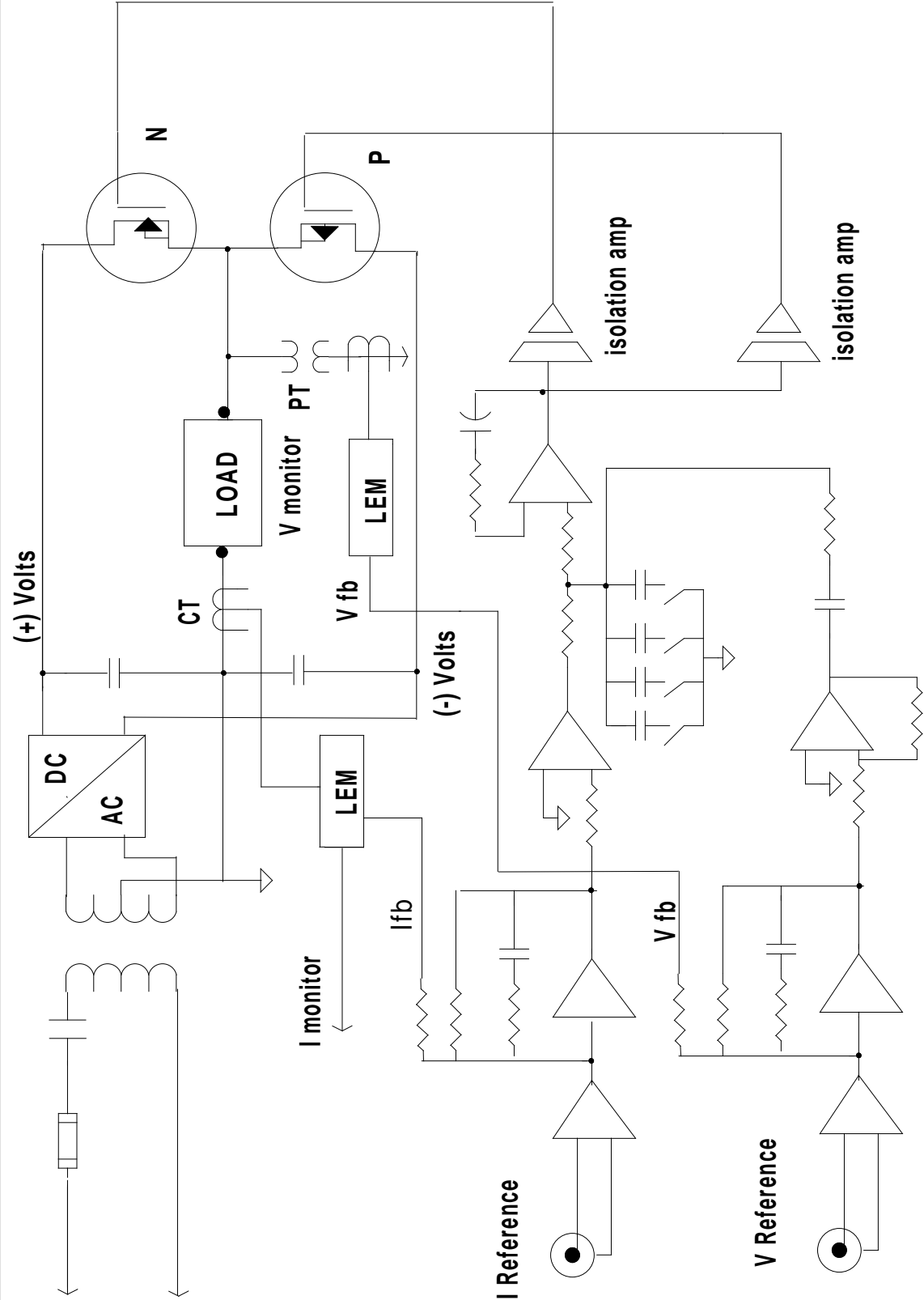


Fig. 5.6-5  
Corrector Power Supply

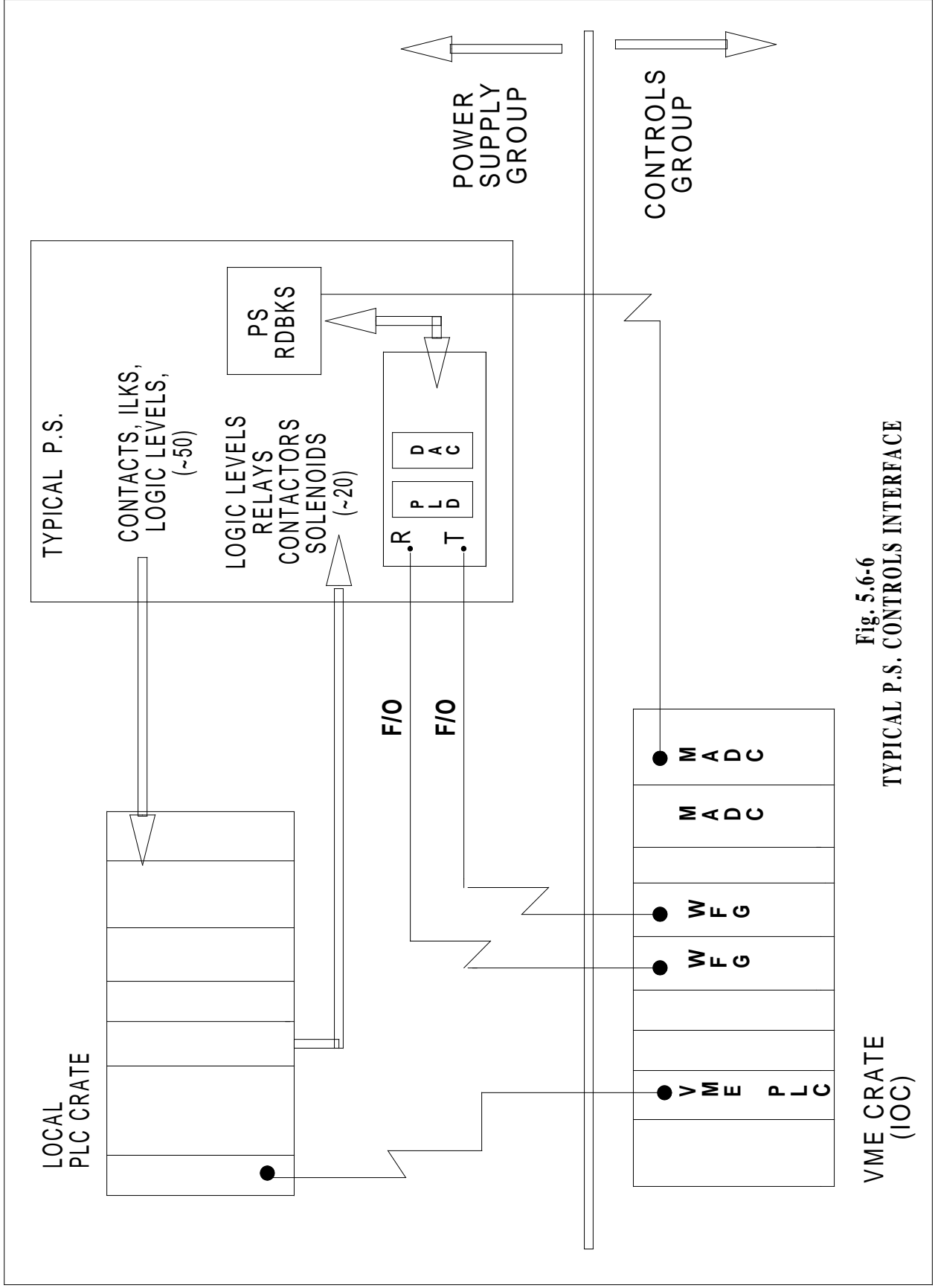


Fig. 5.6-6  
TYPICAL P.S. CONTROLS INTERFACE

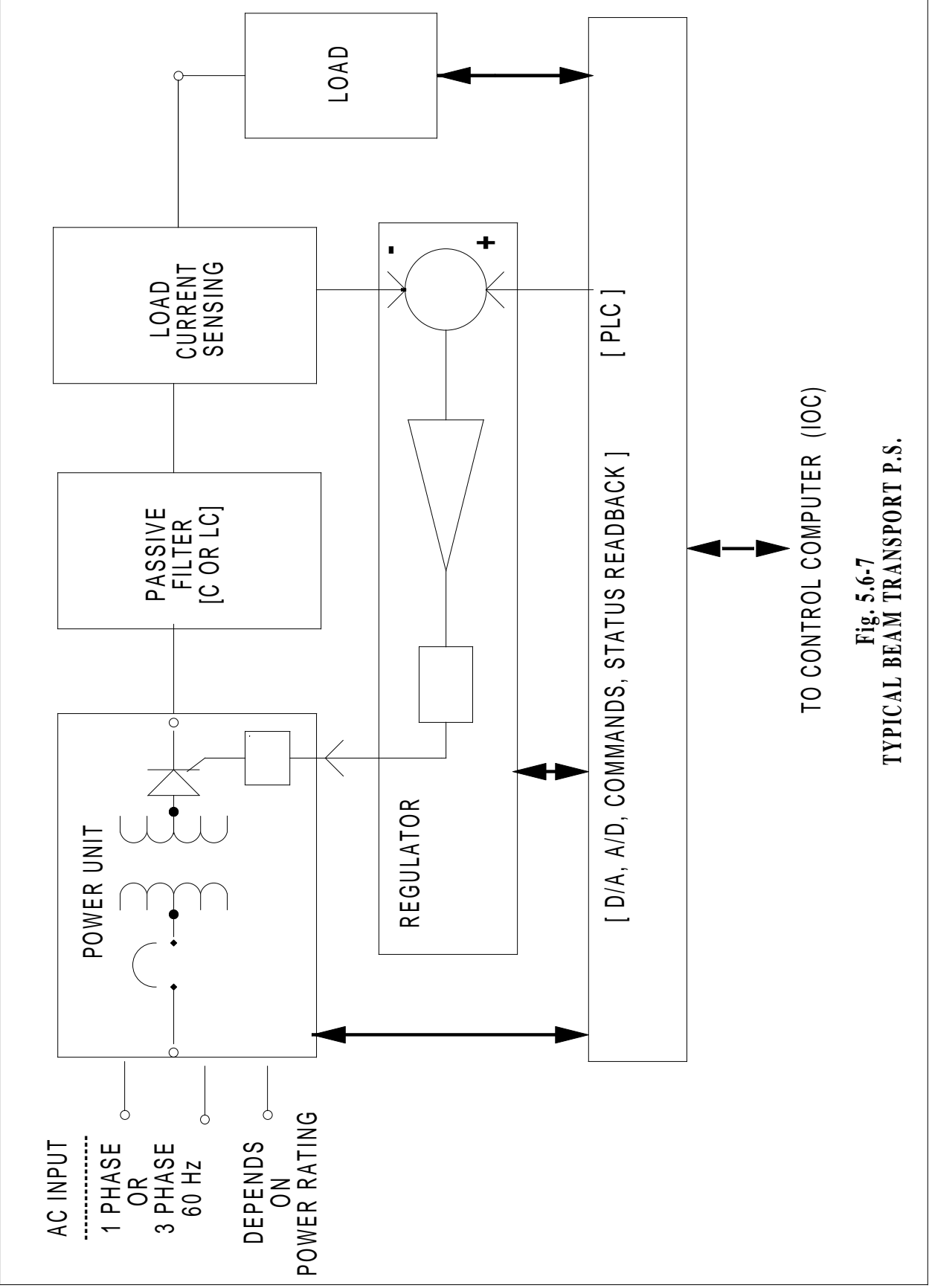


Fig. 5.6-7  
TYPICAL BEAM TRANSPORT P.S.

## 5.7. RING VACUUM SYSTEM (WBS 1.5.5)

### 5.7.1. Scope

The SNS accumulator ring vacuum system will provide a friendly and reliable environment for the proton beam during the one-millisecond accumulation cycle that it spends in the ring.

### 5.7.2. Design Requirement

To avoid the e-p instability, the production of electrons due to beam-residual gas ionization must be minimized. This requires the operating pressure of the vacuum system in the accumulator ring to be  $10^{-9}$  Torr or less.

The ionization cross sections,  $\sigma_i$ , of the 1 GeV protons on the residual gas molecules can be calculated using Bethe formula (Baconnier, 1985):

$$s_i = 4p \left( \frac{h}{m_e c} \right)^2 \left( M^2 \left[ \frac{1}{b^2} \ln \left( \frac{b^2}{1-b^2} \right) - 1 \right] + \frac{C}{b^2} \right)$$

with  $4\pi(h/m_e c)^2 = 1.87 \times 10^{-20} \text{ cm}^2$ , and  $M^2$  and  $C$  the experimentally determined coefficients for different molecules. With a residual gas composition of 40%  $\text{H}_2$ , 40%  $\text{H}_2\text{O}$  and 20%  $\text{CO}$  in the accumulator ring, the average  $\sigma_i$  for 1 GeV proton ( $\beta = 0.875$ ) will be  $\sim 6 \times 10^{-19} \text{ cm}^2$ . At the designed vacuum of  $1 \times 10^{-9}$  Torr, the residual gas density,  $n$ , is equal to  $\sim 3 \times 10^7$  molecules/ $\text{cm}^3$ . The rate of electron production is then given by:

$$\frac{dn_e}{dt} = n s_i N(t)$$

with  $N(t)$  being the instantaneous number of protons in the ring. Integration and averaging of the above equation over the one millisecond cycle gives  $\sim 3 \times 10^{-4}$  electrons per proton, which is negligible (Ruggiero, 1997) in comparison with the production of the electrons from other mechanisms.

### 5.7.3. Ring Vacuum Layout

The accumulator ring, with a circumference of 220 m as shown schematically in Fig. 5.1-1, has four arc regions and four long straight regions. The vacuum system can be conveniently divided into eight vacuum sectors, four arc vacuum sectors and four straight vacuum sectors, isolatable with all-metal pneumatic gate valves positioned at both ends of the straight sections. The arc vacuum sectors are  $\sim 32$  m long, consisting of eight halfcell vacuum chambers each 4 meters long. The straight vacuum sectors are  $\sim 23$  m long, consisting of four quartercell chambers as well as special chambers for injection, collimation, rf, instrumentation and extraction. A list of ring vacuum components and their parameters are given in Table 5.7.1.

**Table 5.7.1. Accumulator Ring Vacuum System Components**

Description	Number of Units	Length
Halfcell Chambers	32	4 m
Straight Region Quadrupole Pipes with BPM	16	~1.2 m
Straight Region Special Chambers	16	~4.2 m
RF-Shielded Gate Valves	8	
Sputter Ion Pumps, 200 l/s	64	
Titanium Sublimation Pumps, 1000 l/s	64	
Cold Cathode and Pirani Gauges	16	
Residual Gas Analyzers	8	
Turbopump/Dry Pump Stations, 200 l/s	8	

Only UHV-compatible materials, i.e., metals and ceramics, are used in the construction of the vacuum system. No elastomer or organic materials are allowed. Stainless steel, for its good mechanical/vacuum properties and the ease of fabrication, has been selected as the preferred material for the halfcell and quartercell chambers. Conflat-type flanges and seals will be used to join the chambers together. In a few locations with potentially high background radiation, such as injection, extraction and collimator regions, quick-demountable type flanges and seals will be used, therefore minimizing the radiation exposure during machine maintenance periods. All chambers will be chemically cleaned and assembled in a clean environment to minimize contamination.

### 5.7.3.1. Halfcell Chambers

Fig. 5.7-1, dimensions in inches, shows a standard arc sector halfcell chamber. The 2 meter long dipole chamber will have an elliptical cross section of 23 centimeter (H) x 16 centimeter (V) inner dimensions. It will be curved with a bending angle of 11.25 degrees and made of 316LN stainless steel. The top and bottom halves of the dipole chamber section will be made by forming and rolling sheets which are then TIG welded together. Alternatively, the dipole chamber can also be extruded and then welded at two mitered locations, which requires a slightly larger horizontal width. To minimize the deflection of the chamber under the vacuum load, the wall thickness of the dipole sections will be ~ 4 mm (Brodowski, 1998). There will be a tapered transition from the dipole chamber to the round quadrupole pipe. The quadrupole section has an I.D. of 19 cm and will be made of seamless stainless steel tubes.

To meet the required precision, the beam position monitor (BPM) housing will be machined from a heavy wall stainless steel cylinder. The BPM housing and the electrodes will be aligned on an X-Y table before being e-beam welded to the quadrupole pipe. The quadrupole section will then be joined to the dipole section with an automatic welder on a precision fixture. The short pump section contains the bellows and the pump port and will be made of 316L stainless steel. The flange end of the pump section will be tapered to match the elliptical cross section of the adjacent dipole chamber. To minimize the radiation induced stress corrosion, the thin wall bellows will be made of Inconel. The pump port with an 8" Conflat-type flange will be

screened with >80% transparency for evacuation. Side ports of 2-3/4" Conflat flanges will be provided at the pump section for other vacuum hardware such as vacuum gauges, residual gas analyzers and roughing valves. The pump section and the 12" end Conflat flanges will be TIG welded to the dipole/quadrupole chamber. The completed half cell chambers will be wrapped with a thin layer of kapton insulation before installation into the "opened" magnets.

### 5.7.3.2. The Straight Section Chambers

Each straight vacuum sector will have a special chamber for housing the injection, the collimators, the rf cavities, or the extraction equipment as well as four quartercell chambers. The quartercell chamber consists of a quadrupole pipe, a BPM section, a pump port, a bellows, and flanges and will be made of stainless steel. The fabrication of the quartercell chambers will be similar to that of the halfcell chambers. The design of the special chambers will follow closely the design of the special components to ensure that both the beam and the vacuum requirements are met. Large Evac-type V flanges and the Helicoflex Delta seals will be developed for some of these special chambers.

### 5.7.4. Pump Down, In-situ Bake, and Conditioning

The eight ring vacuum sectors will be isolatable with all metal gate valves. Vacuum sensors (i.e., vacuum gauge and ion pump readings) upstream and downstream of the gate valves will interlock the valves, thereby protecting the entire ring from catastrophic failure. The valves also allow the repair and modification of the components without venting other regions to ambient air. Turbomolecular pump stations backed by dry mechanical pumps will be used to pump down the vacuum sectors and to maintain the vacuum during an in-situ bake. The arc vacuum sectors and the major portion of the straight vacuum sectors will not be in-situ baked. However, a few special components, such as injection and extraction kickers which have large quantity of high-outgassing ferrites inside the vacuum chambers, must be in-situ baked to lower their outgassing by a few decades to the  $10^{-12}$  (Torr-l)/(sec-cm<sup>2</sup>) level. These chambers will be wrapped with custom heating jackets and instrumented with thermocouples. The bakeout will be carried out using mobile bakeout carts with industrial programmable logic controllers and PC-based software to control and monitor the bakeout process.

After initial roughing, the high vacuum pumps will be conditioned and activated. The high linear conductance provided by the large aperture of the halfcell and quartercell chambers makes distributed pumping unnecessary. Lumped pumps will be used. One sputter ion pump of ~ 200l/sec will be installed at each chamber. In addition, titanium sublimation pumps of ~ 1000l/sec each, built inside the sputter ion pump housing, will be used to augment the sputter ion pumps. The net pumping speed at the pump port will exceed 500 l/sec.

The thoroughly cleaned stainless steel chambers will have a unit outgassing rate,  $q$ , of ~  $1 \times 10^{-11}$  (Torr-l)/(sec-cm<sup>2</sup>), several days after pump down from atmosphere. Pressure inside the chambers can be calculated by:

$$P(x) = Q \left( \frac{L}{S} + \frac{L^2 - x^2}{2C'} \right)$$

with Q being the outgassing per linear length ( $=q \times \text{the perimeter} \approx 1 \times 10^{-9} \text{ \{Torr-l\}/\{sec\text{cm}\}}$ ), 2L the distance between pumps ( $2L = 400 \text{ cm}$  in the arc sectors), 2S the pumping speed at the neck of the pump ( $2S = 500 \text{ l/s}$ ), C' the linear conductance of the chamber ( $\sim 3 \times 10^5 \text{ \{l cm\}/sec}$  for  $\text{H}_2$ ,  $\sim 1 \times 10^5 \text{ \{l-cm\}/sec}$  for  $\text{H}_2\text{O}$  and  $\sim 8 \times 10^4 \text{ \{l cm\}/sec}$  for CO), and x the distance to the nearby pump (x = 0 at the pump and x = L halfway between the pumps). The pressure distribution in the halfcell chamber with no beam is shown in Fig. 5.7-2. The average pressure will be  $\sim 7 \times 10^{-10}$  Torr.

With beam present, protons will ionize the residual gas molecules. The newly created ions, repelled by the beam-wall potential, will bombard the chamber wall and desorb molecules. Each ion with  $\sim \text{keV}$  energy (Hseuh, 1997) will desorb  $\sim 5$  molecules from the unbaked stainless steel surface. The equilibrium pressure in the chamber with the beam will then be given by (Fischer, 1973):

$$P(I,x) = \frac{Q}{C'W^2} \left[ \frac{\cos Wx}{\cos WL - \frac{WC'}{S} \sin WL} - 1 \right]$$

where  $W^2 = I \sigma_i \eta / C'$ , I being the average proton intensity over the 16 millisecond cycle, and  $\eta$  being the average number of molecules desorbed from the stainless steel surface by an incident ion. The pressure distribution inside the halfcell chambers is plotted for  $\eta = 5$  and  $\eta = 10$  also in Fig. 5.7-2. Due to the large linear conductance of the chambers and the high pumping speed available, the pressure increase due to ion desorption is less than 10% even for  $\eta = 10$ . No pressure bump instability is expected.

The pumping requirement in the four straight regions will be modeled with the detailed design of these regions. The designed vacuum will be achieved by positioning large pumps adjacent to the high outgassing components such as the extraction kickers.

### 5.7.5. Vacuum Instrumentation

Two sets of Pirani and cold cathode gauges (CCGs) will be installed at each vacuum sector as primary vacuum gauges. The convectron type Pirani gauges cover the pressure range from 1000 Torr down to  $10^{-3}$  Torr, while the inverted-magnetron CCGs cover the pressure range from  $10^{-3}$  Torr to  $10^{-10}$  Torr. One quadrupole type residual gas analyzer (RGA) will be installed at each vacuum sector and will provide a quick analysis of the partial pressures around the ring. The sputter ion pumps (IP) will be powered by 5kV high-voltage switching controllers, which are capable of reading current down to sub microampere levels. The pump current, proportional to pressure, will give a more detailed pressure profile around the ring. The titanium sublimation pumps (TSP) will be powered by constant-current type power supplies and will be energized for only a few minutes each week. All the gauges, the residual gas analyzers, the controllers and the power supplies are commercially available.

Due to the radiation level in the tunnel, all the electronics including gauge controllers, ion pump controllers and TSP power supplies will be located at the ring support building. A schematic diagram of the vacuum instrumentation is depicted in Fig. 5.7-3. All controllers will have remote control capabilities in addition to front panel switches. They will communicate with the vacuum programmable logic controllers (PLCs) through RS-485 type serial links for remote monitoring and control. Four PLCs are needed for the vacuum systems, two for the ring, one for HEBT and one for RTBT. The PLCs with PC-based LabView type application software will provide the interlock logic and the on-line menu for the operation of the sector gate valves. An ethernet link will connect the PLC to the front-end computer and the main control console for monitoring, logging, and control of the vacuum devices. The residual gas analyzers will be operated with LabView type software through a portable PC. Hardwired interlocks will connect the PLCs to the beam permit chassis and abort the beam in the event of a vacuum fault.

### **5.7.6. References**

- Baconnier, Y., Proceeding CERN Accel. School, CERN 85-19, pp267-300, Nov. 1985.  
Brodowski, J., Private Communication, January 1998.  
Fischer, E. and Zankel, K., CERN-ISR-VA/73-52, Nov. 1973.  
Hseuh, H.C., BNL/SNS Tech. Note #15, February 1997.  
Ruggiero, A.G. and Blaskiewicz, M., BNL/SNS Tech. Note #8, January 1997.

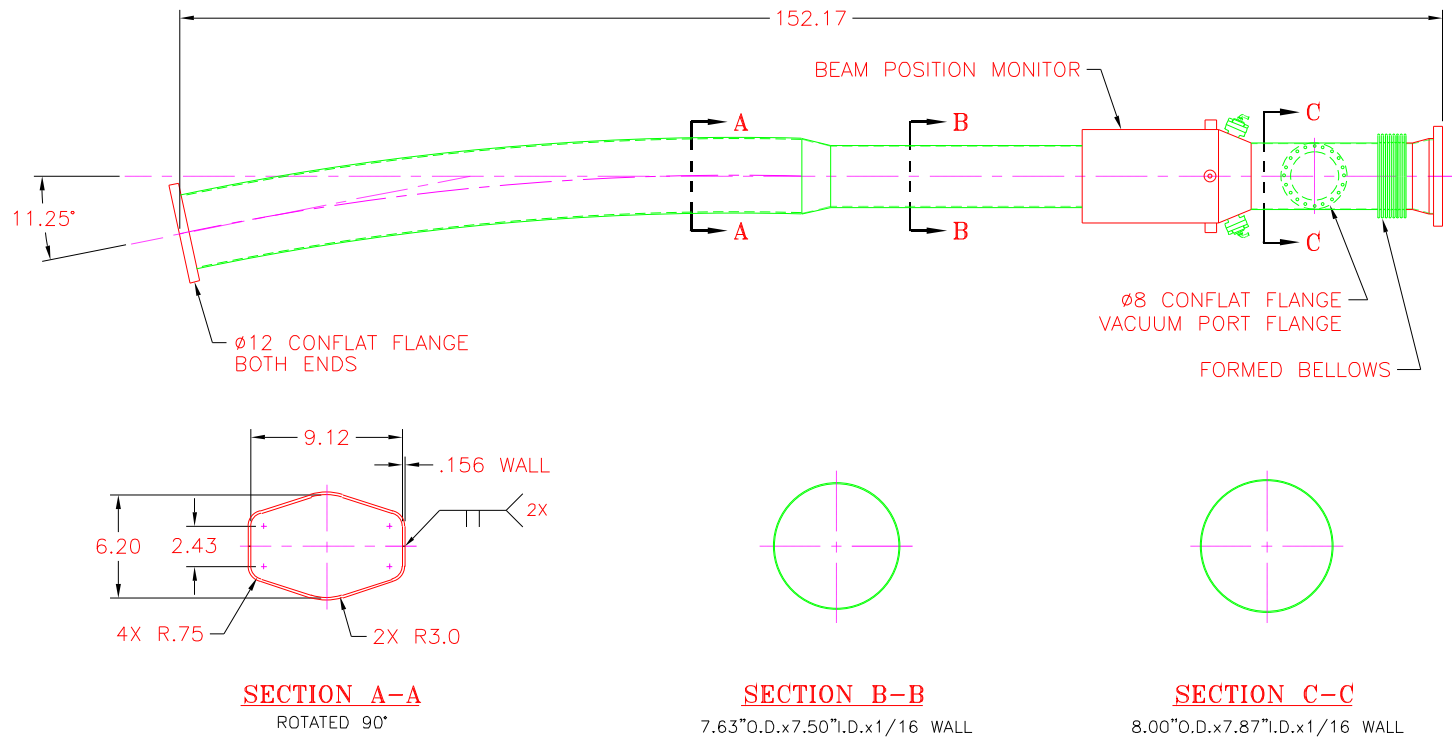


FIG. 5.7-1 SNS ACCUMULATOR RING  
ARC SECTOR HALFCCELL  
VACUUM CHAMBER ASSEMBLY

**Fig. 5.7-2.**

**Pressure in SNS Accumulator Ring Arc Sectors  
with different desorption coefficients**

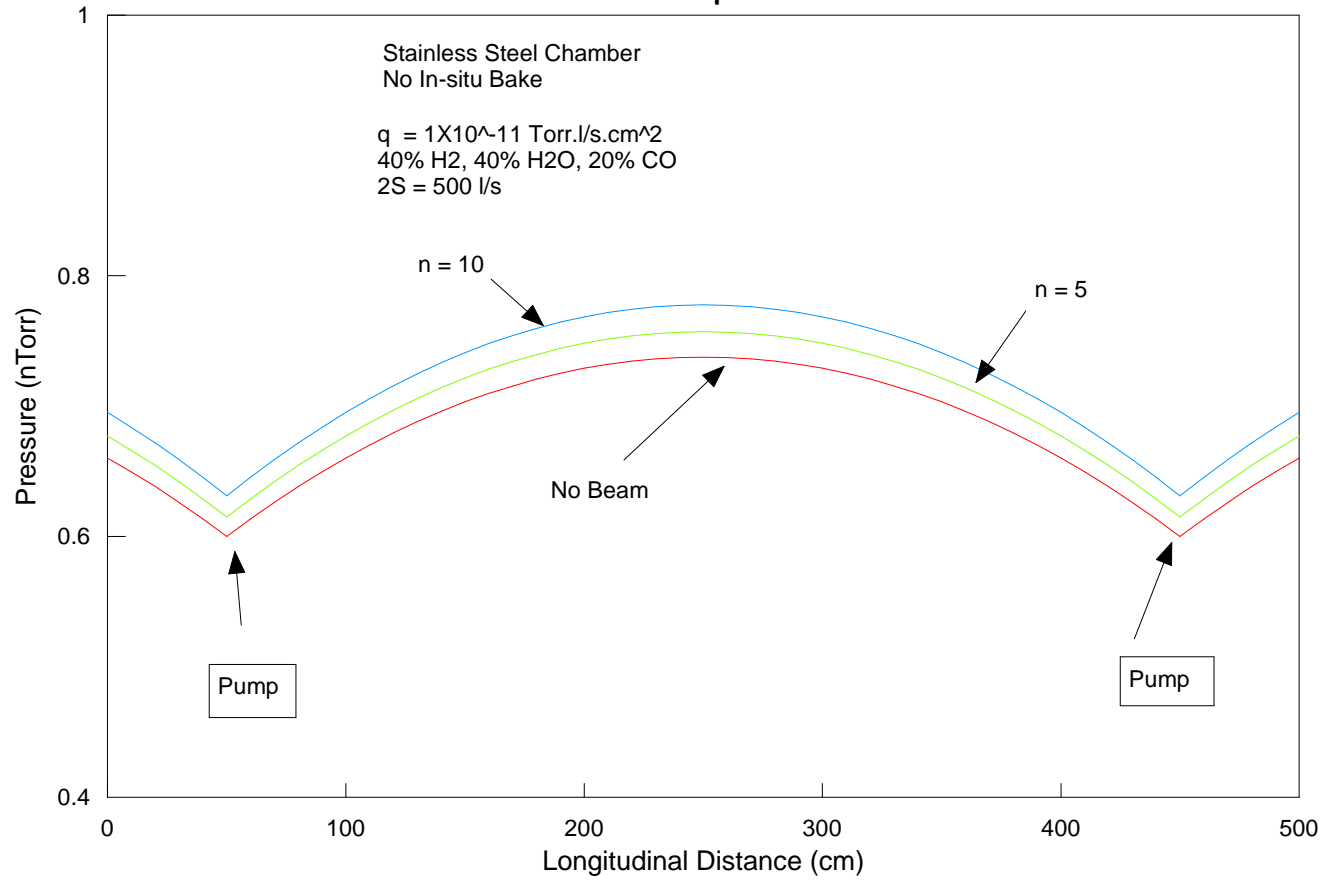
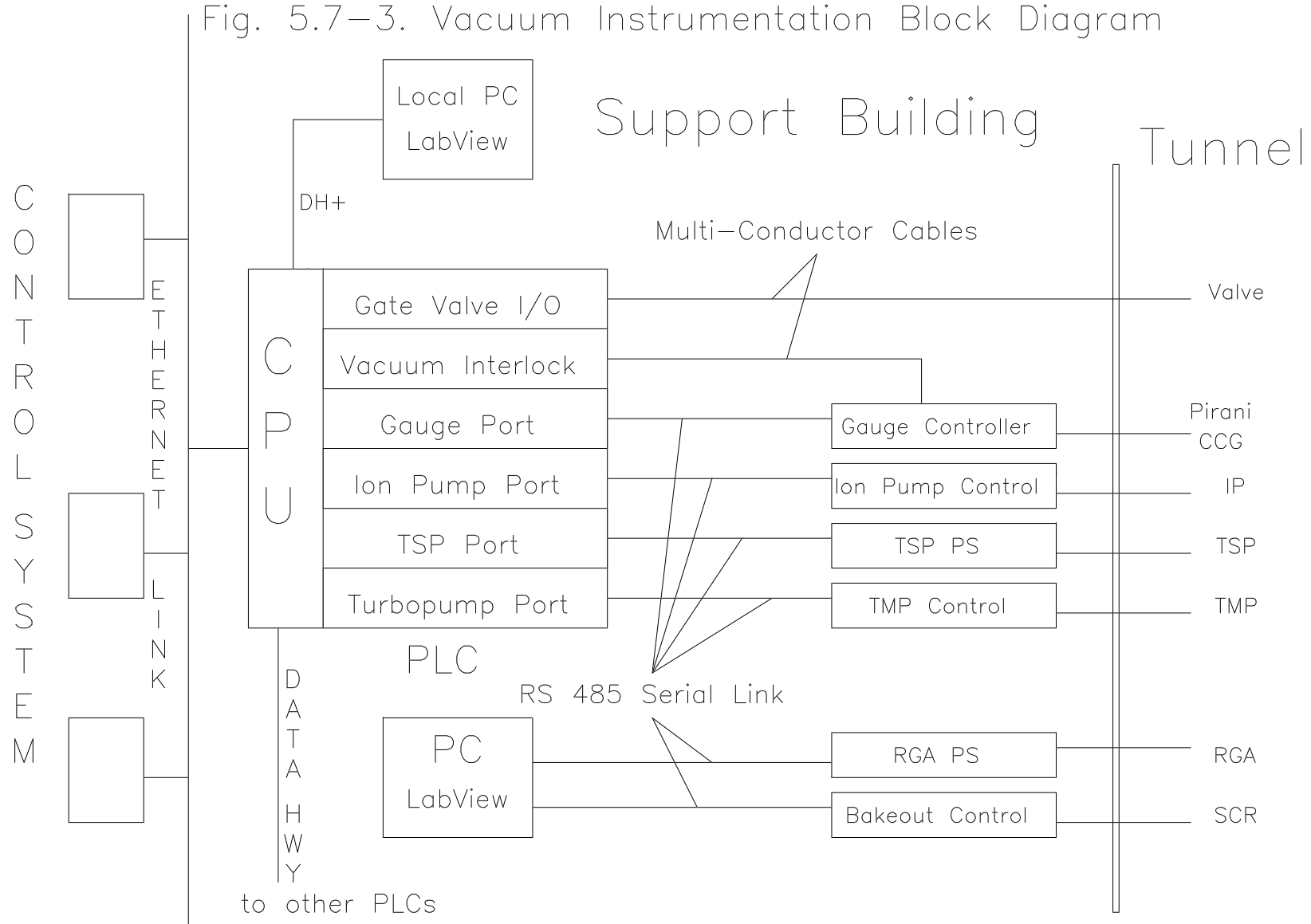


Fig. 5.7-3. Vacuum Instrumentation Block Diagram



## 5.8 THE RF SYSTEM (WBS 1.5.6)

### 5.8.1 Scope

The SNS includes an accumulator ring with a circumference of 220.7 meters that is designed to accumulate  $2 \times 10^{14}$ , 1-GeV-kinetic-energy protons in 1 ms, via charge exchange injection of H<sup>-</sup>. After the beam is accumulated, a kicker magnet will extract the beam in one turn. A 250 ns gap is required to allow for the 200 ns kicker rise time, and the accumulator ring design requires a radio frequency (rf) system to maintain the gap during the injection process. This section describes the accumulator ring rf system.

### 5.8.2 Design Requirements

The requirements for the rf system are listed in Table 5.8-1. Previous work (Blaskiewicz, 1996) has established that a dual harmonic rf system with  $h=1$  and  $h=2$  components has significant advantages over a single frequency system. A barrier bucket rf system maybe even better but there are unresolved issues, such as beam loading, which require more R&D. Therefore, the baseline design for the ring rf system is a dual harmonic system running with  $h=1$  and  $h=2$ . The possibility of upgrading to a barrier cavity system will be considered.

The design has a rf amplitude of 40 kV at  $h=1$  and 20 kV at  $h=2$  with the voltages phased so that the small amplitude synchrotron frequency vanishes. The relevant parameters of the rf system are summarized in Table 5.8-21. Along with the zero current calculations, longitudinal beam dynamics simulations have been done. The code includes space charge, wall resistance, and beam loading for  $h=1$ . Fig. 5.8-1 shows the simulation results.

### 5.8.3 Cavity Design

The harmonic numbers of one and two require cavity frequencies of 1.188 MHz and 2.376 MHz. A variability of  $\pm 5\%$  will be built into the cavities to accommodate changes in beam energy. This would be a slow mechanical adjustment, probably turning a knob on a variable capacitor, and would be very infrequent.

For the SNS,  $h=1$  system we expect to use three cavities, with two gaps per cavity and 6.7kV per gap. There will be one power amplifier per cavity to compensate the heavy beam loading at  $h=1$ . The SNS  $h=2$  rf system will consist of one cavity with two gaps at 10kV per gap, driven by a single power amplifier. Both types of cavities will be identical except for the external capacitance across the gap. Each cavity will have a flange to flange length of about 1.7 meters and two cavities will fit between adjacent quadrupoles in a straight section. All four cavities will occupy one half of one straight section. The current design calls for an unbiased inductance per gap of  $15\mu\text{H}$ , which is determined by the maximum rf field the ferrite can support. A bias field will be needed to align the ferrite domains so that the necessary field can be reached. The biased inductance will be between 7 and  $10\mu\text{H}$ . For  $10\mu\text{H}$  as the biased cavity inductance, the external capacitance will be 1.8 nF for  $h=1$  and 0.45 nF for  $h=2$ . This yields a total R/Q of  $450\Omega$  for  $h=1$  and  $300\Omega$  for  $h=2$ .

### 5.8.4 Design of the Power Amplifier

The design of the entire rf system and the power amplifier in particular is driven by beam loading requirements. From Fourier analysis of Fig.5.8-1 the beam current at  $h = 1$  has an amplitude of 52 Amps at the end of the SNS cycle. The  $h = 2$  beam current is only 4 Amps at the end of the cycle. The design requires the power amplifier to fully compensate the beam current while providing the very-small quadrature component to drive the gap voltage. In some sense this may be pessimistic but the consequences of this assumption to the overall system cost are not great, whereas the benefits for system performance and reliability are very valuable.

Given the difference in beam current harmonic amplitudes only the  $h = 1$  system needs to be considered. With two gaps driven by each power amplifier the PA must be capable of delivering current with a harmonic amplitude of 104 Amps at a voltage with a harmonic amplitude of 6.7 kV. The Thompson TH558 tetrode is well matched to these requirements. Detailed design considerations may be found in Blaskiewicz,1997. The TH558 was designed in the 70's and is used in more than 200 sockets, mostly for radio stations. With this device the tetrode resistance will be  $375 \Omega$  so that the total shunt impedance seen by the beam will be  $4.5 \text{ k}\Omega$  for  $h=1$  and  $1.5 \text{ k}\Omega$  for  $h=2$ . The quality factors will be  $Q=10$  for  $h=1$  and  $Q=5$  for  $h=2$ .

### 5.8.5 Cavity Tuning

A cavity tuning supply is included in the design. Its primary purpose is to maintain the bias needed to align the ferrite domains. Additional uses include maintaining the cavity resonant frequency during the injection of 40 amperes of dc beam current and ensuring that the cavity resonant frequency remains optimal when there are changes in the linac energy. It is also possible that dynamic cavity tuning will be a useful option. Creating a dc magnetic field in the ferrite rings of the accelerating cavities, thus changing their permeability,  $\mu$ , brings about the tuning. However, the  $\mu$  of a ferrite depends on its past history and there is a time delay between changing the bias field and changing  $\mu$ . The time scale is comparable to the SNS cycle time and the role of dynamic tuning on this time scale is a fertile area of R&D. Since the success of that R&D cannot be guaranteed, the present design is not contingent on dynamic tuning.

### 5.8.6 RF Feedforward and Feedback

As the beam accumulates in the ring, the compensation current from the generator needs to increase. This situation will be dealt with using a feedforward system that will adjust the input into the low-level drive. The simulation results shown in Fig.5.8-1 assume that the compensation current increases linearly over the cycle, and an error of 5% in the compensation current makes little difference in the simulation results. Another option would employ a wall current monitor signal to measure the harmonic amplitude of the beam current and send this signal to the drive.

Along with compensating the beam current, it is also necessary to assure that the system is stable to perturbations in beam energy and phase. The beamloading parameter is given by  $Y = I_b R_t / V_g$  where  $I_b$  is the harmonic amplitude of the beam current,  $R_t$  is the effective resistance of the power amplifier and cavity in parallel, and  $V_g$  is the gap voltage. As a rule of thumb, stability requires  $Y < 2$  while the ring design without feedback has  $Y = 6$ . We will reduce the effective  $R_t$  by using one-turn delay feedback that operates only on the low level drive signal and does not require any additional equipment in the tunnel. Using this technique and assuming a quality

factor of  $Q=10$ , the effective resistance can be reduced by a factor of 4 over a full bandwidth of 200 kHz and stability can be restored for high beam current.

It should be noted that neither of these techniques alters the power requirement from the power amplifier. Basically they all amount to obtaining the best possible drive signal to apply to the power amplifier. The amplifier still has to deliver the current at voltage.

Even with beam loading compensation working effectively it is still essential that the synchronization signal for the linac chopper be derived from the vector sum of the actual gap voltage of the cavities (Brennan, 1988). This assures that even though there will be phase shifts between the low-level drive signal and the actual gap voltages the freshly injected beam will always be deposited in the center of the bucket. The consequences of this slowly varying phase during the macro pulse should be considered for the beam loading in the linac.

### **5.8.7 Barrier Cavity Upgrade**

It is likely that the hardware used for the conventional rf system can be upgraded to a barrier cavity system without significantly changing the high power components and cost. With 8 gaps and 10 kV per gap the beam dynamics appears feasible. Barrier cavity operation will use the  $h=2$  gap capacitance. For a gap voltage of 10 kV and  $R/Q = 150 \Omega$  per gap, the peak power amplifier current is 130 A. Roughly, the tube current will be a square wave with a base value of zero amperes for half the revolution period, and 130 A for the rest of the revolution period. In actual operation, the current pulse will be smooth, and losses in the cavity will need to be compensated. The problem of beam loading in a barrier cavity system is currently under investigation.

### **5.8.8 References**

- Blaskiewicz, M., J.M. Brennan, Y.Y. Lee, BNL SNS Tech Note 9, (1996)  
Blaskiewicz, M., J.M. Brennan, A. Zaltsman, BNL SNS Tech Note 36 (1997)  
Brennan, J. M., L. Ahrens, J. Alessi, J. Brodowski, J. Kats, EPAC, p1003, (1988)

**Table 5.8-1 Requirements for the Ring RF System**

Proton beam energy	1000.0 MeV
Transition gamma	4.933
Macropulse rate	60 Hz
Ring filling time	0.974 ms
Number of injected turns	1158
Protons per macropulse	2.08E+14
Lattice circumference	220.688 m
Injected rms energy spread	2.2 MeV
Ring rotation time	841 ns
Required ring injection pulse length	546 ns
Required ring injection kicker gap	295 ns
Ring extraction pulse length	591 ns
Ring extraction kicker gap	250 ns
Chopped beam on/off current	<1.0E-4

**Table 5.8-2 RF Parameter List**

<b>General Parameters</b>	
Total h=1 voltage	40 kV
Total h=2 voltage	20 kV
Space charge Z/n	i150 Ω
Broadband wall resistance	50 Ω
Proton kinetic energy	1 GeV
Injected bunch length	546 ns
Injected rms energy spread	2.2 MeV
Protons at extraction time	2.08x10 <sup>14</sup>
h=1 beam impedance without feedback	4500 Ω
H=1 beam impedance with feedback	1200 Ω
<b>Zero Current Parameters</b>	
Bucket area	17 eV sec
Bunch area	10 eV sec
<b>Simulation Parameters</b>	
Input	
Macro-particle equivalent length	50 ns
Macro-particles added per turn	10
Number of turns	1250
Output	
Extracted rms energy spread	4.2 MeV
Maximum bunch length	600 ns
Peak bunch current	96 A
Bunching factor	0.42
Gap length at extraction	265 ns

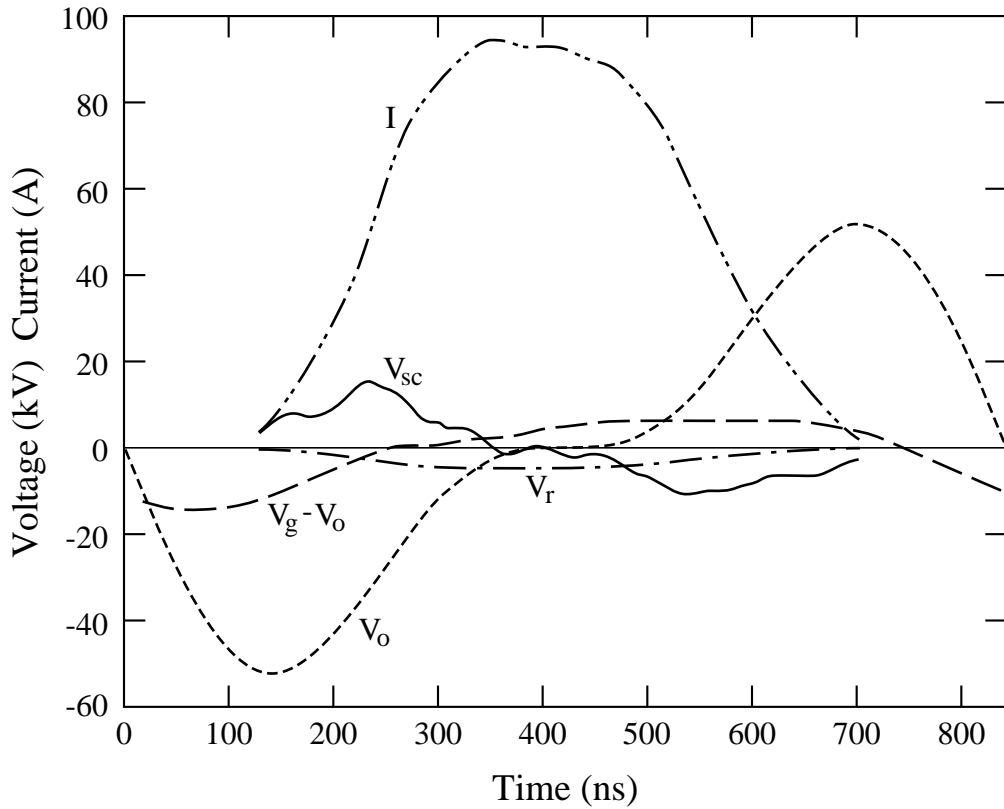


**Fig. 5.8.1: Simulation results for SNS just before extraction including beam loading for  $h = 1$  with one turn delay feedback. Parameters are described in the text and Table 5.8-2.**

**$V_o$  = Ideal RF Voltage**

**$V_g - V_o$  = Actual RF Voltage - Ideal RF Voltage**

**$V_{sc}$  = Space Charge Induced Voltage**

**$V_r$  = Voltage Due To Parasitic Resistance**

**I = Beam Current**

## **5.9 SNS RING BEAM DIAGNOSTIC INSTRUMENTATION (WBS 1.5.7)**

This section will describe all of the beam diagnostic instrumentation that will be in the SNS Ring, which are summarized in Table 5.9-1. Figure 5.9-1 shows the distribution of these devices around the ring.

### **5.9.1. Beam Loss Monitors**

#### **5.9.1.1 Scope**

The primary functions of the Beam Loss Monitor system are to minimize losses by allowing tuning of the beam and preventing injection of subsequent beam following a high loss. Tuning requires that the loss data be continuously acquired and displayed. Programmable threshold detection circuitry will provide an interlock signal tied to the Fast Protect System to prevent beam injection following high loss pulses. This loss monitor system will not be used for personnel protection, which requires fail-safe design and high level certification. Neutron detection is not normally part of the accelerator diagnostics system but may be included as part of the safety system.

#### **5.9.1.2 Design Requirements**

The Ring Beam Loss Monitor (BLM) system will measure the radiation produced by the particles lost from the circulating beam to better than 1 part in  $10^4$  of full intensity. Detectors will be located regularly around the Ring at points of expected transverse losses. Each BLM will be capable of inhibiting further injection if excessive loss is detected. Time resolution will correspond to several turns. Data acquired from the BLMs at a 10  $\mu$ s interval over the full Ring cycle will be available for display and buffered for review in case of beam inhibit.

A limited number of Fast Beam Loss Monitors (FBLMs) capable of observing losses with a single turn will be located at the downstream end of each straight leg and at injection and extraction areas where losses from longitudinal effects might be observed. Data from the FBLMs will be acquired through a separate Bunch Acquisition System, which will take data at a 100 MHz rate.

#### **5.9.1.3 Design Description**

##### Detectors

Ion chambers will be used for the BLM system and scintillator-photo-multipliers will be used to monitor FBLMs.

Ion Chambers are the clear choice for the Beam Loss Monitors in the SNS Ring. Indeed, most accelerators today have made a similar choice. They consist of a gas filled enclosure with a pair or pairs of positive and negative electrodes. Ionizing radiation generates ion-electron pairs along its path, producing a signal as the charges move in the electric field. Argon is used in most accelerator beam loss monitoring applications because it is inert, inexpensive even in high purity, and free of electro-negative carriers such as oxygen that would drastically reduce electron mobility. In some cases small percentages of other gasses, such as methane, are added to enhance the response time. A cylindrical coaxial geometry is the most common, offering simple

**Table 5.9-1 Ring Beam Instrumentation**

DEVICE	QUANTITY	DESCRIPTION
Beam Position Monitors [BPM]	96 planes	Dual plane stripline beam position monitors at each quadrupole
Beam Profile Monitor [BPrM]	2 planes	Residual gas ionization profile monitor
Beam Loss Monitors [BLM]	96	Glass ion chambers located at each quadrupole and at significant loss points.
Fast Beam Loss Monitors [FBLM]	8	Photomultipliers used to look for losses over a single turn or at extraction
Beam Current Monitor [BCM]	1	Simple passive beam current transformer
Fast Current Monitor [FBCM]	2	Wideband beam current transformer
Beam In Gap Monitor [BIG]	1	A monitor of the beam which is outside the RF bucket
Tune Measurement [TUNE]	2 planes	Damper excited, FFT analysis
Transverse Damper [DAMP]	2 planes	Damps transverse instabilities

construction, but parallel plates can provide faster response time, particularly as multiple layers in larger volumes.

Sealed argon filled glass units were developed for the Tevatron at FNAL (Shafer, 1983) are also being used with some modifications in RHIC. The sensitivity of these units is 70 nC/rad. The modifications include non-PTFE connectors and isolated BNCs to break signal ground loops. Measurements made during the RHIC first sextant beam test showed a clean 4-decade range (Witkover, 1997). This was later extended another 2 decades upward by desensitizing the electronics. Response time ranges from 1-2 microseconds for electrons to several milliseconds for ions.

At FNAL, “Paint Cans” containing liquid scintillator were used as the radiation monitors for some years. The PSR also uses this type detector to track fast losses. Scintillator-Photomultipliers offer a wide dynamic range of operation and fast (nanosecond) response but show significant unit-to-unit variation and must be calibrated regularly. Radiation darkening of the scintillator and the glass of the photo-multiplier tube affect the calibration. Due to the unit-to-unit variations and aging, individual controllable HV power supplies be used. The cost of the tubes and their bases is significantly more than ion chambers.

### Location of Detectors

BLMs will be located at each quadrupole in the ring, since the beam is largest (beta-max) at those points, with additional units at injection and extraction and collimators. A number of relocatable BLMs will be placed as operational requirements dictate, bringing the total to 96 channels. The detectors will be mounted as close to the beam pipe as convenient, possibly directly on the vacuum flanges as in RHIC.

Scintillator-photomultipliers (FBLMs) will be installed at the downstream end of each straight section. Several FBLMs will be located in areas such as at injection and extraction where fast losses might provide information about clipping of the bunch ends or losses due to beam in the gap. These will also be useful for observing losses due to instabilities should they occur.

### Electronics

To achieve 1-2  $\mu$ s response only the electron signal is processed, cutting the sensitivity in half. Two approaches to signal conditioning will be investigated. In the first, the signal will be amplified and sampled and held for computer acquisition and display. This provides continuous loss protection but only discrete time acquisition of the losses. In the second, the signal will be amplified and integrated over a 10  $\mu$ s interval and presented for acquisition. “Ping-pong” integrators might be used to eliminate any data dead times. In this case the comparators would follow the amplifier outputs. Because of the wide dynamic range due to the accumulating of beam over 1000 turns, some form of gain change during the cycle will be required. This can be accomplished either in discrete steps or through a programmable gain amplifier. Threshold detectors with programmable reference levels monitor the loss signal and provide a fast beam inhibit within several turns when the trip level is exceeded, allowing the beam to be dumped or inhibited if desired. Data acquisition will be by commercial multi-channel VME digitizers taking data at 10  $\mu$ s intervals with on board storage for the full cycle.

The FBLM signals will be read through VME based fast digitizer channels clocked at the revolution frequency. All of the units at a given location would be buffered and selectable

through a wideband mux to be read into the Bunch Data Acquisition System at 100 mega-samples/second or more to observe losses within the bunch duration.

## 5.9.2 Beam Current Monitors

### 5.9.2.1 Scope

The current circulating in the Ring must be monitored to provide a measure of the cycle intensity. Beam Current Monitors will provide information of the average current, charge density distribution within the bunch and charge which has leaked out of the rf bucket.

### 5.9.2.2 Design Requirements

The beam current in the SNS Ring will be measured non-destructively using several beam current transformers. The design average current (or charge per turn) will vary from 15.4 mA ( $8.1 \times 10^{10}$  protons) for the first turn to 19 A ( $1 \times 10^{14}$  protons) on the last turn injected. Within the bunch the peak current may be twice this value. Charge leaking out of the rf bucket must be monitored since it will be lost and may lead to instabilities. The beam in the gap may be 4 orders of magnitude below that in the bucket so a resolution of better than 5 orders below the bunch peak is required for this measurement.

Average beam current in the SNS Ring will be measured by the BCM. The resolution must be better than 0.1% of full scale and available on a turn by turn basis. The detector, which will be a current transformer, will have a droop of less than 0.1% over the full cycle.

The charge density distribution within the bunch will be measured with the fast current transformer (FBCM). The FBCM must have a risetime of 1 ns or better to observe the 550 ns bunch length, and a droop of at least 100  $\mu$ s. Compensation for this droop will be provided. Acquisition will be through the 100 MHz sampling of the Bunch Data Acquisition System.

The beam which has been lost from the rf bucket and lies between the bunch ends will be measured by a fast beam current with electronics gated to discriminate between the large current in the beam and the small current outside the bucket. Acquisition will be through the 100 MHz sampling of the Bunch Data Acquisition System.

### 5.9.2.3 Design Description

#### Detectors

Two approaches are being considered for the BCM, which will measure the average circulating current. The conventional design uses a standard commercial tape wound Supermalloy core with a 9-inch ID and a 1 inch by 1 inch cross-section. With 1000 turns on the winding this will have an inductance of approximately 50 Henries which will produce a droop time constant of several seconds. Resistors periodically tapping the coil will damp resonances due to the various coil capacitances and inductances. The risetime of this transformer will be about 10  $\mu$ s, which is slow enough that the gap between bunches will not be readily discernable, but will be too slow to see turn-by-turn stacking. The other approach uses a faster rise transformer but with noticeable droop. With 100 turns on the same type core the risetime will be 10 – 20 ns, fast enough to fall to the baseline between bunch ends. The droop time constant will be about 10 ms, causing about a 10% error in the baseline. This can be compensated for in the

electronics. By taking the integral of the current in the bunch and sampling at the end of the bunch, the turn-by-turn charge can be displayed. This design will better information but is more complicated than the conventional approach.

The FBCM will use a commercially available sensor, a Fast Current Transformer (FCT), manufactured by Bergoz, with a risetime of 600 ps but at the sacrifice of a droop time constant of 100  $\mu$ s.

The BIG transformer, which will require a 10-25 ns risetime and a 1 second droop, will have to be developed specially for this application. Test with the 100 turn coil indicate that the rise and droop time constants are possible, however, further work is required to determine if the fall after the bunch will settle to  $10^{-5}$  in a suitable time.

All three units will be housed on a 0.3 meter section of beam pipe with a ceramic break to prevent the image currents from passing through the transformer aperture. A properly designed outer cover will allow the wall current to gracefully pass around the transformer section. Separate transformers will be used since the electronics must be tailored for each application.

### Electronics

The electronics for the BCM will depend on which design approach is selected. In the case of the conventional transformer the long droop time constant negates the need for a baseline restorer and a simple amplifier will suffice. The signal will then be digitized with the 200 kilo-sample/second ADC used for the BLM acquisition. This output will also be available for direct viewing if desired. If the design that allows stacking to be viewed is selected then a baseline restoration circuit is required. This will be followed by an integrator and a sample and hold. The current will be integrated during the bunch time and acquired by a sample and hold at the end of the bunch. The integrator will then be reset and the baseline restorer triggered to acquire the next revolution baseline. An ADC running at the revolution frequency will read the output sample and hold. The analog signal will also be available to display the current stacking.

The FBCM will require a wideband programmable gain amplifier such as the Analog Devices AD600. This is a very low noise ( $1.4 \text{ nV}/[\text{SQRT}(\text{Hz})]$ ), wideband (DC – 35 MHz) current mode op-amp with a programmable input ladder attenuator of 0-40 dB, which appears to be well suited to this application. The 100  $\mu$ s droop time constant of the FBCM will require a baseline restoration circuit which samples the signal in the gap between bunch ends on each revolution, holds this level and subtracts it from the signal during the bunch time. The output of the FBCM amplifier will then go to the Bunch Data acquisition System for digitization at 100 Mega-samples/second. The baseline-restored output will also be available for direct viewing.

In contrast to the FBCM, with the Beam-In-Gap (BIG), it is not the current in the bunch but rather the much smaller current in the gap between the bunch ends that is of interest. Thus the large bunch signal must not be allowed to saturate the transformer core or the electronics. Correct selection of the core parameters will prevent its saturation, but the resulting signal will be so large that the electronics may lock-up and not recover to view the beam in the gap. To prevent this a fast (10-50 ns) switchable attenuator must precede the amplifier and provide 80 to 100 dB of attenuation. Commercial rf switches are rated at 60 dB isolation but tests have shown that more than 72 dB is typical at under 30 MHz. A programmable gain amplifier such as the AD600 will follow the input attenuator. Calculations of the noise indicate a resolution of  $10^{-5}$  is possible. Data acquisition following the amplifier would be the same as for the FBCM except that it must be timed to occur within the gap rather than the bunch. Baseline restoration is not

straightforward as for the BCM and FBCM where the “zero” sample is taken during the gap. For this reason a different transformer design with a 1-second droop time constant will be used. Even then the offset by the end of the cycle may be much larger than the beam in the gap. Since the data from the BIG will be acquired by the 100 MHz ADC, and the droop time constant of the transformer and load are known, arithmetic correction might be used.

R&D will be required to determine if the attenuator isolation can be achieved and the baseline correction is feasible.

### **5.9.3 Beam Profile Monitor**

#### **5.9.3.1 Scope**

Knowledge of the profile and the beta-function at that location allows the emittance to be calculated. Injection errors due to poor painting or mismatch, and instabilities, which will cause emittance growth through the cycle, can also be observed. Measurement of the profile in each plane will provide this information.

#### **5.9.3.2 Design Requirements**

The profile must be measured non-destructively to prevent beam loss and activation of the ring. The profiles must cover a range of  $\pm 80$  mm with a bin size of 2.5 mm. The effect upon the beam, whether due to scattering or orbit distortion, must be minimal. Measurements must be available throughout the cycle, preferably on each turn, but not every cycle: typically at start-up, for studies and for parameter set logging.

#### **5.9.3.3 Design Description**

Interceptive techniques using scrapers or thin carbon wires rapidly moved across the beam pipe (Flying Wires) will cause too much loss and soon be destroyed by the beam. An ionization profile monitor makes use of the interaction of the beam with residual gas molecules in the vacuum chamber. Depending on the bias voltage polarity, the ions or electrons generated are accelerated to an array of collectors that provide the profile information. To prevent the high space charge field due to the beam from spreading the profile, an electric field much stronger than the space charge field must be applied. With large apertures, such as in the SNS Ring, this will lead to very high voltages. If electrons are collected then a parallel magnetic field may be used to confine them within the Larmor radius, as in RHIC where the space charge problem will be even more severe.

For an applied field of 2500 V/cm, (50 kV) ions will have a typical transit time of the order of a microsecond while electrons will be collected in 2 ns, suitable for turn-by-turn measurements. The electrons will be displaced by the beam space charge field and acquire a transverse velocity. For a Gaussian density distribution, a beam of  $2 \times 10^{14}$ , beta max of 16 and an emittance of 120 pi mm mrad, the peak electric field will be 990 V/cm (Weisberg, 1981) which will impart a transverse velocity 33% of that due to the applied field. This will result in significant profile broadening unless a stabilizing magnetic field is applied parallel to the electric field. For a 1-kG field the Larmor radius will be under 0.1 mm for electrons created with 10 eV or less. To prevent the magnet from causing a distortion of the circulating beam orbit, half-length magnets of the same field strength but opposite polarity will be located fore and aft of the

detector. The range of 160 mm will be covered using 64 channels, each of which will be about 2.5 mm wide, much larger than the Larmor radius.

For a vacuum of  $1 \times 10^{-9}$  Torr and  $2 \times 10^{14}$  protons, the central electrode will collect 2-300 pico-A/cm length. Microchannel plates can provide a gain of up to  $10^7$  making the signal sufficient for single turn measurements. However during the early turns, especially for collectors away from the beam center, the statistics are too low to be meaningful. To improve the statistics a local pressure bump to  $10^{-7}$  Torr will be required during the time profile measurements are being made. Careful design of the controlled gas leak and the inclusion of a pneumatic controlled mechanical vacuum isolation valve between the leak and the chamber will be required to guard against an uncontrolled pressure increase.

Provisions to gate the microchannel plate bias voltage will be required to prevent plate depletion.

A 1-meter section of beam pipe in an each of 2 straight sections has been reserved for the profile monitors.

## **5.9.4 Beam Position Monitors**

### **5.9.4.1 Scope**

The Beam Position Monitor System will provide closed orbit measurements for the Ring. Stripline detectors will be located in each of the 48 quadrupoles.

### **5.9.4.2 Design Requirements**

Because of the large number of detectors the beam position monitors (BPMs) must present low impedance to the beam to prevent instabilities. Calculations indicate that at  $1 \times 10^{10}$  protons of circulating beam, circuit noise will provide a resolution of 1- mm RMS, improving to 50 microns at  $2 \times 10^{14}$  protons. Position measurements will be made on a turn-by-turn basis with data from multiple cycles stored locally for recall if a beam fault should occur. Data for computation of the closed orbits will be available from the front-end processor on each cycle if desired.

### **5.9.4.3 Design Description**

The dual plane stripline BPMs will be located adjacent to the quadrupole, nestled under the coil ends. It will be keyed to the quadrupole for positive location. The design will make use of techniques developed in the RHIC units. The electrodes will be 30 cm long and subtend an arc of 70 degrees.

The analog electronics (Fig. 5.9-2) will consist of an impedance matching front-end diplexing 0.1 – 5 MHz filter, followed by an amplification stage. Another low pass filter precedes the 12-bit ADCs that sample the signal at 41 mega-samples/second (MSPS). The over-sampled data is then stored in on-board shared VME memory. The data will be digitally processed at the front end to provide the position information. The local memory will be of sufficient size to store several cycles of position history data (useful following a beam inhibit/dump). Upon request averaged, single revolution or the full memory may be obtained.

The wide dynamic range in signal will be covered in 2 ranges. An analog DPDT switch will direct the signal through the 0 dB or –40 dB paths, then into a 256 state programmable gain

(40 dB) amplifier. Switching will require 1-2 turns so only a few gain changes per cycle will be used.

Triggering should be straightforward since the rf is of constant frequency. Delay modules with separate channels for each BPM and nano-second setability will trigger the ADCs.

## **5.9.5 Damper/Tune Measurement**

### **5.9.5.1 Scope**

Transverse beam instabilities may develop which will lead to beam loss. The Damper will detect and correct these instabilities in either plane. Measurement of the tune of the ring will be provided by the Damper system.

### **5.9.5.2 Design Requirements**

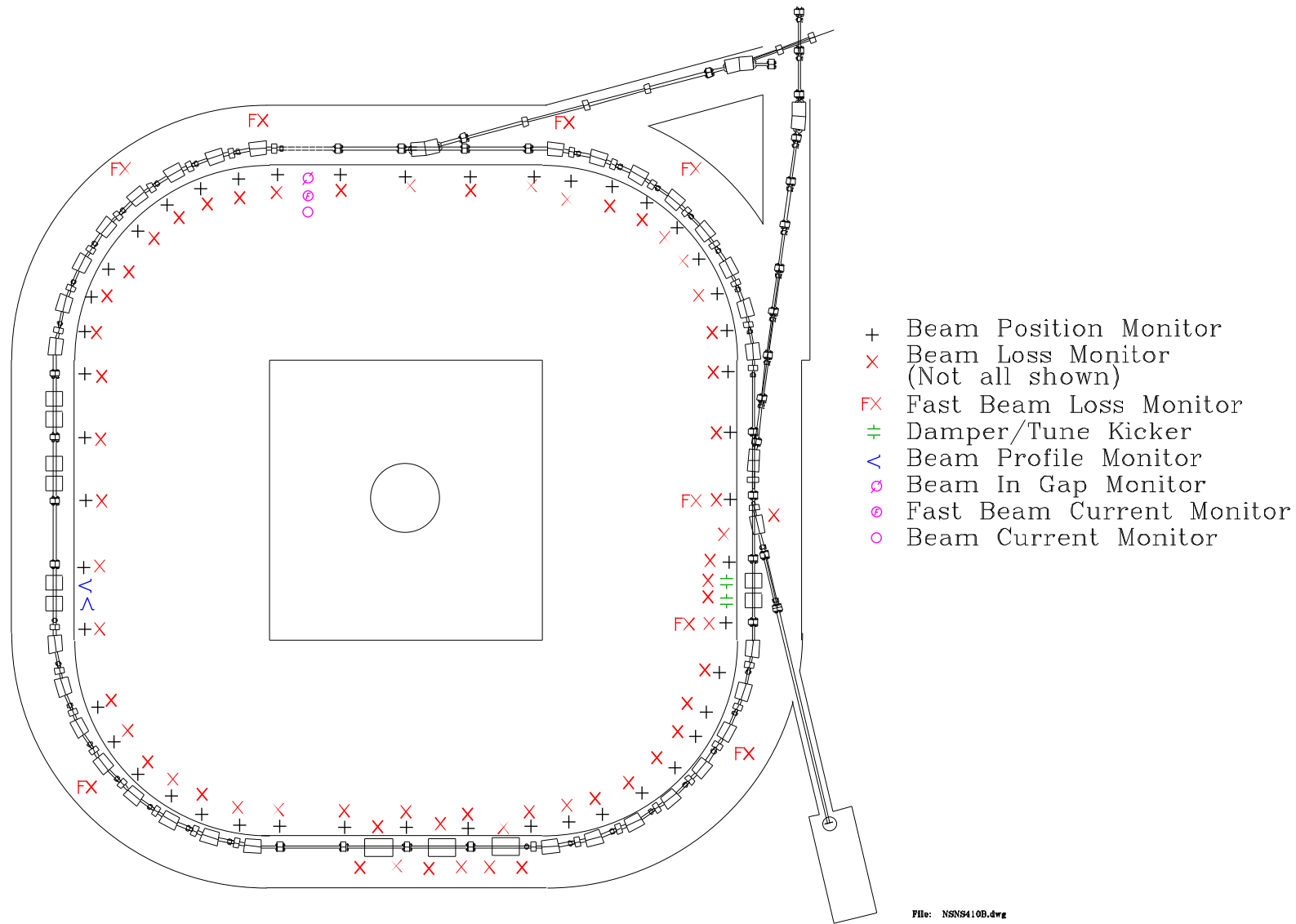
Analysis of the transverse instabilities in the ring (Section 5.2.2.4) will determine the power and bandwidth requirements of the damper. Each plane will be located in a 1-m section of the ring. Measurement of the tune will be done by using the damper kicker to excite the beam oscillations.

### **5.9.5.3 Design Description**

A system similar to that in the AGS (Smith, 1995) will be installed to damp both horizontal and vertical transverse oscillations in the beam orbit. The AGS system takes signals from the beam position pickups and digitally processes them to obtain orbit data. The average orbit is subtracted to determine the excursion of the bunch and a correcting kick amplitude is obtained from a look-up-table (LUT). The kick is delayed using a FIFO and applied to the bunch on a later turn using a wideband 500 Watt rf amplifier to drive a stripline. The tune measurement will be made using the damper to kick the beam. The digital acquisition and processing electronics for each beam position monitor has sufficient memory to store the position for the entire cycle. An FFT analysis of this data is normally used to find the fractional tune. Since the cycle period for the SNS ring is so short, the precision of the FFT method may be limited. While a simple FFT analysis has an estimated error of  $1/N$ , where  $N$  is the number of samples, several other techniques offer  $1/N^2$  or better errors. (Bartolini)

## **5.9.6 References**

- Bartolini, R. Et al, "Algorithms for Precise Determination of the Betatron Tune," CERN SL-96-048
- Shafer, R. E. Et al, 1983, "The Tevatron Beam Position and Beam Loss Monitoring Systems", p 609, Twelfth Intl. Conf. on H. E. Accel.
- Smith, G. A., Castillo, V., Roser, T., Van Asselt, W., Witkover, R., Wong, V., "Digital Transverse Damper for the Brookhaven AGS," Proc. 1995 PAC p 2678
- Weisberg, H. L., 1981, "Beam Profile Monitors for the AGS," AGS Div. Tech. Note 173, July 8, 1981
- Witkover, R., et al, 1997 "RHIC Beam Loss Monitor System Design," Proc. 1997 Part. Accel. Conf, To Be Published



File: NSNS410B.dwg

Fig. 5.9-1

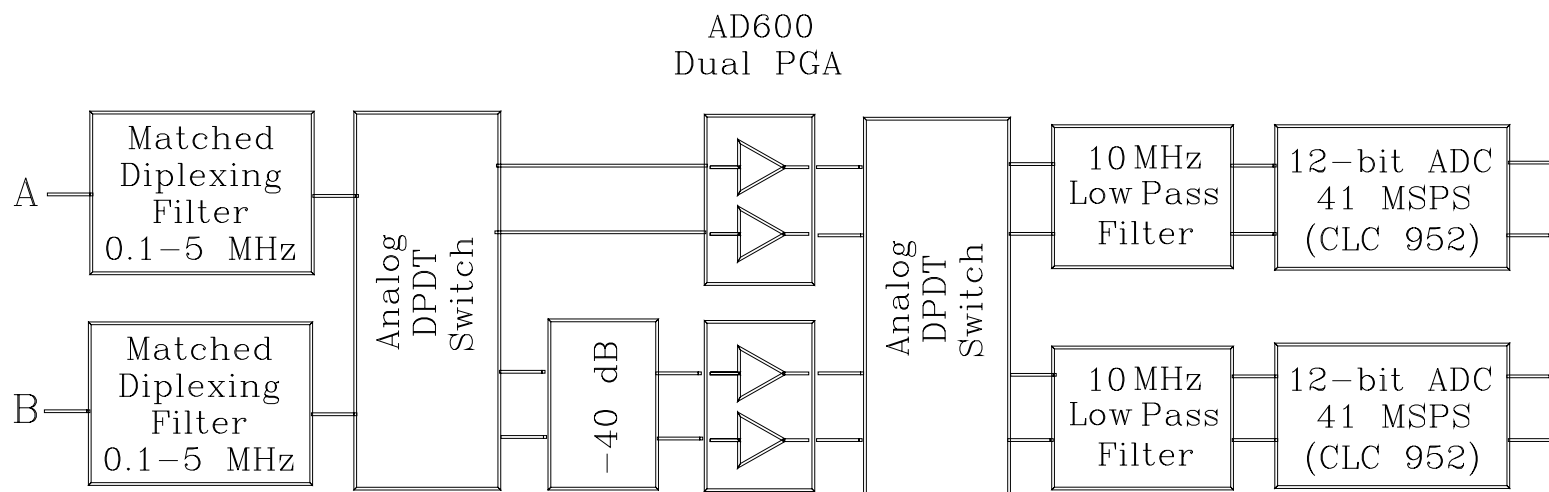


Fig. 5.9–2 Analog Electronics for dual plane stripline BPM

## 5.10 COLLIMATORS AND MOVABLE SHIELDING (WBS 1.5.8)

### 5.10.1 Scope

Collimators are placed at strategic positions within the ring and transport lines to remove any protons not in the desired orbit or do not have the desired momentum. In addition, it is desirable that both the secondary particles generated by the capture of these protons and any resulting radioactive isotopes be contained within the structure of the collimator. In this manner any imperfections in the ring or transfer line components can be compensated for by strategic placement of the collimators.

Moveable shields will be used to protect operating and maintenance personnel in the event that they are required to gain access to highly activated areas. In addition, the use of moveable shields will make it easier to comply with the ALARA rules.

### 5.10.2 Design requirements for the collimator

The design requirements for the collimator are the following:

- 1) Halo proton attenuation by a factor of  $10^{-4}$ ,
- 2) Minimize production of secondary radiation, and its subsequent leakage,
- 3) Remove heat (1 kW),
- 4) Mechanically compatible with ring operation (mitigate fatigue failures due to cyclic heating),
- 5) Minimize radiation damage and secondary activity.

### 5.10.3 Design description

In order to meet these requirements a layered structure was designed. A design consisting of layers in the direction of the proton beam which are initially transparent to protons, and become progressively less transparent with depth into the collimator. In addition a high-density shield will be added around this structure, particularly in the backward and forward directions, to attenuate any reflected and transmitted protons respectively. The protons are stopped in the approximate center of the collimator, and thus the bulk of the secondary particles will also be generated there. Since these secondary particles are primarily produced isotropically their leakage path length will be maximized in this manner with a high probability of capture or attenuation. In the case of neutrons a black layer is included at each end in order to minimize further their leakage in the direction of the beam. This design will therefore minimize the activation of surrounding accelerator components.

The conceptual design is shown on Fig. 5.10-1. The protons travel from left to right, with the beam confined primarily to the inner diameter of the collimator. Halo particles are found between the collimator inner diameter and the beam tube inner diameter, and are assumed to pass into the collimator volume. On their way into the collimator the halo particles will first encounter a graphite transition piece between the beam-tube diameter and the collimator diameter. This piece is 20-cm long, and has a conical front end. Protons at the operating energy pass through graphite with relative ease, and produce a small number of secondary particles. The collimator containment vessel wall fits behind the graphite piece, it is 1-cm thick and made of steel. The next 15 cm consist of a borated light water volume. This region is relatively transparent to high-energy protons, but lower energy neutrons, such as those that might result from a

spallation reaction, would be thermalized in this region and be absorbed by the boron. It would thus be black to low-energy neutrons. All the zones to this point have the same composition in the radial direction. The following zone has a radial variation at a radius of 20 cm. Within the 20 cm radius it consists of randomly packed stainless steel spheres cooled by borated light water, and outside this radius they consist of solid iron plates. This arrangement is chosen to ease the assembly of the collimator, ensure heat removal, and minimize the cost. Randomly packed beds of particles are particularly efficient at heat transfer, since their area per unit volume is greater than any other practical arrangement of the same characteristic dimension. Furthermore, the cost of small spheres of stainless steel is lower than machined discs of the same material. The void (coolant in this case) fraction of randomly packed spheres is approximately 35%; thus the solid fraction in this zone will be 65%. The particle bed zone will consist of 3-millimeter diameter stainless steel particles, with a length of 95 cm. The protons will lose the bulk of their energy in the first 80 cm of this zone, and since the production of neutrons per proton is modest for stainless steel at these energies the secondary production of neutrons is relatively low. Once the protons have lost the bulk of their energy, they will enter the remaining 15 cm of the particle bed zone. However, there is a probability of generating secondary protons in addition to the neutrons. Fortunately the yield of secondary protons is low compared to the neutron yield, due to the fact that the protons have to overcome the potential barrier before escaping the excited nucleus.

**Table 5.10-1 Masses and overall dimensions for the collimator**

<b>Component</b>	<b>Dimensions (cm)</b>	<b>Mass (kg)</b>
Graphite Transition piece	20 (L)	18
Front iron shield	65 (L)	8989
Collimator vessel	150 (OD)	900
Front Borated water	15 (L)	
Stainless steel particle bed/ Borated water	95 (L) x 20 (OD)	625
Iron (inside vessel)	80 (L)	5200
Radial iron shield	155 (L) x 190 (OD)	10240
Back iron shield	65 (L)	8989
Back borated water	15 (L)	
<b>TOTAL</b>		<b>34961</b>

Finally, the back 15 cm of the collimator consist of the same borated light water used in the first 15 cm of the collimator. This volume will ensure that many of the remaining spallation neutrons are slowed down and captured. The collimator is encased in 20 cm of solid iron in the radial direction. In the front and back directions the shield thickness is increased to 65 cm. The collimator thus has an overall radius of 75 cm and a total length of 242.6 s (including the iron

shield). The thick iron shield acts to stop/attenuate any protons that are reflected or are created within the collimator. In addition any high-energy neutrons which may escape the collimator will be attenuated in these shields, thus minimizing the activation of the surrounding (upstream and downstream) ring components. In addition, the thick shields should minimize the activation of the air and tunnel walls. Table 5.10-1 summarizes the masses and overall dimensions for the collimator configuration described above.

#### 5.10.4 Analysis and Results

The above collimator configuration was analyzed using the Monte Carlo codes LAHET (Prael, 1989), for particles above 20 MeV; and MCNP (MCNP, 1993), for particles below 20 MeV. In addition, a suitably modified version of the ORIGEN (Croff, 1980) code was used to estimate the buildup of spallation products during machine operation, and their decay following shutdown. The radial proton beam profile was assumed to be ring shaped. Those protons passing down the center of the beam tube were ignored, since they would be unaffected by the collimator. The inner radius of the ring shape corresponds to the smallest radius of the cone shaped collimator beam tube, and the outer radius was set at 1 mm less than the radius of the accelerator beam tube at that location, which was 5 cm. A radially uniform distribution of protons across the ring shape was assumed. In future analyses the proton intensity will be allowed to vary in the radial direction. These variations will presumably be either Gaussian or parabolic. The performance of the above collimator design is shown in Table 5.10-2.

**Table 5.10-2 Performance of collimator  
 (Protons crossing surface per halo proton)**

Surface (cm)	Backwards	Forwards	Remark
0.0	2.7E-05	~	Front
45.0	4.4E-03	1.0	Source
65.0	4.6E-03	6.6E-01	Front of collimator
81.6	3.6E-03	5.3E-01	Front of stainless steel particle bed
121.6	6.3E-04	1.0E-01	Mid-way in bed
161.6	2.3E-04	1.4E-02	Back of bed
242.6	~	1.4E-03	Back of collimator

These results show the backward (opposite to the direction of the proton beam) and forward (in direction of proton beam) proton currents in the halo zone of the beam (radius greater than 2.7 cm) per halo proton at various axial positions along the collimator. It is seen that the results start with unity at the source plane (surface 45.0 cm, forward direction), and decreases monotonically to the back end of the collimator. In addition the leakage out of the front end of the collimator is also seen to be small (surface 0.0 cm, backwards direction). Within the collimator it is seen that the proton current in the backward direction varies, with a maximum at the interface between the shield and the collimator containment vessel. The need for the thick iron shield is thus demonstrated

The thick shield should minimize neutron leakage, which in turn will minimize the activation of the tunnel air. Venting the tunnel air will further reduce activation levels. The only

other activated material that can leave the collimator is the cooling water. Potentially  $^7\text{Be}$  and  $^3\text{H}$  are formed and circulate in the coolant. If contained, the  $^3\text{H}$  should be undetectable, since it emits an electron upon decaying to  $^3\text{He}$ . However, the  $^7\text{Be}$  decays via a gamma ray (477.6 keV) and a half-life of 53.28 days. This poses a potential problem, particularly for maintenance work. For the above reason the cooling water will be cooled in a closed loop via an intermediate heat exchanger. The maximum heat load from a collimator is 1 kW. If a temperature rise of  $5^\circ\text{C}$  is assumed, a flow rate of approximately 2.0 gal/min is required.

Estimates of the energy deposition in the collimator indicate the bulk of the power will be generated in the inner 20 cm of the borated light water zone (9%), the front iron shield (10%), the stainless steel particle bed (52%), and the graphite transition piece (20%). All these zones need to be cooled by the cooling water system. The stainless steel particle bed zone is inside the collimator and is cooled by the borated water system. A cooling jacket positioned between the graphite transition piece and the iron shield will cool these two pieces. They will thus be cooled on one surface by cooling water, and by conduction within the body of the respective pieces. Preliminary estimates of the temperature in the two pieces indicate that they are well within their operating limits.

The activation of selected zones within the collimator is shown in Table 5.10-3. The values shown on this table assume that the machine has operated for 180 days at full power (1 MW, with 0.001 of the beam being captured in the collimator). Activation levels are shown for 1 day, 7 days, and 30 days following shutdown. It is seen that the quadrupole magnets have a low activation. The primary activation products being  $^{51}\text{Cr}$ ,  $^{54}\text{Mn}$ ,  $^{56}\text{Mn}$ ,  $^{55}\text{Fe}$ ,  $^{59}\text{Fe}$ ,  $^{65}\text{Ni}$ ,  $^{62}\text{Cu}$ , and  $^{66}\text{Cu}$ . In the iron zones of the magnet structure the same activation products are important, except Cu and Ni. The dipole magnets behind the collimator have a small amount of radioactive buildup. The activity of the solid components within the collimator is well shielded, and the gamma ray leakage out of the cylindrical surfaces of the shield is approximately six orders of magnitude below the source intensity. Furthermore, the activity is contained within the collimator structure. If for some reason the radiation levels should be too high (for maintenance work) then it is possible to arrange for the placement of movable shields around the collimator. It is seen that the air activity is quite modest, and is initially dominated by argon activation, for longer times carbon is the dominant contributor. The stainless steel particle bed is the most activated part within the collimator

Finally, a preliminary estimate of the number of electrons produced per halo proton in the collimator aperture tube was determined to be in the range 0.25 – 7. If this value is considered unacceptably high it is planned to include sweeping electrodes in the collimator aperture to capture the electrons.

Additional shielding might be required to minimize radiation levels during periods of maintenance. This will be accomplished by movable shielding blocks, which will be placed around the collimators should this be necessary.

**5.10.5 References**

Croff, A.G. 1980. “ORIGEN2-A Revised and Updated Version of the Oak Ridge Isotope Generation and Depletion Code,” Oak Ridge National Laboratory, Oak Ridge, Tennessee, ORNL-5621, July.

MCNP—A General Monte Carlo N-Particle Transport Code Version 4A. ed. J. F. Breismeister, Los Alamos National Laboratory, Los Alamos, NM. LA-12625-M (November 1993).

Prael, R. E., and H. Lichtenstein. 1989. “Users Guide to LCS: The LAHET Code System,” Los Alamos National Laboratory, Los Alamos, New Mexico, LA-UR-89-3014, September.

**Table 5.10.3 Activation of selected components after shutdown  
 (Curies)**

Component	Time after shutdown			
	0 Days	1 Days	7 Days	30 Days
Quadrupole (Cu/Fe)*	5.0	1.8	1.1	0.8
Quadrupole (Fe)*	0.2	0.15	0.1	0.1
Air front	0.03	~	~	~
Graphite transition	15.2	3.0	2.8	2.1
H <sub>2</sub> O – <sup>10</sup> B (20 cm radius)	6.6	0.52	0.48	0.36
Stainless steel particle bed	74.3	48.9	41.0	29.2

\* Down stream magnet. Activity tabulated for the complete magnet and for just the iron.

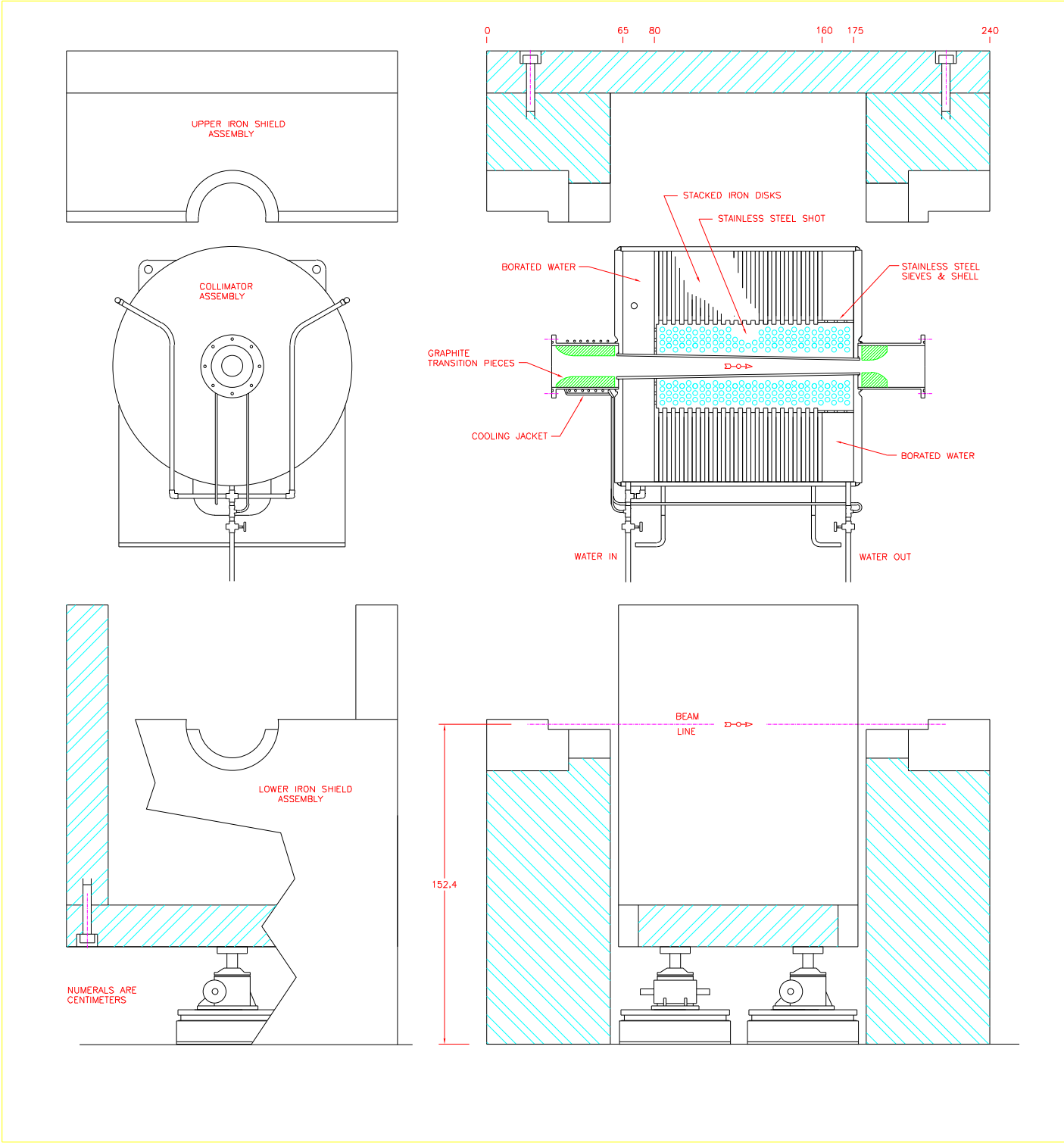


FIG. 5.10-1

COLLIMATOR ASSEMBLY

## 5.11 EXTRACTION (WBS 1.5.9)

### 5.11.1 Scope and Requirements

The beam will be extracted from the accumulator ring at a maximum rate of 60 Hz in a single turn, taking place in less than one beam revolution period of 841 ns. The selected scheme is to use a two-step process consisting of a fast kicker and a Lambertson type magnetic septum magnet. Extraction will take place very soon after the injection stacking process is completed (typically a few revolutions). The accumulated beam will have a gap of 250 ns to enable the magnetic field in the fast kicker to rise to its extraction level within this gap. Extraction from the accumulator has to exhibit a high level of reliability and reproducibility, since it is not desirable to dump beam within the main ring. To this end, all selected components have to operate conservatively within their ratings, and exhibit good MTBF and MTTF figures. A high degree of modularity is also built into the systems for this purpose. Timing for extraction is very crucial. While extraction must occur as soon as possible after injection is complete, nevertheless enough time must be allocated to provide synchronization to the target beam choppers and to the ring rf system (i.e. the beam gap).

Extraction will take place in one of the accumulator ring's long straight sections (section D). The fast kicker provides a vertical kick that clears the magnetic septum and the septum provides the large angle deflection to extract the beam into the RTBT line. A short dipole in the RTBT line is used to straighten out the vertically kicked beam. In the region of the main ring accumulated circulating beam, the fringe field of the septum will be low. A schematic layout of the extraction channel is shown in Fig. 5.11-1. The kicker is centered around the vertical focussing quadrupole (QVD9) and its associated corrector magnet, while the Lambertson magnetic septum is located just downstream of horizontal quadrupole (QHD10). The two extraction magnets and their respective PS systems are described in the following sections. The requirements for the extraction system are summarized in Table 5.11-1.

### 5.11.2 Fast Kicker

The fast kicker system consists of eight sections of rectangular-frame, ferrite core magnets. A closely coupled pulse-forming network (PFN) which is discharged when it receives a synchronized timing trigger powers each magnet. The requirements for the fast extraction system are given in Table 5.11-1. The important advantage of this scheme is that the inductance and hence the voltage per module is reduced to the level where the components can operate more reliably. The increased number of components is compensated for by the fact that the extraction design allows the full beam to be extracted within the acceptance of the RTBT line and transported to the target even with one of the modules missing. This can be seen in Fig. 5.11-2 where the vertical phase space of the kicked beam is shown at the center of the quadrupole preceding the Lambertson septum. The figure shows that the deflected beam fits well within the acceptance even with one of the eight modules missing.

Each magnet section will have a single-turn copper conductor that will be center-fed through the return leg of the ferrite core. A schematic sketch of one of the ferrite kicker sections is shown in Fig. 5.11-3. The sections will have the same gap height but will have differing widths that take advantage of the varying beta function in the extraction region around the quadrupole (QVD9). In order to keep the impedance of each module constant, the lengths will be varied inversely to the widths. Therefore, all modules can be charged to the same voltage. An

assembly of one of the two magnet groups is shown in Fig. 5.11-4. Each group will be assembled under clean conditions and baked prior to ring installation so that ultimate ring vacuum requirements can be met.

The fast kicker pulsers will consist of eight pulse-forming networks (PFN's) that will be discharged simultaneously into their corresponding magnet sections. The discharge will be by hydrogen thyratron tubes that are capable of high currents and fast rise times. To reduce the amount of stray inductance, each of the eight PFN's will be located in the ring next to and closely coupled to its magnet section in the group assembly. For each tube, power supplies for the grid control and power supplies for heating the reservoir and filament will be located in the ring air cooling equipment. The rest of the electronics, consisting of the common charging power supply, timing triggers, interlock controls, and computer interface PLC will be located outside the tunnel in the ring support building. A simplified schematic of a PFN module is shown in Fig. 5.11-5. Noise and interference to other systems will be reduced by isolating the control electronics and triggers and by monitoring with fiber-optic receiver/transmitter circuitry. An important consideration for this is that the grounding for the fast kicker shall be isolated or sectionalized from the rest of the building and equipment grounds. A list of the fast kicker system parameters is given in Table 5.11-2.

The fast ejection system has to be capable of operating at the maximum rate of 60 pps. At this rate the number of pulses accumulated by the switching thyratrons will be quite high and have to be closely monitored. The usual indication of degradation is a slow increase in the tube turn-on jitter time.

### **5.11.3 Lambertson Magnetic Septum**

A Lambertson type magnetic septum will be used to eject the fast kicked beam from the accumulator. The septum will deflect the beam by 15.5 degrees with a field of about 5 kG. The design of the magnet takes into account the requirements of uniform field in the extraction gap and very low fringe field in the accumulator circulating beam gap. A computer simulation is being used to determine the optimum shapes and lengths of the core/conductor to accomplish this. The major parameters are shown in Table 5.11-3. A cross-sectional view for each end and for the layout of the magnet is shown in Fig. 5.11-6. It consists of a machined soft iron core and water-cooled copper conductors. The copper insulation will be epoxy/fiberglass. It will operate dc continuous. The magnet will be curved and will have an Y vacuum chamber for the circulating and extracted beams.

The power supply (ps) for the magnetic septum will be an ac-to-dc converter type, using multiphase SCR's (silicon controlled rectifier). The unit will include a passive, damped LC filter to reduce the ps ripple to acceptable levels. A feedback regulator incorporating voltage and current loops, and fed by dc voltage (DCPT) and dc current (DCCT) sensors will provide the high degree of regulation required. A programmable logic controller (PLC) will accomplish the interlocks and computer interface. The analog control will be a project standard waveform generator. The unit will receive its primary input power from a project supplied 13.8 kV/480 volt substation, and will be physically located in the main ring support building. The power supply will be water-cooled. See section 5.6.2.1 for a further description of this type of ps.

### 5.11.4 Timing and Synchronization

As mentioned earlier, timing for the ejection system is very crucial for fast, clean, lossless beam extraction. The fast kicker must be triggered during normal operating conditions so that its field rises in the circulating beam gap. As soon as a beam is extracted from the ring, charging of the fast kicker modules will begin and take approximately 12 ms, ending roughly one ms before extraction is to take place. When the required charging level has been verified by the Beam Permit System, injection of the next beam pulse from the Source/Linac will begin. This beam pulse will be ejected at the next rf synchronized trigger. This sync is determined by the overall timing system after taking into account the target neutron chopper synced conditions.

Since no beam can be dumped continuously in the ring, the Beam Inhibit System will prevent any additional beam pulses from being admitted into the main ring after an abnormal condition is sensed. An abnormal condition can arise from a number of areas such as high beam loss monitor signals, main ring and RTBT ps's out-of-tolerance, kicker fault, MEBT beam chopper faults, neutron chopper faults, etc. For some of these, it is desirable to kick any circulating beam out of the ring and into the RTBT line and the target

**Table 5.11-1 Requirements for the Ring Extraction System**

Parameter	Base Value	Comment
Extraction Type	Single-turn	Two steps
Maximum Extraction Rate	60 Hz	
First step	Fast kicker	Vertical full aperture kicker
Fast kicker vertical deflection angle	16.8 mrad	
Beam displacement above ring	12 inches	
Beam extraction gap	250 ns	
Fast kicker rise time	<200 ns	0 to 97%
Second step	Lambertson	Magnetic septum
Lambertson horizontal deflection angle	15.5 degrees	
Beam extracts to target with 1 of 8 kickers inoperable	Yes	

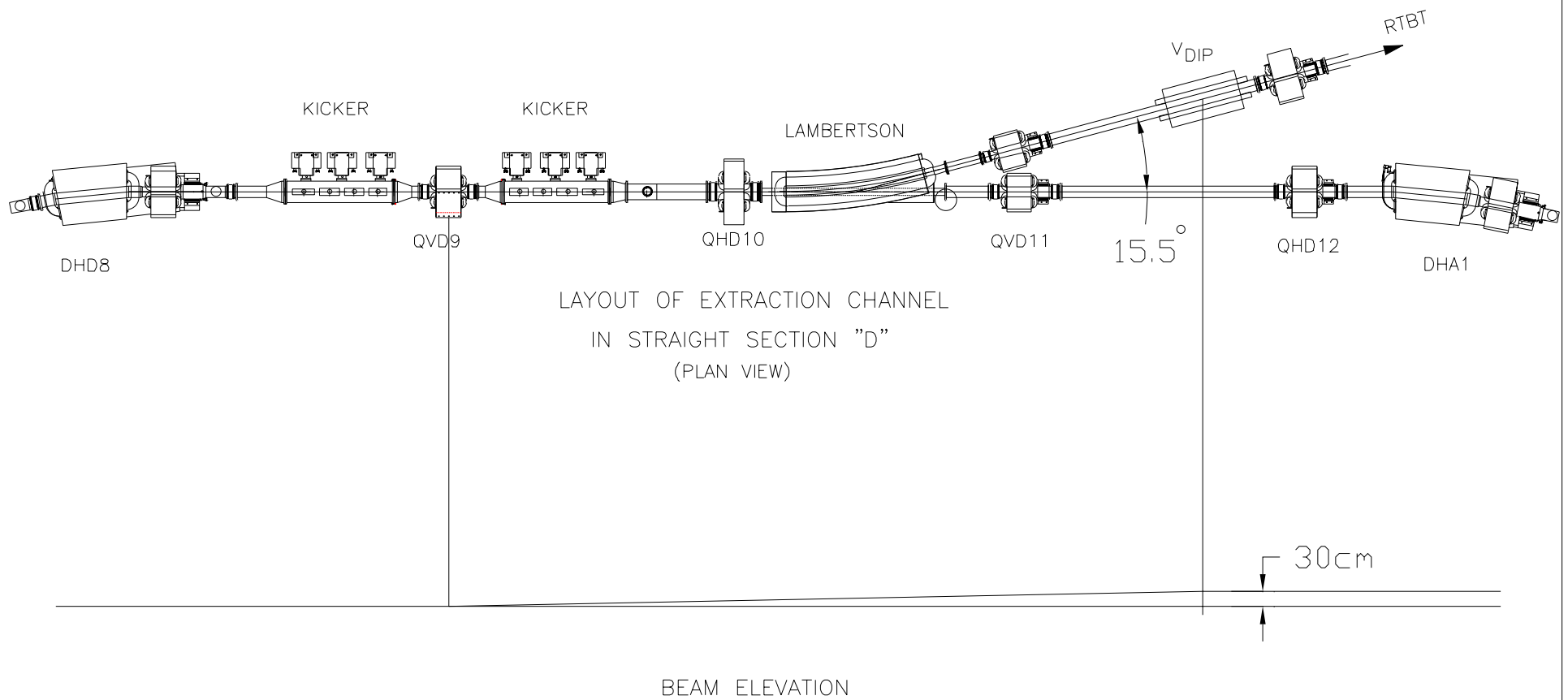
**Table 5.11-2 Fast Kicker Parameters**

<b>Mechanical Parameters</b>	
Type	Rect. Frame; Full Aperture
Core Material	Ferrite
No. Sections	8
Core length/Section	44 cm Max; 37 cm Min
Core Spacing	10 cm
Total Length	2 x 190 cm
Gap (H)	11.5 cm
Width (V)	12.9 cm Min; 15.4 cm Max
<b>Electrical Parameters</b>	
Bend Angle/Section	2.1 mrad
Peak Field	300 Gauss
Peak Current	2.8 kA
Pulse Repetition Rate	60 Hertz
Rise time	200 ns
Pulse Flattop	600 ns
Voltage/Section	17 kVolt
No. PFN's	8
No. DC PS	1
Voltage Rating	40 kVolt

**Table 5.11-3 Lambertson Septum Parameters**

Bend angle	15.5 deg
Core Length	3.1 m
Gap (Field -Free Region)	15cm(H) x 11 cm(V)
Gap (Field Region)	15cm(H) x 11 cm(V)
Septum Thickness	1 cm
B	5 kG
Total No. of Turns	40
Max PS Current	2200 A
Magnet resistance	0.009 $\Omega$
Max V dc	9 V
Max Power	20 kW

Fig. 5.11-1



# Vertical Phase Space of Kicked Beam

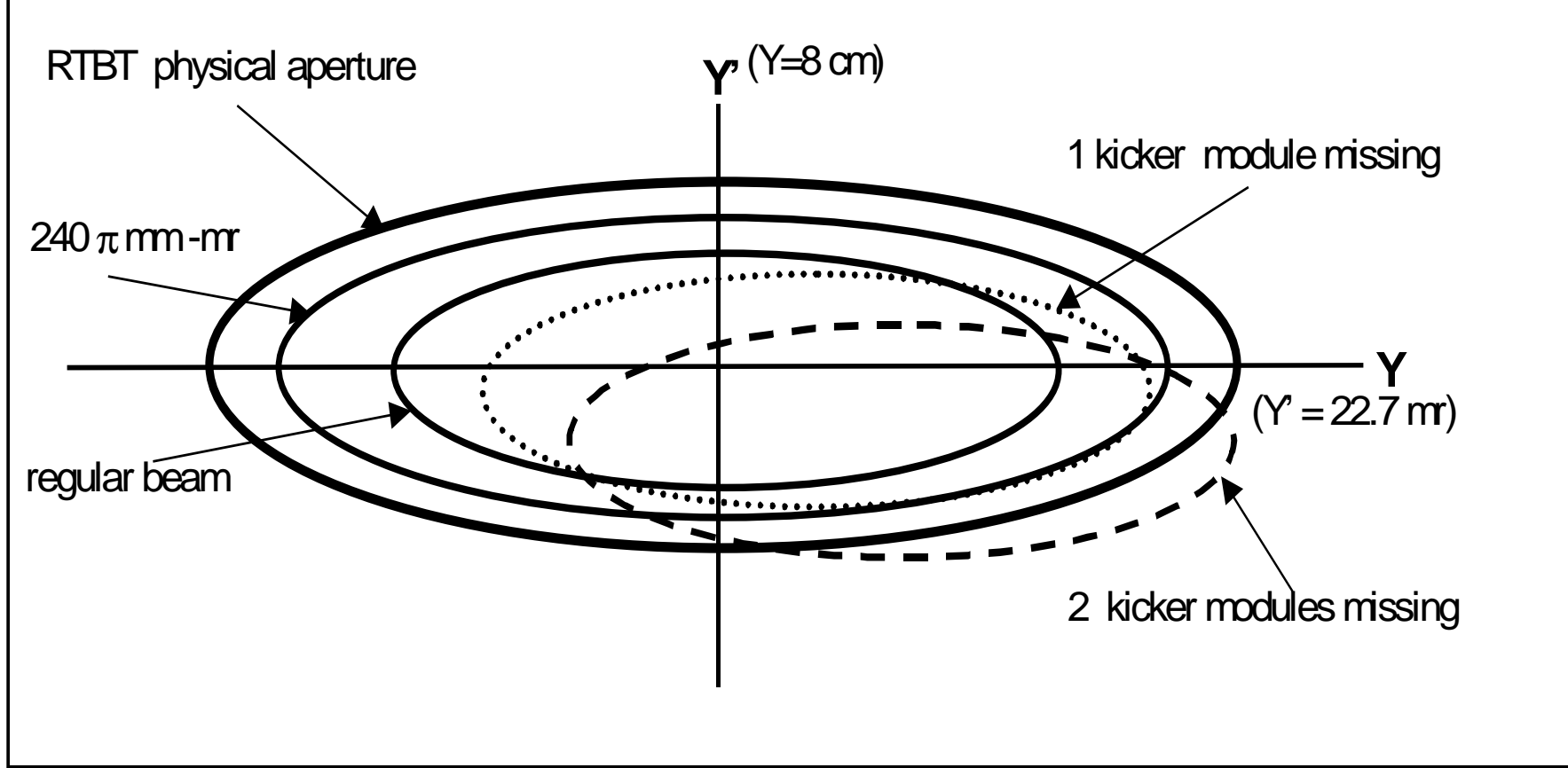
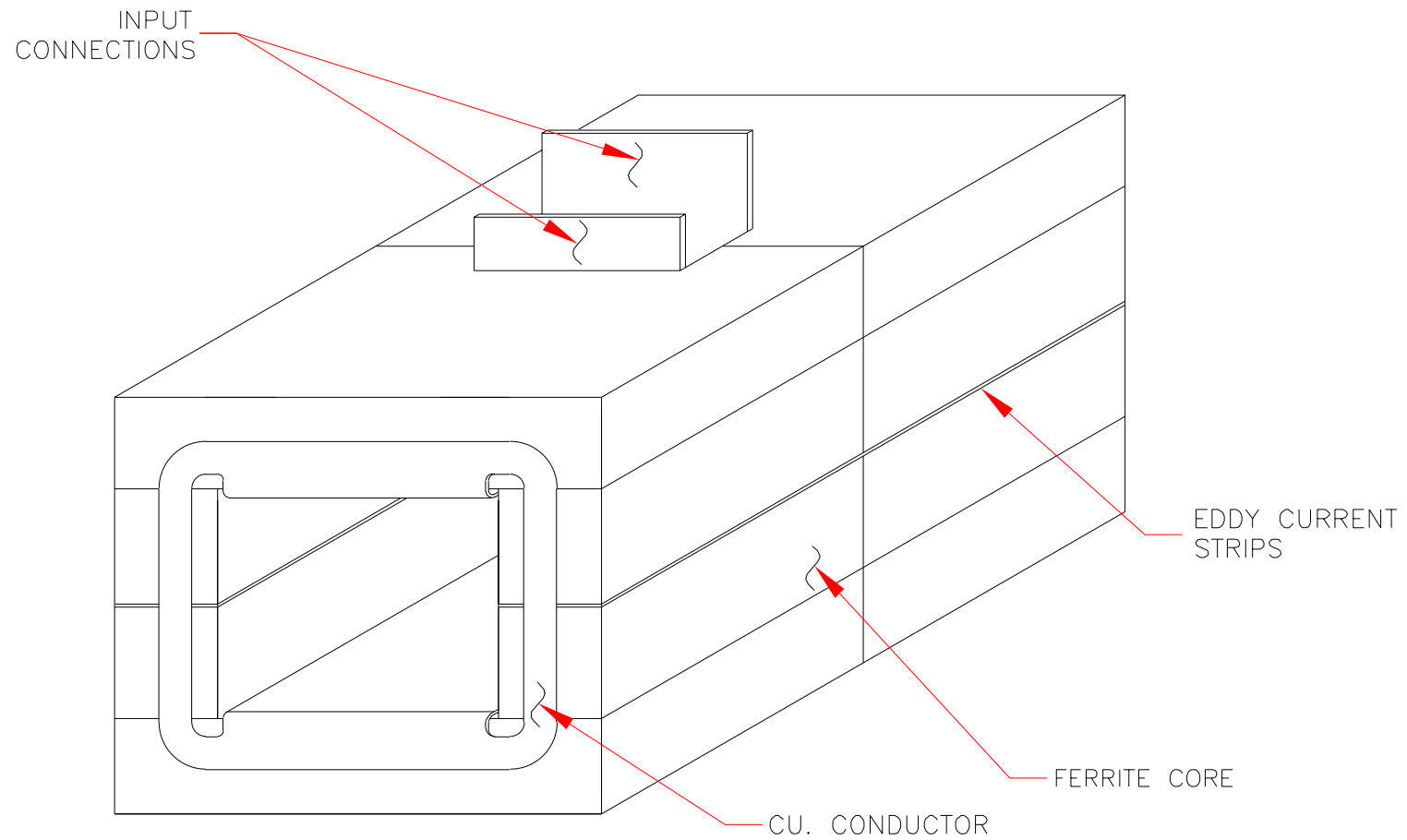


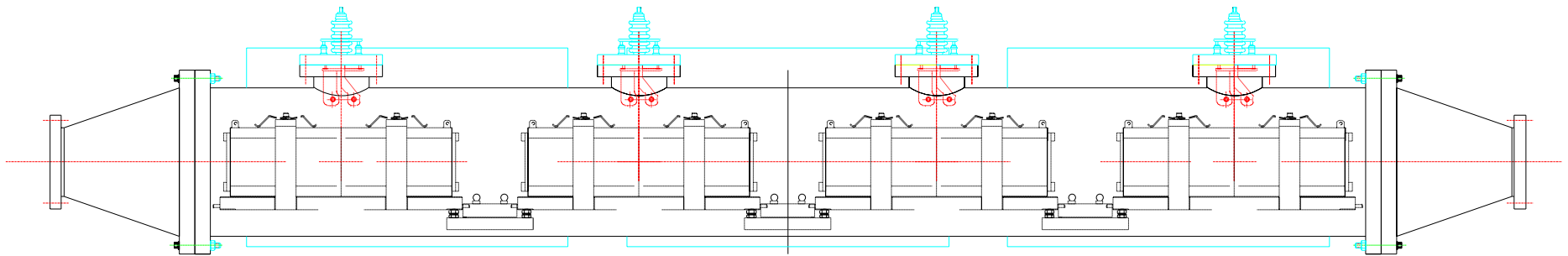
Fig. 5.11-2

Fig. 5.11-3

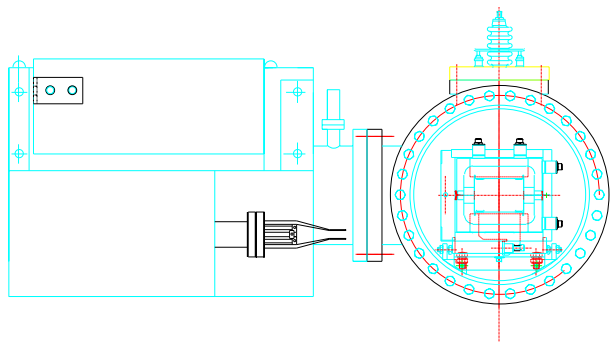


SNS TYPICAL EXTRACTION FAST KICKER MODULE

Fig. 5.11-4



SNS FAST KICKER ASSEMBLY



END VIEW

MAGNET	KICKER, EXTRACTION
A SECTIONS/CHAMBER	2 CHAMBERS/RING
CORE MATERIAL	NiZn FERRITE
GAP H	11.5 cm
GAP W	12.9 cm - 15.4 cm
PEAK CURRENT	2.8K AMP
PEAK VOLTAGE	17K VOLT

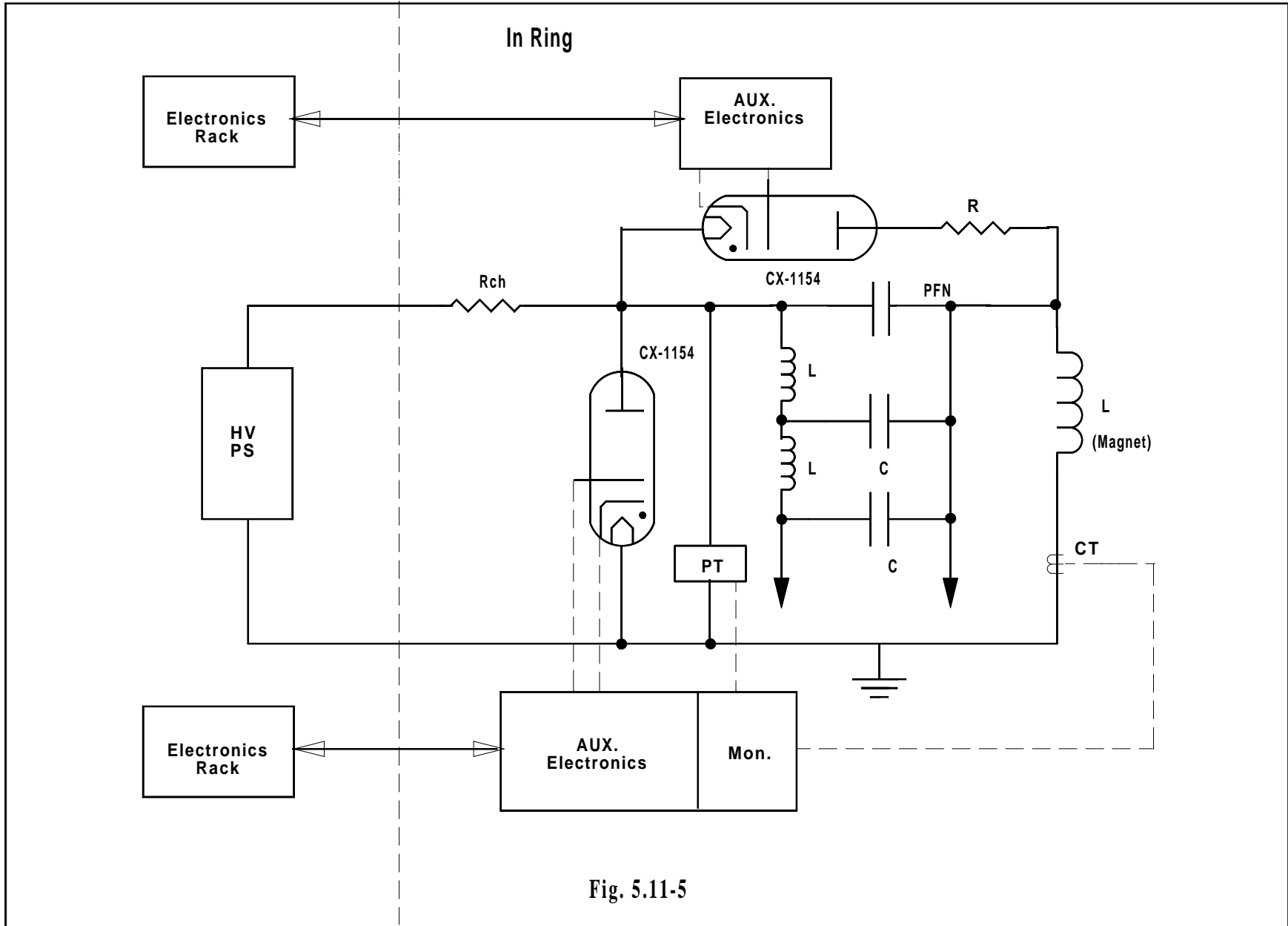
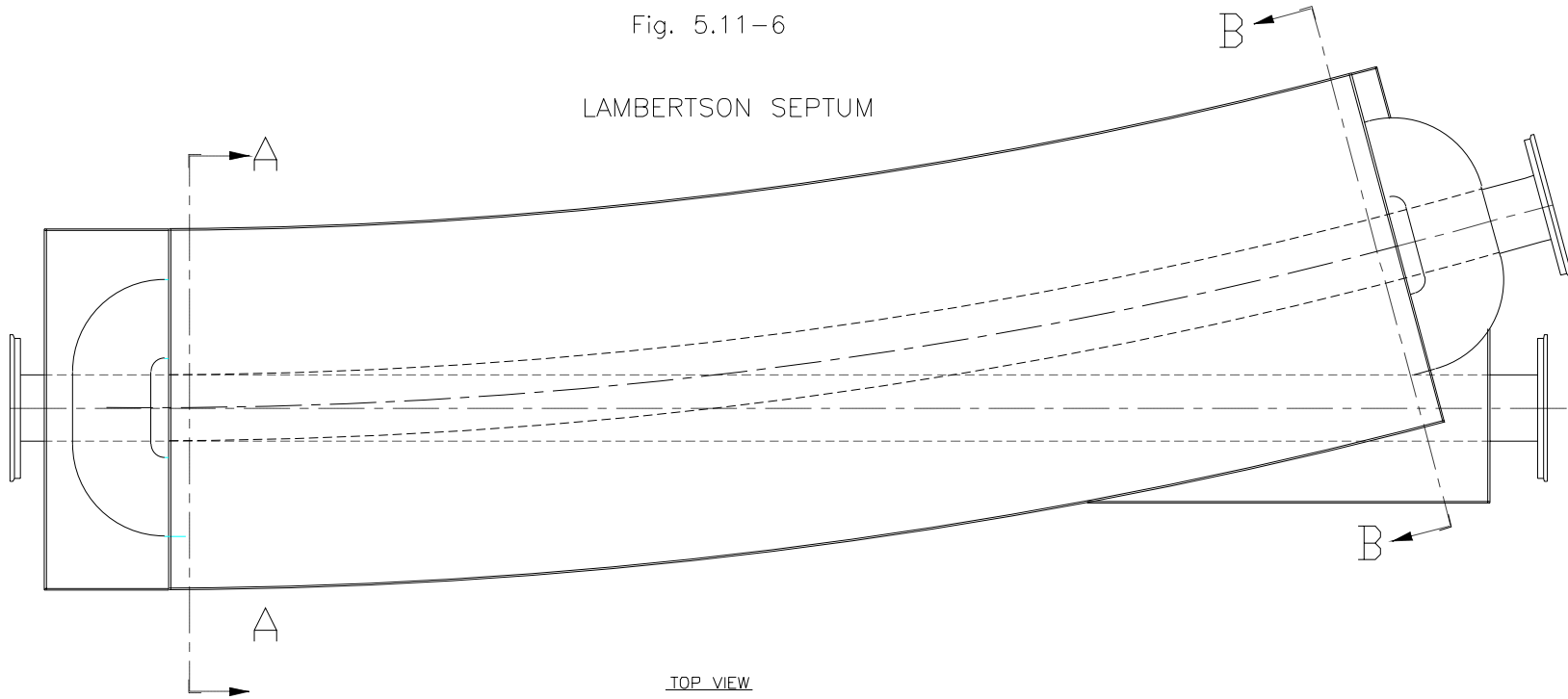


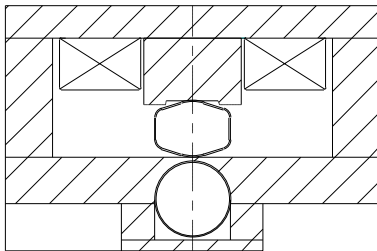
Fig. 5.11-5

Fig. 5.11-6

LAMBERTSON SEPTUM

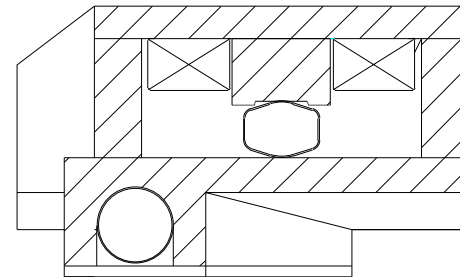


TOP VIEW



CROSS-SECTION A-A  
UPSTREAM END VIEW  
ROTATED 90° CCW

MAGNET, EXTRACTION D.C.	LAMBERTSON, DREL
APERTURE, FIELD	15 cm Horiz. x 11 cm Vert.
LENGTH	3.1 m
APERTURE, FIELD FREE	15 cm Horiz. x 11 cm Vert.
MAX POWER	20 kW
MAX CURRENT	2200 A
COIL	40 TURNS (total)
WEIGHT, COILS	3,500 LBS
WEIGHT, STEEL	20,000 LBS
WATER	4 GPM



CROSS-SECTION B-B  
DOWNSTREAM END VIEW  
ROTATED 90° CW

## 5.12 RING TO TARGET BEAM TRANSPORT LINE (WBS 1.5.10)

### 5.12.1 Scope

The Ring to Target Beam Transport line (RTBT) connects the accumulator ring, at the beginning of the extraction kicker magnet, to the target. It is 180 m long.

### 5.12.2 Design Requirements

The beam requirements at the target are given in Table 5.12-1. Table 5.12-2 gives the Twiss parameters of the beam at the beginning of the extraction kicker magnet and at the target, assuming no space charge forces.

**Table 5.12-1 Beam requirements at the target**

Beam full width	200 mm
Beam full height	70 mm
Time-average beam current density, over beam footprint	< 0.091 A/m <sup>2</sup>
Beam power within target and outside nominal spot	< 5%
Peak time-average beam current density, over 1 cm <sup>2</sup>	< 0.182 A/m <sup>2</sup>
Peak 1-pulse density, over 1 m <sup>2</sup>	1.89 x 10 <sup>16</sup> protons/m <sup>2</sup>

**Table 5.12-2 Twiss parameters at the ring extraction magnet and at the target for 1MW beam**

Twiss parameters	Output of Ring	Target	Units
$\alpha_X$	0.0	0.0	
$\beta_X$	4.15	83.0	mm/mrad
$\epsilon_X$	120	120	$\pi$ mm mrad
$\alpha_Y$	0.0	0.0	
$\beta_Y$	1.967	10.2	mm/mrad
$\epsilon_Y$	120	120	$\pi$ mm mrad

### 5.12.3 Design Description and Functions of the RTBT Line

The RTBT uses a FODO lattice up to the beam spreading section. The 90°/cell phase advance and length of 11.6 m/cell matches very closely the ring lattice. The line has following elements: (a) extraction, (b) beam dump, (c) halo collimation, (d) beam spreader, and (e) diagnostics. The first four functions have essentially been decoupled in the RTBT. The extraction system starts in the ring with a kicker magnet and continues through four cells in the RTBT. Following the extraction system, the beam can be dumped straight through a 15.5° dipole magnet. After this 15.5° bend, two cells are used for the halo collimation. Following another 6 cells of transport, the last five quadrupoles in the line are used for final beam spreading to produce the beam size required at the target. Every quadrupole in the RTBT is followed by a small dipole corrector magnet for steering of the beam in the quadrupole focusing plane. To

reduce the probability of uncontrolled beam losses and to define the beam size precisely on the target, RTBT is equipped with four transverse beam halo scrapers and several types of diagnostic devices. Fig. 5.12-1 shows the layout of the RTBT. To keep uncontrolled beam losses low, a study of the required alignment tolerances (Raparia, 97a), has led to the requirements given in Table 5.12-3.

**Table 5.12-3 Alignment tolerances for the RTBT magnets**

Type of Error	Tolerance
Translation (x and y)	$\pm 0.1$ mm
Pitch and yaw	$\pm 1$ mrad
Rotation	$\pm 0.5$ degrees

Fig. 5.12-2 shows the amplitude functions ( $\beta_x, \beta_y$ ) and the dispersion function ( $\eta$ ) along the RTBT. This line is designed such that it can accommodate the beam current required for the upgrade to 2 MW.

### 5.12.3.1 Extraction dump

Following the extraction section, the beam dump is in a line straight through the 15.5° dipole magnet. This dump can handle up to 200 kW beam power and will be used for accumulator tuning purposes. This line is 28 m long and the optics of this line is shown in Fig. 5.12-3.

### 5.12.3.2 Beam spreader

The beam spreader consists of two doublets and a singlet near the end of the RTBT. These five 36-cm diameter aperture quadrupoles provide the desired beam size at the target, as given in Table 5.12-1. Due to thermal considerations of the target, the beam current density on target must remain below the limits shown in the table. The required current density distribution can be obtained using the injection scheme described in Section 5.4. Fig. 5.12-4 shows the current density distribution at the target using such a scheme. The scattering effects of a 4-mm thick inconel window, 1.25 meter from the target, were included.

### 5.12.3.3 Magnet & Support

The magnet & support system detail is described in Section 5.5. Table 5.12-4 shows the magnet requirements for the RTBT.

**Table 5.12-4 Magnet requirements for the RTBT**

	Type	Number	Field	Aperture	Length
<b>Dipoles</b>	17D310	1	0.50 T	17 cm x 45 cm	3.1 m
	20C30	27	0.02 T	20 cm x 20 cm	0.3 m
	36C30	5	0.02 T	36 cm x 36 cm	0.3 m
	17DV50	1	0.25 T	45 cm x 17 cm	0.5 m
<b>Quadrupoles</b>	20Q50	27	3.4 T/m	20 cm diam.	0.5 m
	36Q80	5	3.0 T/m	36 cm diam.	0.8 m

# Same as the accumulator quadrupoles.

### 5.12.3.4 Power Supplies

The power supply system details are described in Sections 5.6.1 & 5.6.2. Table 5.12-5 shows the power supply requirements for the RTBT.

**Table 5.12-5 Power supply requirements for the RTBT**

	Type	Number Magnets	Number PS
<b>Dipoles</b>	17D310	1	1
	20C30	27	27
	36C30	5	5
	17DV50	1	1
<b>Quadrupoles</b>	20Q50	27	11
	36Q80	5	5

### 5.12.3.5 Vacuum

The RTBT will have a vacuum of less than  $10^{-8}$  Torr. Table 5.12-6 shows the required vacuum components.

**Table 5.12-6 Vacuum components required for the RTBT**

Equipment	Number
Sector Valves	6
Ion Pumps	18
Roughing Pumps	5
Vacuum Gauges	5

### 5.12.3.6 Diagnostics

There must be enough diagnostic devices in the RTBT line to determine beam quality and beam losses in the line, as well as to determine the beam profile as close as possible to the target.

There is one beam loss monitor per quadrupole and one per dipole, with 17 units left for additional (still to be determined) critical locations. Horizontal and vertical beam position monitors are located near each quadrupole. Current toroids will allow continuous monitoring of beam current near the beginning and end of the transport line. Using profiles from four crawling-wire profile monitors located between four consecutive quadrupole magnets in the line, one will be able to infer the beam emittance in the line. These units will have 4 wires, taking profile measurements in four projections - 0° (horizontal), 30°, 60°, and 90° (vertical). From these projections, we will use an algebraic reconstruction technique (Raparia, 97b), to get a detailed 2-dimensional density distribution of the beam. Finally, there will be one harp located near the ring extraction and a pair of harps ~1.5 m in front of the target. The lifetime of the harps should not be a problem, since the current density at the RTBT harps will be lower than in the HEBT line, and the power deposited in the wires will be less than that in harps used in the BNL Booster injection line. Since the harp in front of the target is important for guaranteeing beam flatness, there will be two units, one always in the beam and the second retracted as a spare. Harp measurements that find a beam excursion from the target requirements given in Table 5.12-1, will trigger a fast beam inhibit. A list of the diagnostic devices is given in Table 5.12-7, and the locations are shown in Fig. 5.12-5

**Table 5.12-7 Diagnostic devices in the RTBT**

Device	Number
Beam Loss Monitor (BLM)	50
Beam Current Monitor (BCM)	2
Beam Position Monitor (BPM)	32
Harp (PrM)	3
Crawling Wire Scanner (PrM(WS))	4

**5.12.3.7 Halo scraping (collimation)**

To define the beam size at the target, there are four  $\beta$  collimators in the RTBT line. These collimators are located just after the last 15.5° bend in the line, and each is designed to handle up to 1 kW of beam power (see Section 5.10). The lattice functions and the beam size at the collimator locations are given in Table 5.12-8.

**Table 5.12-8 Lattice functions and beam size at the collimator locations.**

$s(\text{deg})$	$b_x(\text{m})$	$b_y(\text{m})$	$(\epsilon b_{x,y})^{0.5}(\text{mm})$	Col. half aper. (mm)
0	18.9	2.02	47.68	60.41
45	2.02	19.1	47.91	60.69
90	18.96	2.02	47.70	60.43
135	2.02	19.1	47.79	60.53

There is a three-m long collimator just before the target window to prevent beam from hitting outside of the target area.

#### **5.12.4 References**

Raparia, D., Alessi, J., Lee, Y.Y., Ruggiero, A.G., Soukas, A., Tuozzolo, J., Weng, W.T., Witkover, R.L., NSNS/BNL Tech. Note 6 (1997a)  
Raparia, D., Alessi, J., Kponou, A., to be published in the Proc. 1997 Particle Accelerator Conference (1997b)

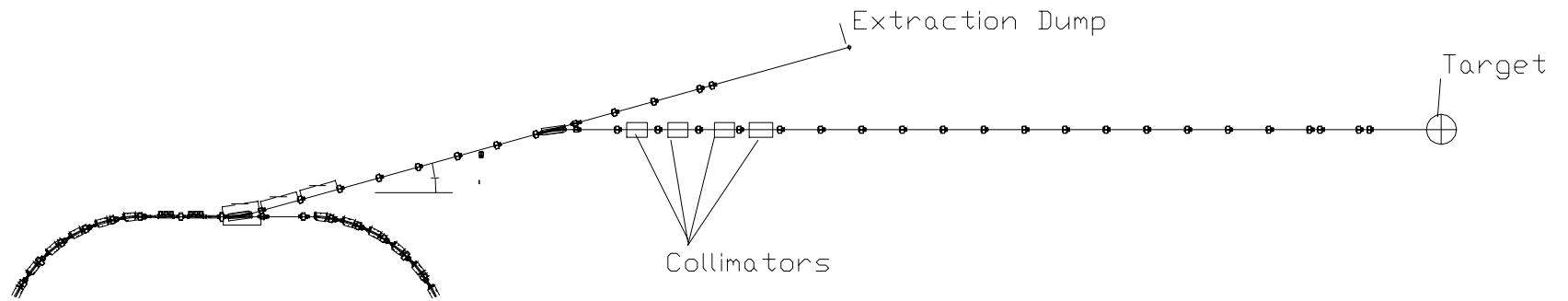


Figure 5.12-1 Layout of the RTBT line.

"SNS RING TO TARGET TRANSFER LINE"

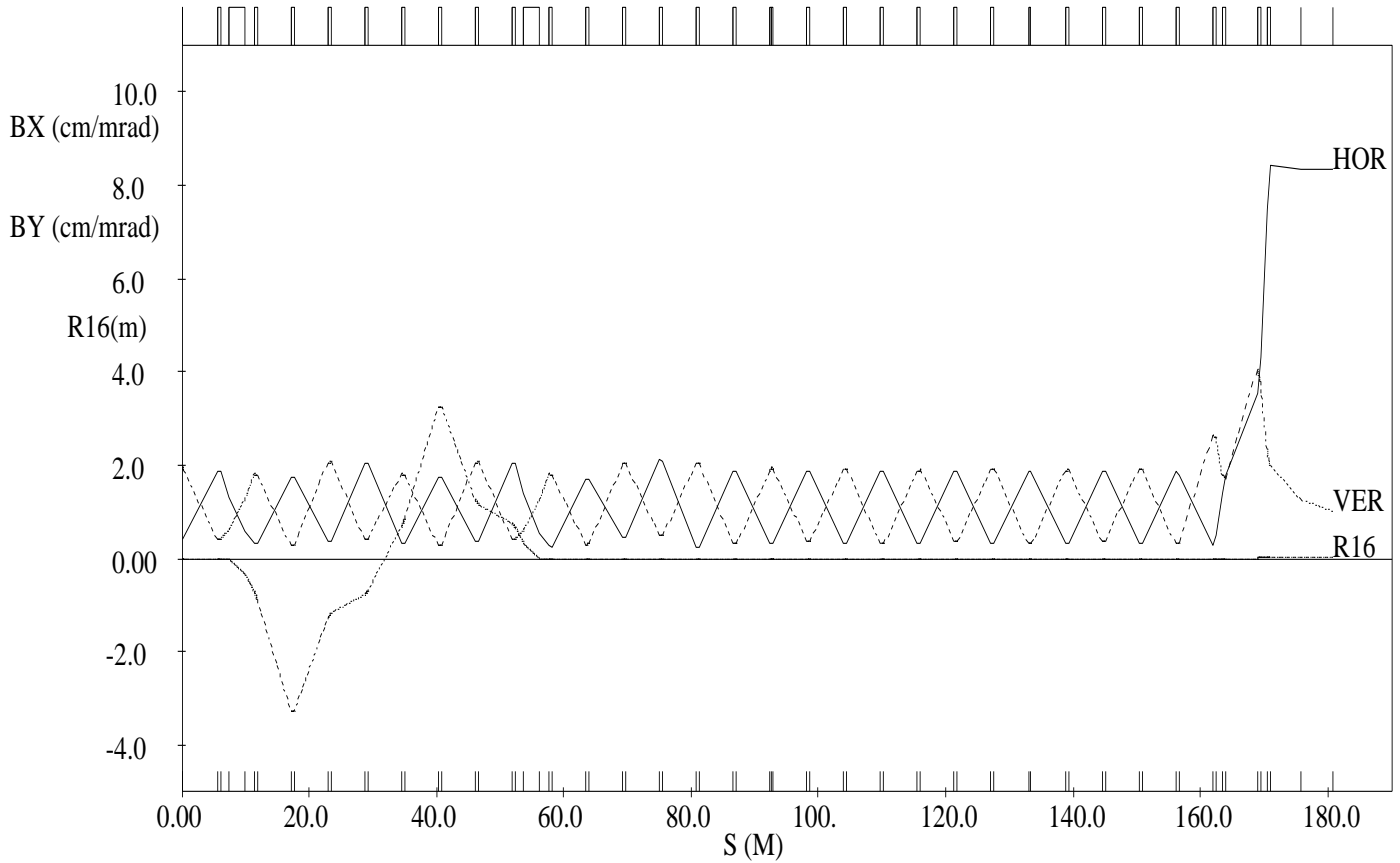


Figure 5.12-2. TRANSPORT output of the beta functions and dispersion function (R16) along the RTBT.

"SNS EXTRACTION DUMP LINE

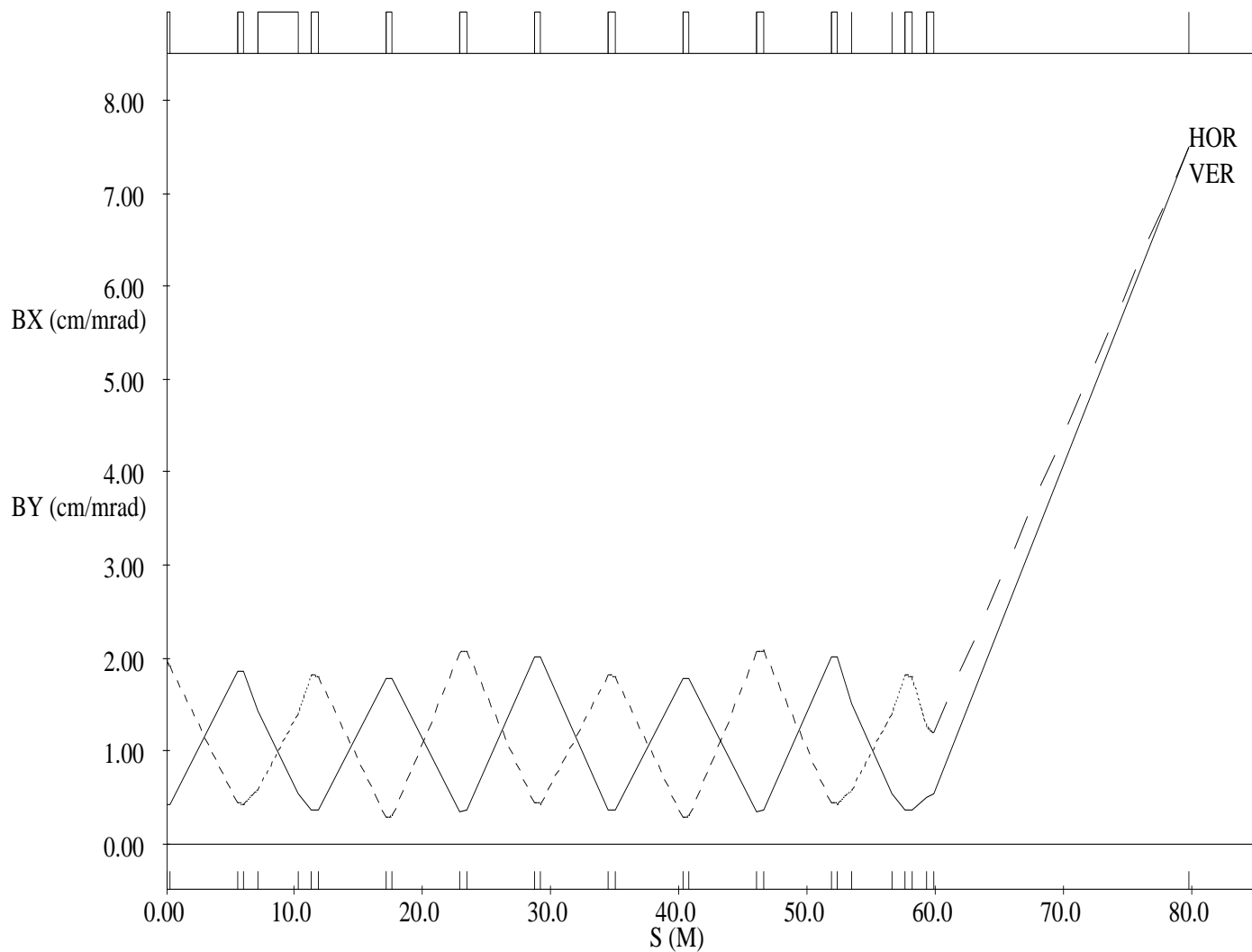


Figure 5.12-3. TRANSPORT output showing the beam transport to the extraction dump.

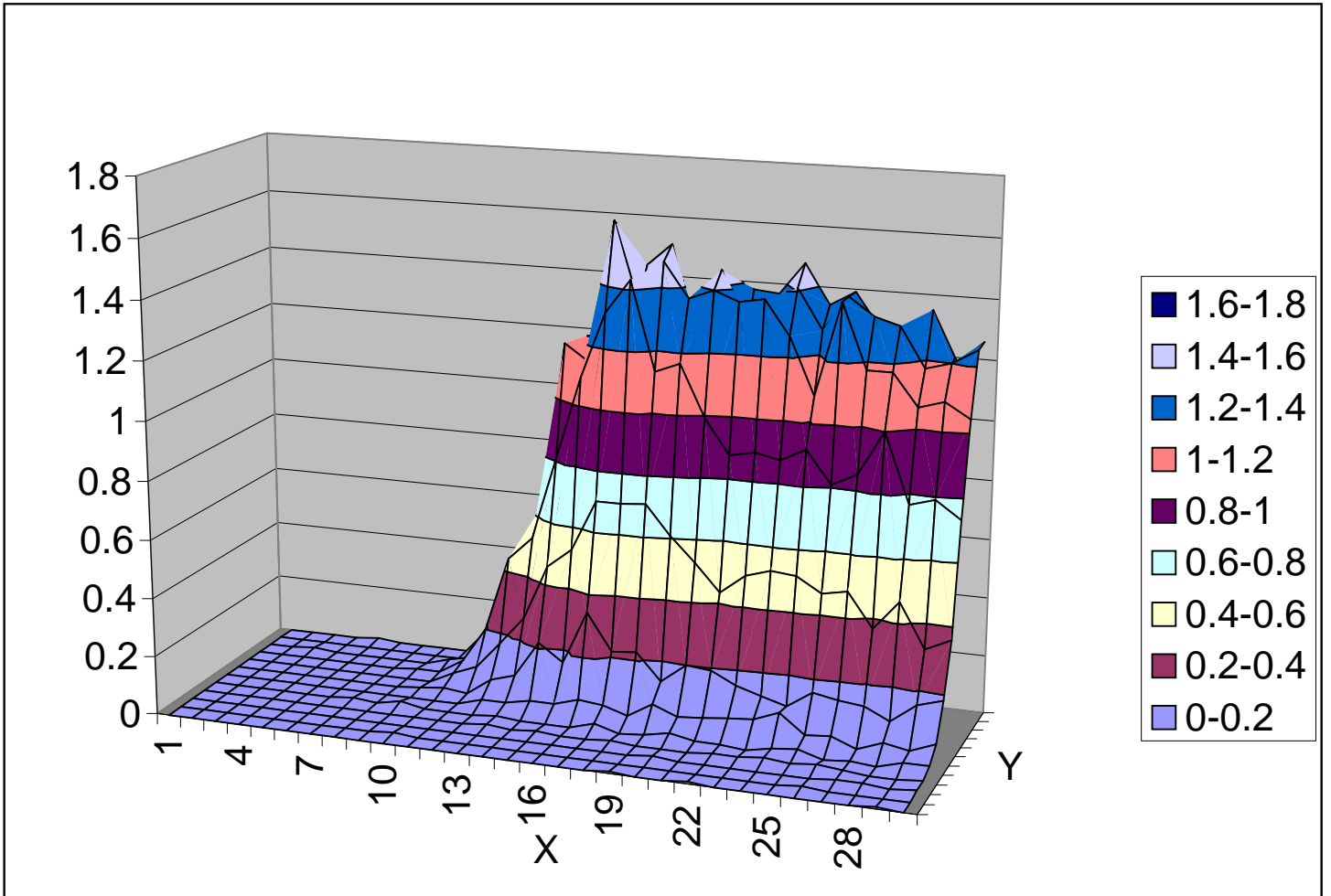


Figure 5.12-4. Current density distribution at the target in units of  $10 \text{ A/m}^2$ . Only one quadrant of the beam footprint is shown.

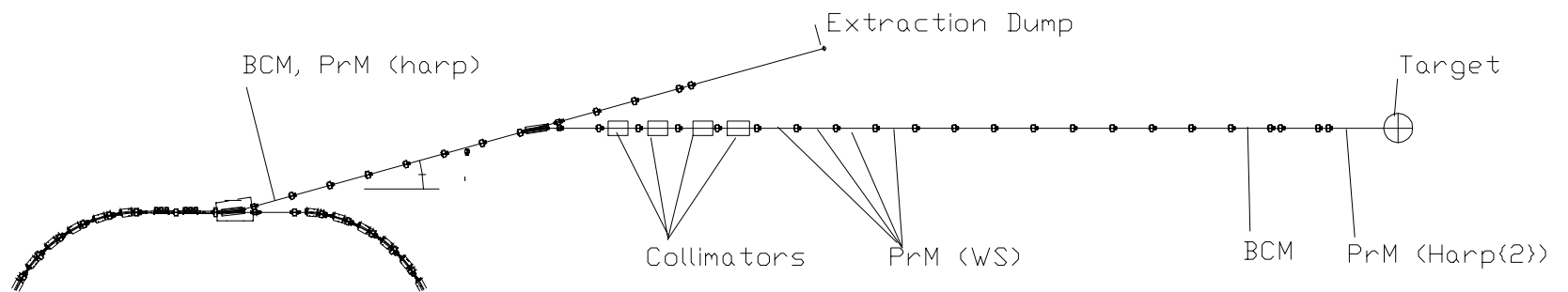


Figure 5.12-5. Schematic showing the location of the Diagnostics in the RTBT line.

## **5.13 RAM CONSIDERATIONS**

In order to meet the project availability goal, the ring system has to operate well above 90% for its availability and reliability. Several strategies are adopted to meet this performance goal.

### **5.13.1 Sound and Conservative Conceptual Design**

Every effort has been and will be made to solve problems with solutions that also provide for operation that is more reliable and for ease of repair. For example, the accumulator ring was designed to have few pulsed components and to be simple to operate; hence, it will be more reliable than most proton synchrotrons. Our decision to put each ring in its own tunnel was primarily dictated by reliability concerns. Another example is careful design to prevent and to collect the beam losses in order to minimize both radiation damage to components and maintenance delays due to high radiation levels. This is an ongoing effort and is the first line of defense against frequent component failures.

### **5.13.2 Conservative Engineering Design and Reliable Components**

Since the reliability of a system/component is a function of its mean time between failure (MTBF) and mean time to repair (MTTR), the overall reliability of a system will be improved by increasing MTBF and decreasing MTTR whenever possible. For critical components, such as the thyatron for the kickers and the tetrodes for the RF power amplifiers, careful search for and comparisons of products from different vendors will be carried out to select those with better MTBF records. Another critical component is the stripping foil system. The design will be of a multiple foil system capable of remote switching from one foil to another in case of failure.

### **5.13.3 Good Bookkeeping and Maintenance Record of Components**

A site-wide database system will be established to record the performance and reliability information for critical components as advertised by the producers and as experienced at the SNS. A superior product to improve the overall reliability will be used to replace a less reliable component.

### **5.13.4 Strategic Schedule for Preventive Maintenance**

There are many ways that a well-thought-out operation and maintenance schedule can improve the availability of the NSNS facility. For example, if one component is known to fail within a certain period of time, it should be replaced before it actually fails. Sufficient stocks of spares of critical components can reduce the MTTR.

### 5.14 UPGRADE PATH

Provisions have been made to upgrade the facility first to 2-MW and eventually to 4-MW capability. The upgrade from 1 to 2 MW will be achieved by doubling the linac current from 28 mA to 56 mA and doubling the number of stored protons in the ring. The upgrade from 2 to 4 MW will be accomplished by providing a second ring and providing beams from both rings at the same target. In that case, a splitter kicker will be provided to switch the linac beam for different rings, and the present entrance to the HEBT line will be modified.

The accelerator physics design goal for the accumulator ring is 2 MW. However, not every system is built to be capable of taking a 2-MW beam. Table 5.14-1 summarizes the capability of each system and the additional upgrades needed for 2-MW operation.

**Table 5.14-1 Upgrade path for the ring system**

	<b>Phase I</b>	<b>Upgrade Work</b>
<b>Accelerator Physics</b>	Design for 2 MW	None
<b>HEBT</b>	1 MW	More Shielding
<b>Injection</b>	1 MW	New Foil, New Kicker
<b>Magnets</b>	2 MW	None
<b>Power Supply</b>	2 MW	None
<b>Vacuum</b>	2 MW	None
<b>RF System</b>	2 MW	None
<b>Diagnostics</b>	2 MW	None
<b>Collimator</b>	1 MW	More Shielding
<b>Control</b>	2 MW	None
<b>Extraction</b>	1 MW	New Kicker
<b>RTBT</b>	2 MW	None
<b>Beam Dump</b>	2 MW	None

## **5.15 REQUIRED RING FACILITIES**

### **5.15.1 Scope**

The following facilities are required for the operation, support, and maintenance of the HEBT and RTBT beam transport lines, the injection and extraction systems of the accumulator ring, and the accumulator ring.

### **5.15.2 Light Laboratory Area and Technician Shops**

Two tech shop areas are required for mechanical and electrical technicians to assemble and repair clean mechanisms and electronic chassis and modules. Workbenches and light machine shop tools such as drill presses, brakes, milling machines, and lathes shall be available. Workbenches are to be provided with solder stations, hand tools, measuring equipment, and small parts. A central caged area for heavier tools such as hard soldering torches and tanks, drill chucks, vacuum cleaners, pumps (both water and vacuum), etc. shall be available for general use. These two areas shall be at least 5000 square feet apiece.

### **5.15.3 Assembly Area**

A larger high bay area will be set up for assembly or repair of large equipment such as electromagnets or power supplies. It is recommended that a building crane be provided for moving the assembled magnet cells, RF cavities, collimators, etc. A 25-ton capacity will be required. Access into the building for flatbed trucks, trailers, and forklifts will also be required. All of the tools that have been listed in section 5.15.2 shall be provided as well as heavier machine shop types such as lathes, milling machines, and high temperature ovens for bakeout and curing, etc. A separate work area shall be set aside, behind adequate concrete shielding, for working on "hot" items that have seen accelerator service. The building crane will allow these "hot cells" to be configured and reconfigured as needed for the number and type of equipment requiring repair.

A test bay with adequate safeguards is required for testing the electromagnets, septum magnets, collimators, etc. The test equipment typically consists of oscilloscopes, meters; temperature measurement equipment (thermocouples and infrared), survey or aligning tools, residual radiation or contamination measuring equipment, etc. A high current dc power supply as well as a smaller supply for the corrector magnets shall be available for testing. This area shall be 7500 square feet. Two hundred kVA of ac power are required. A closed-loop water-cooling system and heat exchangers that provide approximately 100 gpm (35°C supply temperature max/300 kW cooling) are required.

### **5.15.4 High Voltage Assembly and Test Lab**

The assembly and testing of high voltage equipment such as RF cavities, and fast kicker magnets and pfn's requires isolated areas that are clean and have high ceilings (20 ft). Separate bays set up for the safe high voltage powering of these specialty devices are required for personnel safety. Each of the two shall measure at least 40 feet by 60 feet. 480-volt ac power and closed-loop water cooling of typically 100 gpm (35°C supply temperature max/300 kW cooling)

are needed. Power supplies for hv rf testing, for capacitor charging, and for high-potential testing shall be available on a continuing basis.

### **5.15.5 "Clean" Assembly Area**

The assembly of high vacuum equipment, extraction kicker magnets, and internal beam line instrumentation equipment to be used in the ring and beam lines requires clean, dust free area of adequate size to handle vacuum chambers up to 5 m long. Welding, brazing and bakeout capabilities shall be provided. The area is best set up as a long assembly line where equipment goes from one step to the next and will require a space of at least 40 feet X 100 feet

### **5.15.6 Storage Areas**

The accumulator ring is a specialty type machine that requires equipment and ready spare parts that are not readily available commercially. Operational spares must be stored near the accelerator. Caged storage areas, lockers, and bins which are lockable shall be provided. Some spares for beam line equipment will be stored under vacuum, but continuous pumping will not be required.